Development of Advanced 3D Medical Analysis Tools for Clinical Training, Diagnosis and Treatment

A thesis submitted for the degree of **Doctor of Philosophy** (PhD)

by

Emmanouil D. Skounakis

M.Sc. in Data Communications Systems

M.Sc. in Electronic and Computer Engineering

Electronic and Computer Engineering

School of Engineering and Design

Brunel University

United Kingdom

May 2013

Author's Declaration

I hereby declare that I am the sole author of this thesis.

I authorise Brunel University to lend this thesis to other institutions or individuals for the purpose of scholarly research.

Signature:

Date: 10/5/2013

I further authorise Brunel University to reproduce this thesis by photocopying or by other means, in total or in part, at the request of other institutions or individuals for the purpose of scholarly research.

Signature:

Date: 10/5/2013

Abstract

The objective of this PhD research was the development of novel 3D interactive medical platforms for medical image analysis, simulation and visualisation, with a focus on oncology images to support clinicians in managing the increasing amount of data provided by several medical image modalities.

DoctorEye and *Automatic Tumour Detector* platforms were developed through constant interaction and feedback from expert clinicians, integrating a number of innovations in algorithms and methods, concerning image handling, segmentation, annotation, visualisation and plug-in technologies.

DoctorEye is already being used in a related tumour modelling EC project (ContraCancrum) and offers several robust algorithms and tools for fast annotation, 3D visualisation and measurements to assist the clinician in better understanding the pathology of the brain area and define the treatment. It is free to use upon request and offers a user friendly environment for clinicians as it simplifies the implementation of complex algorithms and methods. It integrates a sophisticated, simple-to-use plug-in technology allowing researchers to add algorithms and methods (e.g. tumour growth and simulation algorithms for improving therapy planning) and interactively check the results. Apart from diagnostic and research purposes, it supports clinical training as it allows an expert clinician to evaluate a clinical delineation by different clinical users.

The *Automatic Tumour Detector* focuses on abdominal images, which are more complex than those of the brain. It supports full automatic 3D detection of kidney pathology in real-time as well as 3D advanced visualisation and measurements. This is achieved through an innovative method implementing *Templates.* They contain rules and parameters for the *Automatic Recognition Framework* defined interactively by engineers based on clinicians' *3D Golden Standard* models. The *Templates* enable the automatic detection of kidneys and their possible abnormalities (tumours, stones and cysts). The system also supports the transmission of these *Templates* to another expert for a second opinion.

Future versions of the proposed platforms could integrate even more sophisticated algorithms and tools and offer fully computer-aided identification of a variety of other organs and their dysfunctions.

To my mother **Roubini Skounaki**

She died suddenly during this research
from Acid Leukaemia (Cancer)
on 26 December, 2010

Acknowledgements

Working on my PhD has been a really great experience. It is difficult to describe the feeling during the process of writing the first papers and proposals, giving talks, while working with other scientists.

I would like to say a heartfelt thanks to my supervisor Dr. Konstantinos Banitsas for his unflagging support, invaluable comments on my work, and continuing regard throughout this research. I feel privileged to have worked with him all these years for his dedication to this research and his unrelenting assistance and support. I look forward to continuing collaborating with him in the future.

I would also like to thank the following people:

➢ Doctors Dr. Norbert Graf - University Hospital of the Saarland, Germany and M.D. Stavros Tzoulakis - Venizeleio General Hospital, Heraklion, Crete, Greece, for their support concerning the clinical trials, their invaluable input to the design and functionality of the platforms and the clinical data.

➢ Dr. K. Marias - Computational Medicine Laboratory, Foundation for Research & Technology Hellas - Institute of Computer Science, for giving me the opportunity to work there in the development of the *DoctorEye* medical platform (teamwork project supported by the EC ICT project *ContraCancrum*, contract No: 223979).

➢ *Clear Canvas Company* for allowing free access to their code for the *DocrorEye's* DICOM images handling process [Clear Canvas, 2013].

➢ Angelos Armen for the implementation of the 3D visualisation module of the DoctorEye's platform.

➢ My friend Evangelos Kandounakis for his support in writing this thesis.

Very special thanks to my wife Maria for her invaluable support, love and understanding, to my children Stavros, Aristea and Roubini and to my sister Areti for their continuous encouragement.

Finally, I would like to thank my mum, Roubini Skounaki who died of cancer during this research, for her infinite support throughout everything. As a teacher, you taught me to love studying and inspired me to continue my studies to get this PhD. Thank you with all my heart …

Abbreviations and Acronyms

2D	Two-Dimensional
3D	Three-Dimensional
ACR	American College of Radiologists
ATD	Automatic Tumour Detector medical platform
Bit	Binary digit (0 or 1)
BrainIX	DICOM MRI sample image datasets
CA	Connectivity Analysis process
ContraCancrum	Clinically Oriented Translational Cancer Multilevel Modelling project
CT-Scan	Computed Tomography Scan
CSF	Cerebrospinal fluid is a clear colourless bodily fluid produced in the choroid plexus of the brain
DAT	A common file format for data files
DCM	DICOM medical images
DICOM	Digital Imaging and Communications in Medicine protocol
DLL	Dynamic-link library
DSC	Dice Similarity Coefficient (Evaluation metric)
DrEye	DoctorEye medical platform
DoctorNo	A suite of plug-ins for the DoctorEye medical platform
EC	European Community
GS	Golden Standard model (The Clinician's volume model)
GUI	Graphical User Interface
IAD	Imaging-enabled Assistive Diagnosis System
In Silico	Expression used to mean *via computer simulation*
Linux	Computer Operating System
MIP	pH-sensitive Molecularly Imprinted Polymer (type of 3D view)
MRI	Magnetic Resonance Imaging
MT	Medical Technician's volume model (Automatic process)
NEMA	National Electrical Manufacturers Association
PACS	A picture archiving and communication system (PACS) is a medical imaging technology which provides economical storage of, and convenient access to, images from multiple

	modalities
ROI	Region of Interest
SDK	Software Development Kit (a set of routines that allows the development of applications)
Snaxel	Snake pixel point (used in the Active Contours – Snake segmentation method)
TCP/IP	Transmission Control Protocol / Internet Protocol (Internet protocol suite)
VB	Visual Basic
VR	Value representation as a character string, describes the data type and format of the attribute's value in DICOM Images
VTK	Visualisation Toolkit (open-source libraries, freely available for 3D computer graphics)
XML	Extensible Markup Language (defines a set of rules for encoding documents in a format that is both human-readable and machine-readable)

Table of Contents

List of Figures

List of Tables

Nomenclature

Δθ	Angular spacing between adjacent projections (MRI Scanners)
θ_j	The jth projection angle (MRI Scanners)
A	Represents a local maximum value in the histogram
B	The point where the histogram starts to rise again
C	Speed of the ultrasound (Ultrasound Imaging)
Bit	Binary digit (0 or 1)
Byte	Unit of digital information (consists of 8 bits)
D	Distance of the reflecting object from the transducer (Ultrasound Imaging)
Down	Represents the distance from a local maximum value and the point where the histogram starts to rise again (in the Automatic Segmentation Framework)
DSC	Dice Similarity Coefficient (Evaluation Metric)
GS	Golden Standard model (The Clinician's volume model)
gv	Grey-scale value (from 0 to 255)
h(gv)	Histogram value for a specific grey-scale value *gv*
Lm	Threshold in the histogram to separate groups of objects
M	Number of projection views (MRI Scanners)
Max	Maximum value of the histogram
MT	Medical Technician's volume model (Automatic process)
NormMax	Normalised maximum value of the histogram (defined by the user)
P(i)	The initial location of the Snake (Greedy algorithm)
P′(i)	The search location of the Snake (Greedy algorithm)
T	Time of the pulse from emission to reception (Ultrasound Imaging)
Threshold	Value used to define homogeneous regions (*Thresholding Segmentation methods*)
Window Level	Mid value between the brightest and dullest pixel value
Window Width	Is the difference between the brightest and dullest pixel value

Chapter 1 - Introduction

1.1 Motivation

The rapid evolution of advanced medical image modalities such as the modern Magnetic Resonance Imaging (MRI) scanners and their extensive use in the clinical environment produces a huge amount of data. Consequently, there is a need for clinicians to examine a large number of slices of MRI datasets on a daily basis.

Nevertheless, the complexity of medical images renders the diagnostic process a difficult and time consuming task.

Speed of process of medical images and accuracy in the delineation of organs and their potential abnormalities are central to the clinical environment. In an effort to assist clinicians in their diagnostic task, a number of medical image processing systems have been developed.

However, apart from the fact that these systems involve high costs regarding purchase and use, they also have a complex environment requiring previous knowledge in the field of image processing, factors which are often discouraging for the clinicians and the medical staff. Developers of such systems, in an effort to achieve a balance between accuracy and complexity, give priority to accuracy of the detection of important areas which however takes a toll on the simplicity of use. Usually, they integrate manual and semi-automatic algorithms and methods which require a lot of time to achieve an acceptable result. Moreover, in many cases, the extremely large number of images contained in a dataset renders this process ineffective.

Therefore, there is a clear need for more advanced medical systems in the field of medical imaging, which must meet two crucial requirements.

First, they must integrate fully automatic processes in order to simplify the image processing task in a user-friendly environment.

Secondly, the results of the processing of the medical data must be accurate

enough from the clinicians' point of view.

All in all, the motivation behind this research is to develop more sophisticated systems to address management of large amounts of medical images, so as to achieve accurate, easy and quick processing and simplify complex procedures from their input to their 3D representation.

1.2 Aims and Objectives

To improve on the above situation, two platforms were developed: *DoctorEye* and *Automatic Tumour Detector.* Both platforms have the following aims:

- facilitate the management of the increasing number of medical images using user-friendly tools to ensure accurate and timely diagnosis in the clinical environment

- support medical data exchange (telemedicine)

- assist in the training of clinicians to recognise and treat pathologies

- allow clinicians to conduct virtual experiments in silico to develop new treatments

- support researchers with experimentation, to develop new, more effective algorithms and methods in the field of medical imaging

These aims were achieved by carrying out the steps below:

- A study with a focus on the most commonly used medical image modalities to identify the most appropriate one. The objective was to utilise a modality ideal for soft tissues which does not emit radiation and produces medical images with the highest resolution and the least noise so as to get the most accurate results from the segmentation process.

- A comprehensive study of the DICOM (Digital Imaging and Communications in Medicine) technology specifications. This provided the required understanding to remove sensitive data of the patient and to use important information included in the DICOM files for the realistic representation of 3D models of the important areas.

- In-depth understanding and research of methods concerning image handling processes, advanced image correction tools and techniques and 3D visualisation processes are required for the development of the platforms.

- A comprehensive literature review of various brain segmentation algorithmic approaches, full-automatic segmentation frameworks for abdominal images and annotation systems.

- Effective collaboration with expert clinicians, clinical staff and engineers was established in order to design user-friendly environments of the platforms to meet the needs of clinicians.

- A multi-user and multi-functional annotation system was implemented to support training of clinicians in the accurate identification of organs and their potential pathology.

- A sophisticated Templates technology was integrated to enable clinicians automatically detect organs and their potential pathology as well as to send the outcome of the analysis to another clinician for a second opinion.

- A sophisticated plug-in technology was developed to support researchers in experimentation with new segmentation/classification algorithms.

1.3 Contribution to Knowledge

This research presents two novel, interactive platforms which integrate many innovations in the field of digital image processing for 3D medical image handling, analysis, simulation and visualisation, focusing on oncology images.

The platforms were developed through constant interaction and feedback from expert clinicians integrating a thorough analysis of their requirements while having the ultimate goal of assisting in accurate delineation of organs and their potential abnormalities.

They allow clinicians to work with a large number of 3D tomographic datasets containing complex images, in a simple way, and also to efficiently annotate

multiple regions of interest in the same session.

Manual, semi-automatic and full automatic segmentation techniques with advanced correction tools combine with sophisticated multi-functional systems for annotation and visualisation to assist in the quick and accurate delineation of regions of interest. In particular, the full automatic segmentation framework contributes to the combination of ease of use and robust results compared to all existing segmentation methods for abdominal images.

A multi-user, multi-functional annotation system supports the comparison of the delineations produced by several users working on the same medical dataset. In this way, this innovative procedure can be useful in training clinicians concerning identification of areas of interest and their potential pathology.

Moreover, a sophisticated and simple in use plug-in technology allows researchers to add components related to oncology such as tumour growth and simulation algorithms for improving therapy planning.

The platforms ensure stability, usability, extensibility and robustness, with promising results as they have been tested by different users and over a large number of heterogeneous tomographic datasets.

Thus, these platforms serve as *3D Medical Analysis Tools for Clinical Training, Diagnosis and Treatment*.

1.4 Thesis Structure

This thesis describes the development of advanced medical image analysis tools in five chapters. The following contains a brief description of these chapters.

The first chapter introduces the motivations, aims and objectives, contribution to knowledge and the thesis structure.

Chapter two presents the foundation technical background necessary for the full understanding of this research, as well as a literature review of segmentation/annotation methods.

Each of the next three chapters is divided into two parts to describe

technologies integrated into the *DoctorEye* and *ATD* platforms.

Chapter three explains the technical challenges faced during the development of the proposed medical analysis platforms. This chapter starts with a presentation of the design and the architecture of the platforms followed by a detailed description of the integrated methods and algorithms. The chapter elaborates on scientific areas such as image handling, segmentation (Manual, semi-automatic and full-automatic), image correction tools and techniques, annotation and 3D visualisation. At the end of each part, there is also a description of the experimental process for each platform.

Chapter four presents the experimental results and discussions for both medical platforms. For *DoctorEye*, experimental results are presented in connection with the mode of use (training / clinical / research) while for the *ATD* platform results come from the full automatic use.

Chapter five concludes the research, with a summary, contributions and suggestions for further research, for both platforms separately.
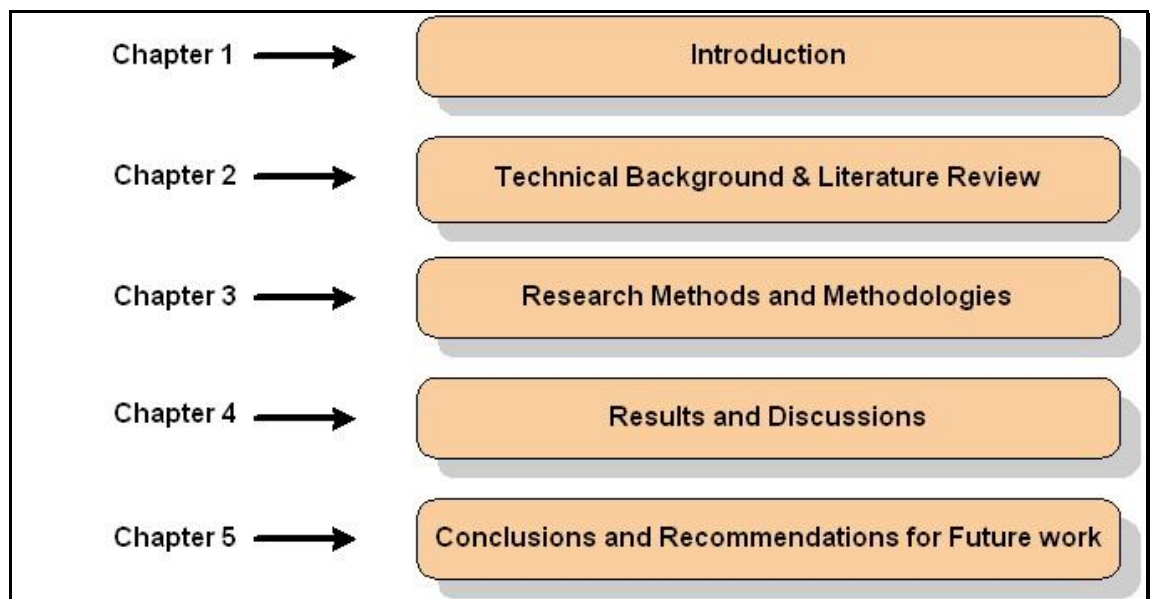
Figure 1.1: Structure of the thesis

Chapter 2 – Literature Review

2.1 Introduction

Cancer is a leading cause of fatality among other diseases. Still, there is no known way of preventing cancer, but early detection allows treatment before cancer is metastasised to other parts of the body.

Modern tomographic systems like the new Magnetic Resonance Imaging (MRI) scanners, offer clinicians high resolution medical images allowing a more specific look at radiologic anatomy.

They offer the ability to detect masses and distortions of tissue better, quicker and more efficiently than ever before. This makes MRI imaging a very popular technique in cancer imaging, allowing doctors to extract critical pathophysiological information in order to establish early diagnosis and assess the stage of the disease.

However, it is often the case that a radiological department and specifically oncologists deal with a large number of MRI multi-frame slides where tumour identification and delineation can be a thorny and time consuming process.

2.2 Technical Background

It is crucial to understand that not all medical image modalities provide high resolution images for the purposes of accurate identification of areas of interest.

Thus, a study in the functionality of the most commonly used modalities is essential for the selection of the most appropriate one which provides medical images with the highest resolution.

Moreover, modern medical image modalities depend on the DICOM medical image technology. Knowledge of this technology is required. The reason is that DICOM images contain data that must be utilised in the medical image analysis tasks, such as the thickness of the slices and the distance between them, which are essential for the realistic 3d representation of the organs and

their dysfunctions. Other sensitive data of the patient needs to be excluded (anonymisation process).

2.2.1 Medical Images – The need for a standard

Medical imaging is the technique and process used to create images of the human body or parts of it *in silico (via computer simulation)*, for clinical purposes in order to diagnose or examine diseases or for studying the normal anatomy and physiology in medicine.

The transition from the classical studying of an X-ray film clipped to a light box to onscreen image processing has produced a variety of image modalities in clinical practice.

The medical imaging industry has developed a wide range of sophisticated image modalities, storing the collected data (images) in different file formats.

This raised compatibility issues in the past, when clinical practice required comparison of data coming from different modalities and manufacturers.

The need for a standard for compatibility reasons led to the introduction of the DICOM (Digital Imaging and Communications in Medicine) standard.

2.2.2 The DICOM Standard

The DICOM standard resulted from co-operation between the American College of Radiologists (ACR) and the National Electrical Manufacturers Association (NEMA).

This standard specifies a protocol for handling, storing, and transmitting medical data and ensures a *plug and play* integration of all information systems in clinical environments.

The DICOM protocol defines how information can be efficiently transferred between compliant equipment, while its TCP/IP protocol compatibility allows the exchange of medical data between applications over the Internet.

The DICOM file format consists of two parts of information: The DICOM File

Meta Information and the DICOM Data Set.
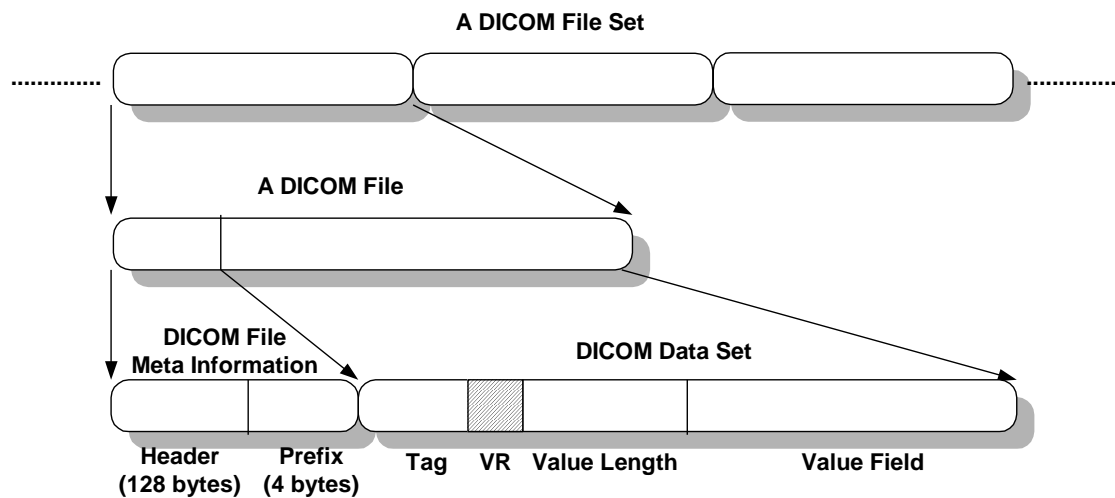
Figure 2.1: Schematic layout of the DICOM file format

The DICOM file Meta information consists of two parts: a 128 byte header and a 4 byte DICOM prefix (Figure 2.1).

The *Header* (128 bytes) is included in DICOM files to support compatibility with commonly used computer image file formats. The *Header* is not always used, for example when all 128 bytes are set to 00H (NULL). In all other cases the header must be interpreted.

The *Prefix* (4 bytes) contains the characters *DICM* to identify the file as DICOM *(medical file).*

The DICOM dataset comprises of a set of Data Elements which contain a number of Data Element Fields (Tag, Value representation, Value length and Value field).

Tag is an ordered pair of two 4-bit unsigned integers to define the *Group* (first 4 bits) and the *Attribute* (last 4 bits) of the information contained (Table 2.1) in the format of Group, *element* (XXXX XXXX) that identifies the element.

Value representation (*VR*) as a character string, describes the data type and format of the attribute's value.

Value length is a 16-bit or 32-bit unsigned integer that defines the length of the

following *Value field (attribute value)*.

Value field is an even number of bytes containing the attribute data (values of the Data Element), encoded according to the *VR*.

2.2.3 Working with DICOM (Medical) Images

Medical images are in the form of DICOM format (dcm files). This means that every image contains information categorised in *Modules* some of which are listed below:

- Clinical Trial Subject Module Attributes
- General Equipment Module Attributes
- Patient Module Attributes
- Patient Study Module Attributes
- Patient Summary Module Attributes
- Therapy Module Attributes

Every *Module* contains *Attributes* with corresponding *Tags* (with numerical names) and a short description containing information (Table 2.1).

The following table depicts some of the attributes included in medical images:

Table 2.1: Therapy Module Attributes [DicomLookup, 2013]

Tag	Attribute	Type	Description
(0018,0036)	Interventional Therapy Sequence	3	Introduces sequence of items describing interventional therapies
(0018,0038)	>Interventional Status	2	Temporal relation to therapeutic intervention Specialized as Enumerated Values: PRE INTERMEDIATE POST NONE Required if Interventional Therapy Sequence (0018,0036) is present.
(0018,0029)	>Interventional Drug Sequence	3	Sequence that identifies the interventional drug. May be present if Interventional Therapy Sequence (0018,0036) is present.
(0018,0035)	>Intervention Drug Start Time	3	Time of administration of the interventional drug. May be present if Interventional Therapy Sequence (0018,0036) is present.
(0018,0027)	>Intervention Drug Stop Time	3	Time of completion of administration of the intervention drug.
(0054,0302)	>Administration Route Code Sequence	3	Sequence that identifies the Administration Route. This sequence shall contain exactly one item.
(0018,0039)	>Therapy Description	3	Further description in free form text describing the therapy. May be present if Interventional Therapy Sequence (0018,0036) is present.

This information is extremely important at the stage of clinical diagnosis and treatment since the history of the patient, older clinical trials and results can be accessed, to assist clinicians.

2.2.4 Medical Image Modalities

Existing medical image modalities with wide use include X-ray (1895, mainstay of medical imaging until 1970), CT-Scan (1971), Ultrasound and Magnetic Resonance Imaging - MRI (1980).

X-rays are very short wavelength electromagnetic radiation with a range between 0.01 and 10 nanometres.

They are generated by an X-ray vacuum tube, where high voltage is used to accelerate the electrons released by a hot cathode. These electrons move at very high speed and create a beam of X-rays emitted through a patient onto a film which provides a measure of the ray attenuation in tissue (Figure 2.2).
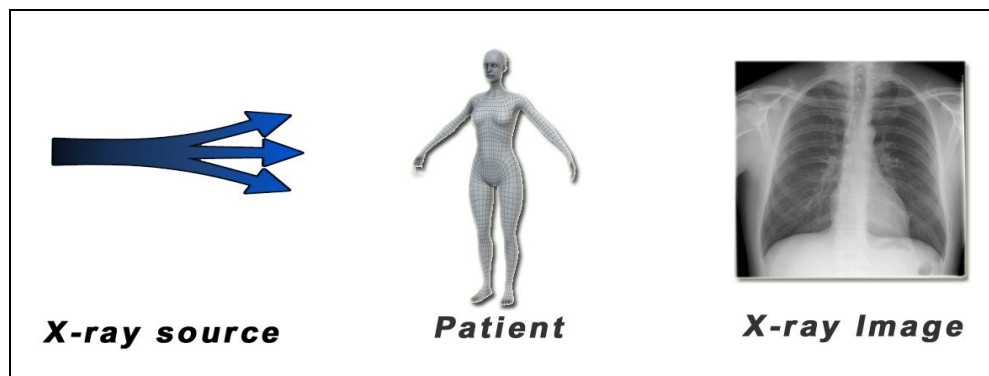
Figure 2.2: Chest X-ray Image

X-rays provide low resolution images, which necessitates the need for contrast enhancement techniques.

X-ray technology is widely used today since it is excellent for imaging bones. However it provides low resolution images and thus it is not ideal for soft tissues and also emits excessive radiation.

Figure 2.3 shows an example of an X-ray breast film-mammogram to which two contrast enhancement techniques have been applied to enhance microcalcification areas.
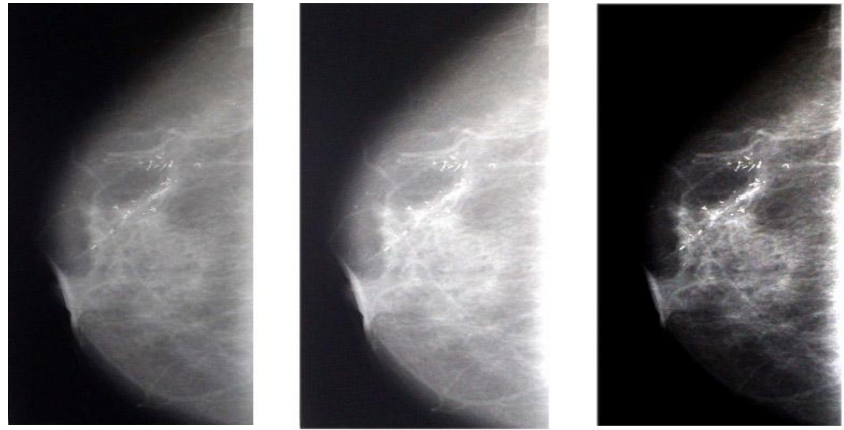
Figure 2.3: An X-ray breast film-mammogram. The second image is enhanced through histogram equalisation algorithm and the third image is enhanced through feature adaptive contrast method. Figures come from the textbook [Medical Image Analysis, 2003]

Computed tomography (CT) systems, based on X-ray technology, produce series of 2D *slices* through the body*,* in order to create 3D models of the body and its internal organs.

Figure 2.4: CT scan in process

The process here requires the following steps:
- An X-ray image is acquired though the main system (X-ray beam and the detector).
- By rotating to the next angle a new X-ray image is acquired, and so on for 360°.
- In the end, all projections are assembled.

In modern CT-scanners multiple X-ray sources and detectors are used,

enabling simultaneous collection of multiple projection images.
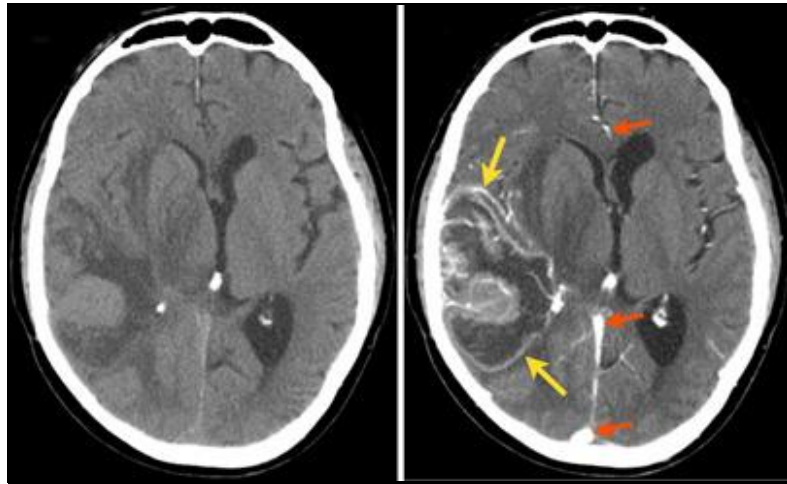
Figure 2.5: Computed tomography (CT) of the brain. Brain diseases can be recognised with contrast enhancement. Figure comes from [Computed Tomography, 2013]

Computed Tomography (CT) technology is also widely used today in clinical practice as it provides 3D anatomical information about the body preserving topology (bones). Disadvantages include unsuitability for all soft tissues and emission of excessive radiation.

Ultrasound produces images of tissue and blood vessels using high-frequency sound in a similar manner to the sonar system of a submarine. It emits ultrasounds and detects echoes. These returning echoes are analysed and the boundaries of an area in the body are mapped out.
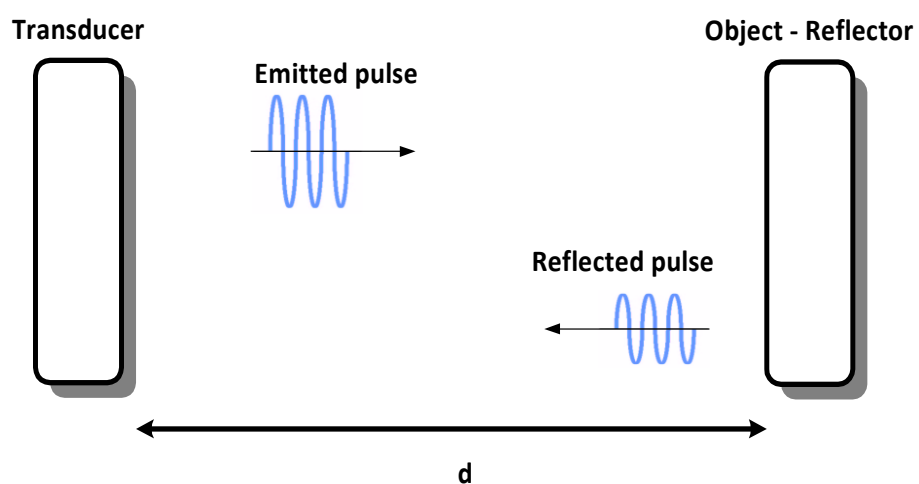
Figure 2.6: Ultrasound Imaging - Basic Principle

The basic principle of the ultrasound technology is based on the following equation:

$$d = \frac{ct}{2}$$ Eq. 2.1

Where *d* is the distance of the reflecting object from the transducer, *c* is the speed of the ultrasound and *t* is the time of the pulse from emission to reception.

The images created are related to the differing sound transmission characteristics of different tissue areas.
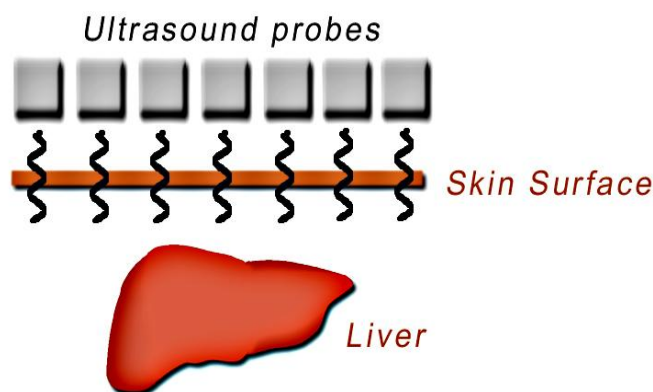
Figure 2.7: Ultrasound Imaging – Medical Applications

This technology is used today in:
- viewing the fetus in pregnancy (Fetal ultrasound)
- diagnosing osteoporosis (Bone sonography)
- visualising blood flow through a blood vessel (Doppler ultrasound)
- viewing the heart (Echocardiogram)
- listening to the fetal heart beat (Doppler fetal heart rate monitors)

A major disadvantage is noise in the pictures in the case of bony structures due to the absorption of ultrasound waves.

Figure 2.8: Ultrasound Modality and Image sample

MRI (Magnetic Resonance Imaging) is one of the most contemporary medical imaging techniques used to visualise in high resolution internal areas of the body.

Paul Lauterbur and Peter Mansfield won *The Nobel Prize in Physiology or Medicine 2003*, for their discoveries concerning *Magnetic Resonance Imaging* (MRI).

In contrast to CT-scanners, this technology does not use X-ray radiation, but powerful magnets and radio waves to create images of the body.

Electromagnetic Radiation Energy
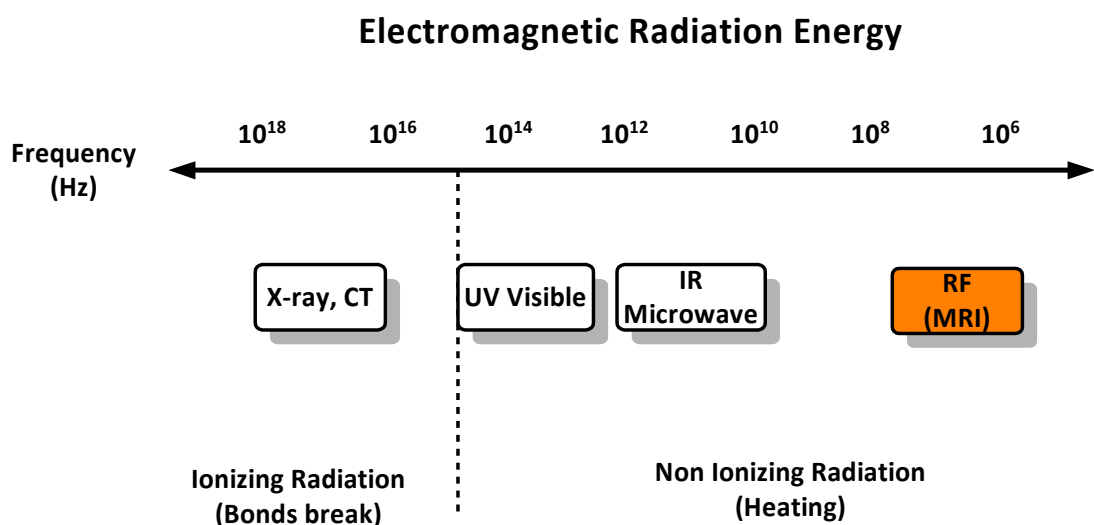
Figure 2.9: Electromagnetic Radiation Energy in X-ray, CT and MRI technologies

The main idea here comes from the fact that there is a difference between the nuclear magnetic relaxation times of tissues and tumours, thus scientists consider the magnetic resonance technique useful for the detection of diseases.

In a strong magnetic field Hydrogen nuclei (protons) spin in phase with one another and align with the field. Relaxed protons induce a measurable radio signal.

MRI technology produces series of images (slices). These image slices are then reconstructed by computation (Equation 2.4.4 – Simple Back projection).

$$\hat{f}(x,y) = \sum_{j=1}^{m} p(y\cos\theta_j - x\sin\theta_j, \theta_j)\Delta\theta \qquad \text{Eq. 2.2}$$

Where θ_j is the jth projection angle, m is the number of projection views and $\Delta\theta$ the angular spacing between adjacent projections.
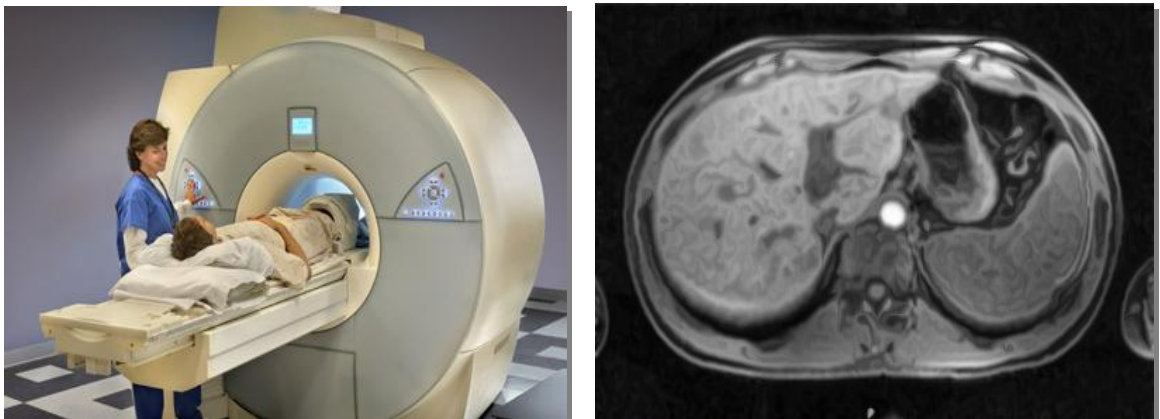
Figure 2.10: MRI Modality and Image sample. Figures come from [How MRI works, 2013]

The fact that it creates high resolution images renders this technology useful for the observation of morphological – structural abnormalities.

Since it has the ability to discriminate between subtle differences in tissue characteristics, it is the most widely-used modality in clinical practice for image guided surgery.

2.2.5 Selecting Modalities and DICOM Tags

Of the four medical image modalities mentioned above, MRI produces higher resolution medical images. This is the reason why these medical images have been used in our experiments instead of X-ray, CT-Scan and Ultrasound images.

Moreover, one more reason why we focus on MRI imaging modalities is the fact that they have been mostly used recently by clinicians.

Concerning the attributes (tags) of the DICOM images, some are valuable in several image processing tasks.

For example in the creation and visualisation of a 3D model of the body we need to have prior knowledge of the resolution that the modalities provide in the 3 dimensions x-y-z.

In other words, this information is necessary in order to present a 3D model of the body with real metrics.

2.3 Overview of Brain Segmentation Algorithms

Image segmentation is the process of detecting multiple segments (sets of pixels) in an image giving a more meaningful representation of the content.

Medical image segmentation has been a subject of considerable research. Many methods have been proposed for the delineation of regions of interest of the brain area which fall into two categories: structural and statistical.

Structural methods (such as edge detection algorithms) are based on the spatial properties of the image (e.g. edges) in order to extract boundaries between different brain tissues [Bomans M. et al, 1990], [Dellepiane S., 1991], [Clarke P., et al 1995]. A downside to these methods is vulnerability to artifacts and noise. One of the most popular structural methods is the Region growing algorithm [Fujita H. et al, 2006].

Statistical methods label pixels according to probability values, which are based on the intensity distribution of the image.

In the case of the presence of solid objects with well separated intensities from the background and the neighbouring-objects, thresholding-based techniques are used. However, in complex medical images, they are not always effective [Brummer M., 1992].

Parametric and nonparametric statistical approaches are widely used in segmentation of brain MRIs.

Nonparametric methods are adaptive but require a large number of correctly labelled training points in advance, since no prior knowledge about the functional form of the distribution exists. A downside here is the difficulty of obtaining a large number of training points, even for those who have experience with them. A commonly used nonparametric method is the K-Nearest-Neighbours.

The only parametric approach for brain segmentation which has been used to date is the finite Gaussian mixture model when the Gaussian likelihood distribution is assumed.

2.4 Overview of full-automatic Segmentation Algorithms for Abdominal Images

To date, we can find several attempts aimed at improving the abdominal image segmentation process.

2.4.1 Overview of the Kidney Segmentation methods

Recently, several sophisticated algorithms have been devised for accurate automatic detection of kidneys addressing the challenge of increased difficulty in their delineation, due to their intensity variation.

Prevost et al. [2012] have automatically localised the kidney with a novel ellipsoid detector and then applied deformation of this ellipsoid with a model-based approach in the segmentation process achieving a DSC (Dice Similarity Coefficient) of 87.5%. Similarly to this platform, they calculate the accuracy of automatic segmentation outcome by comparing it with the result of the semi-automatic segmentation method coming from the radiologist's work (Ground Truth).

Lin et al. [2006] have presented an effective model-based approach for kidney segmentation with an average correlation coefficient of 88% while Gloger et al. [2012] have deployed Bayesian concepts for a probability map generation to achieve an automatic kidney Parenchyma volumetry with a DSC of 90.3%.

Rao et al. [2005] use deformable shape models (called m-reps) to automatically segment kidneys yielding a DSC of 88.8 %. Rusinek et al. [2007], use an automated graph-cuts (GC) segmentation technique for dynamic contrast-enhanced (DCE) 3D MR renography achieving a DSC of 96% for the kidney and 90% the cortex and the medulla. The authors of this system report that their method is very fast (approx. 20 min) compared to the time needed for a manual segmentation of about 2.5 hours.

A framework for a fully automatic grey-level based segmentation of kidneys has been presented by Campadelli et al., [2008] that employs a fast matching technique with a similarity volume overlap of 95%.

Other researchers have proposed a 3D minimal path segmentation method with an average overlap ratio of 93% [Li and Fei, 2008].

Finally, Akbari et al. [2012] have presented a combination of texture features and a statistical matching of the geometrical shape of kidneys, for an automatic segmentation in 3D MRI images with a mean DSC of 90.6%.

Compared to those methods, the proposed *Automatic Segmentation Framework* yields a higher mean DSC of 97,2% for the recognition of kidneys. The processing time needed for a 24 MRI dataset, is about 1 minute; much faster compared to the above mentioned methods.

2.4.2 Abnormality Detection Overview

Concerning abnormality detection, Chen et al. [2011] have presented a finite element method based on 3D tumour growth prediction for kidney tumours, with an average true positive fraction of 91.4% on all tumours.

A new approach for the automatic classification of normal and acute rejection transplants from Dynamic Contrast Enhanced MRI's has also been introduced by Farag et al. [2006] with an overall accuracy of 93,3%.

El-Baz et al. [2007], [2008] have presented a method to distinguish between normal and acute rejection transplants from Dynamic Contrast Enhanced MRI's with an overall accuracy of 97%.

Khalifa et al. [2010] have presented a non-invasive image-based approach for early detection of acute renal rejection with overall accuracy of 96,1%.

Tamilselvi et al. [2011] used an improved seeded region growing method and classification of kidney images with stone sizes and focused on the kidney image segmentation and diagnosis for stone detection having a DSC of 95%.

S. Kumar et al. [2011] use an automatic segmentation algorithm for segmenting liver and tumour based on thresholding, and region growing techniques. The tumour is segmented with the use of the alternative FCM clustering algorithm and the DSC for liver and tumour is 95.8 and 89.8 respectively.

K. Kumar et al. [2012] have tested three neural network algorithms for diagnosis of kidney stones diseases. They claim that the multilayer perception with two hidden layers and the back propagation algorithm is the best model for diagnosis of kidney stone disease with an accuracy of 92%.

Wang et al. [2013] focuses on the automatic segmentation of liver, intrahepatic vessels and tumours. Their method is based on a combination of patient-specific shape and a minimally supervised segmentation algorithm. The average run-time of the classification algorithm in the segmentation stage was 18 minutes with eight iterations.

Finally, Jose et al. [2012] methodology is closer to our own. Their automatic segmentation method is based on association rule-mining to enhance the diagnosis and classification of kidney images. Along with the primary method, they use conditions and criteria to adjust their system thus achieving results with an average accuracy of 92%.

2.5 Overview of the development of Annotation Systems

While numerous existing projects are developing specialised platforms and tools to speed up the process of data analysis in different biomedical

applications, most of the open access solutions often require engineering skills to understand their complicated user interface, rendering their clinical use difficult.

However, in the actual clinical environment, accurate delineations are required without the need of knowledge of specific and complicated procedures concerning medical image processing.

Generally, there is a variety of medical image-annotation platforms including VANO [Peng H. et al, 2009], CMAS [Lin I. & Chao H., 2006], Hybrid System [Mechouche A. et al, 2008], Annotor annotation software [2007], Amira multifaceted software platform [2006] and ITK SNAP segmentation software [2006].

DoctorEye and *ATD* are novel, flexible and easy to use platforms, for intuitive segmentation / annotation of organs and their potential dysfunctions.

Their development is clinically driven. In particular, *DoctorEye* follows an open modular architecture focusing on plug-in components.

Clinicians who have used these over a large number of datasets, find the environments of the two platforms simple and user friendly and also claim that only a basic knowledge of annotation / simulation processes is required to use both systems.

The main advantages of the proposed platforms over existing ones include:
- fast and accurate delineation of large datasets (even in areas with complicated shapes)
- the ability to set multiple labels that allow the user to annotate and manage many different areas of interest in each selected slide
- a clinically driven design and functionality which ensures that they have the potential to be used routinely in the clinical practice

A feature that adds value to the *DoctorEye* platform is that while it offers standard functionalities for oncology image analysis, annotation / segmentation and 3D visualisation, it also allows the easy incorporation of more specific and sophisticated plug-ins that can empower the clinician to use modern technologies for enhanced diagnosis and therapy design.

As an example, computational *in-silico* models of cancer growth and simulation of therapy response could easily be plugged in, allowing modelling assisted therapy decision making.

The development of the *DoctorEye* platform as a teamwork project is part of the *ContraCancrum EU-ICT* research project and is currently used by clinicians for oncology 3D annotation and visualisation.

2.6 Summary and Discussion

Of all the algorithmic approaches and methods mentioned in Chapter 2 concerning *Segmentation Algorithms*, *Full automatic segmentation frameworks for abdominal images* and *multi-level Annotation systems*, a choice had to be made - in each of these three issues - based on specific criteria.

Concerning segmentation algorithms, the *Region Growing* algorithm was selected for the delineation of important areas by clinicians, on the grounds that it does not require any sophisticated or previous knowledge of segmentation algorithms or complicated adjustment of parameters.

Additionally, as will be explained in the following sections, the integration of this algorithm in the platform was conducted in such a way that the delineation process becomes interactive and faster while maintaining accuracy.

As regards full-automatic segmentation frameworks for abdominal Images, first the Perona-Malik diffusion filter [Perona P. & Malik J., 1990] was used to homogenise areas in the images (Section 3.2.10.2).

Next, a modified *Region Oriented Segmentation method* was selected to be the basis for the development of a 3D Segmentation framework.

Compared to the full-automatic segmentation methods mentioned in section 2.4, the proposed *Automatic Segmentation Framework* integrated in the *ATD* platform, yields a higher mean DSC of 97,2% for the recognition of kidneys and 96,1% for their abnormalities (Tumours, Stones and Cysts).

It must also be noted that although all the above mentioned methods detect kidneys, some methods detect tumours as well [Chen X. et al, 2011], [Kim D.Y.

& Park J.W., 2004].

Furthermore, the multi-level, multi-functional *Annotation system* developed was clinically driven to ensure ease of use by clinicians.

Chapter 3 - Methods and Methodology

Chapter 3 elaborates the methods and methodologies integrated in the *DoctorEye* and *ATD* platforms.

3.1 The *DoctorEye* Project

3.1.1 Introduction

The complicated functionality and the high cost of use of existing medical platforms are two inhibitive factors for using them in clinical practice. Doctors find them difficult to understand and to use since they require prior knowledge of image processing techniques and training.

So, the main idea behind this project was the development of a medical platform which can be used by clinicians with no prior knowledge of segmentation and annotation methods for easy and accurate delineations of organs and their dysfunctions supporting 3D visualisations with real metrics.

An additional concept was that the development of the architecture of the platform should support plug-in technology in order to allow researchers to add their algorithms and analyse the results in an easy way.

Last but not least, the platform should also enable *Expert Clinicians* to train other clinicians for more accurate diagnosis and treatment.

3.1.2 Platform Design

The platform was developed from scratch based on the .NET framework architecture [Benefits of the Microsoft .NET Framework, 2013] and can be used in any Windows-based computer with the .NET framework version 2.0 or later.

However, .NET framework permits, in concept, the porting of the application in many other *Linux* based environments, using the *Mono project* [The Mono project, 2013] functionality and libraries, so the user can run an application using the *No-Touch Deployment* [Benefits of the Microsoft .NET Framework, 2013]. The *Mono project* is a software platform designed for developers to

easily create cross platform applications.

The graphical user interface (GUI) is based on *Microsoft Office 2007* applications to ensure a user-friendly environment. This new implementation interface gives the user the option to change the appearance of the interface by choosing one of the embedded *Skins* in the tab *Home* on the ribbon, next to the *View* option (Figure 3.1).

Figure 3.1: DoctorEye: Snapshot of the main window. The user is able to easily navigate through the available slides and select the one to process

The ribbon contains three tabs corresponding to three clearly defined steps necessary for the process of creating the 3D models *in silico*, a feature that simplifies the whole process and makes it user-friendly.

More specifically, the tab *Home* supports the image handling process (Zoom, Navigation, View and Skins), while the *Image Annotation* and *Visualisation* tabs support their corresponding processes.

3.1.3 DoctorEye Architectures

There are two major issues when working with a large number of big images, such as medical images (dcm files), simultaneously.

The first issue concerns the anonymisation of the personal data process (removal of the patient's data from the images) while the second issue is related to the management of the system's memory to avoid overflow events.

In order for the application to work with anonymised data (medical images), and to be stable in terms of efficient memory management so as not to present overflow events, four stable versions of the *DoctorEye* platform have been developed.

The first attempt (*DoctorEye ver 1.0*) was implemented with *Visual basic 6.0* using the library *dicom.dll* [Dicom.dll software, 2013] to anonymise medical images so as to contain no data of the patients. This library was created by Marco Parvis – Politecnico di Torino (2001) and was based on the original work of George J. Grevera dicom2pgm.cpp file (1995). The DLL exports six functions, four of which (ReadDicom, ReadDicomHeader, ReadDicomVariant, SetImageIndex) are related to the DICOM files. The other two functions (ReCreateArray, ReCreateArrayV) are related to the bitmap files necessary for DICOM images so that they can be displayed in the VB environment. Although the issue concerning the anonymisation process was resolved, for effective memory management, a complex and sophisticated design of the system was still required.

The second attempt (*DoctorEye ver 2.0*) was based on the *DicomObjects* libraries [DicomObjects, 2013]. These libraries were very practical as they performed many functions. However, the issue here was the need for registration and activation on every computer using this application since their use was time-limited as they expired within 60 days after activation.

The third attempt (*DoctorEye ver 3.0* – Figure 3.2) was based on the *Clear Canvas* libraries [ClearCanvas, 2013]. Their use is free as no registration or activation is required, rendering them practical for the development of beta versions of medical platforms.

This version is based on an asteroid construction of the object model *ToolsHost* which allows the processing of a medical Image dataset with multiple images (Figure 3.2).
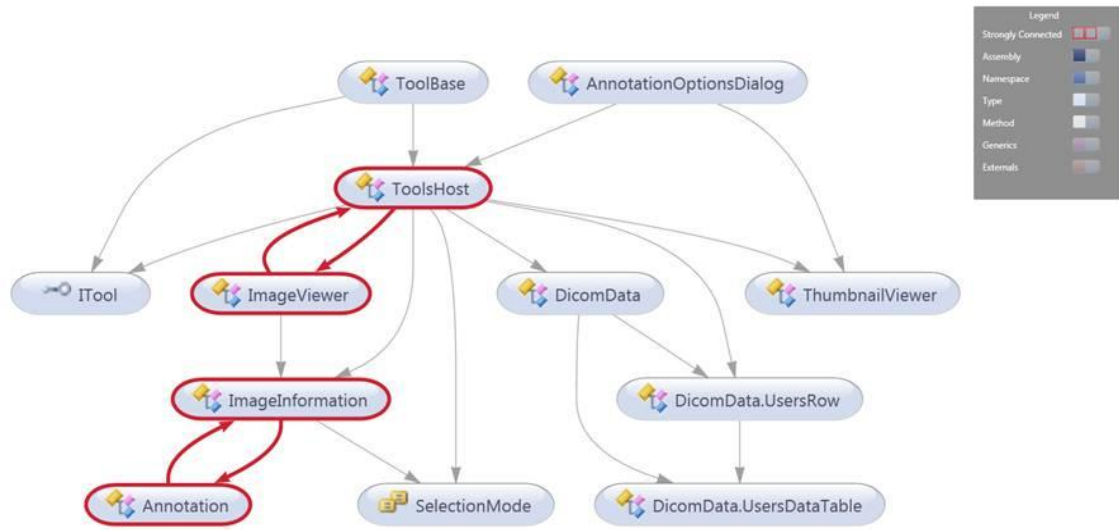
Figure 3.2: DoctorEye architecture version 3x

The final version (*DoctorEye ver 4.0* – Figure 3.3 & Figure 3.4) is completely reconstructed and contrary to previous versions, supports the processing of multiple medical datasets (each one containing multiple images).
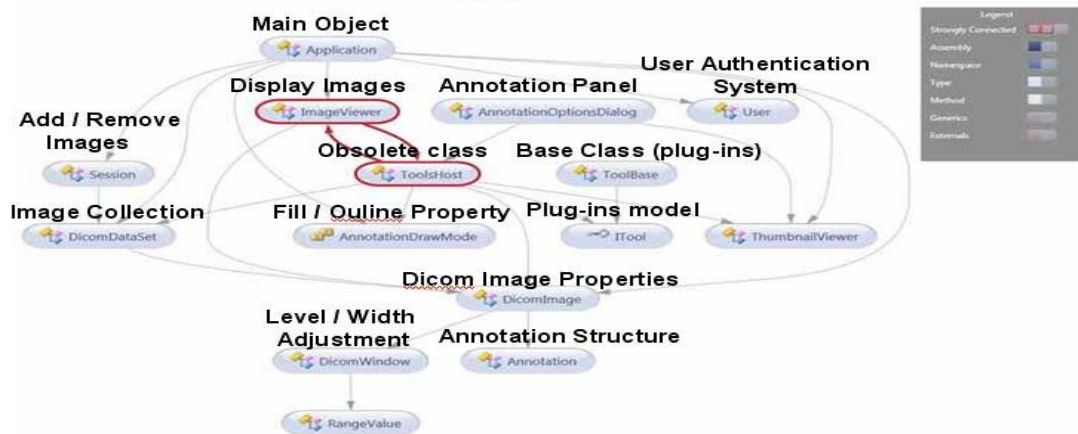
Figure 3.3: DoctorEye architecture version 4x

With this version, it is possible to perform processes, such as the comparison of the information coming from the same patient prior to and after treatment.

Figure 3.4: DoctorEye structure version 4x

3.1.4 Architecture ver 3x vs Architecture ver 4x

Table 3.1: Differences in architecture between *DoctorEye* ver 3 and 4

Changes	Version 3x	Version 4x
Root Class (the main class on which the Object Model is based)	Asteroid construction of the Object Model based on the object *DoctorEye.ToolHost* which controls all the other objects.	Tree architecture of the Object model based on the object *DoctorEye.Application.* Every object acts independently, without relying on the *ToolHost*. This new architecture allows the management of more than one image datasets simultaneously.
Relation between objects	The main classes as shown in Figure 3.2 (illustrated with red colour) are *circular references* where the *Parent object* calls methods from the *Child object* directly and vice versa).	In the new Object model there are no *circular references*. *Events* allow all objects to interact with each other (*Event-driven programming*).

User Interface	The platform can handle one dataset containing multiple images.	The platform can handle multiple datasets containing multiple images simultaneously.
Plug-ins	The platform supports plug-in insertion to work with one dataset.	The platform supports plug-in insertion to work with many datasets simultaneously.

The need to work with more than one dataset simultaneously both on the platform as well as with potential plug-ins (as shown in Table 3.1.4) led to the development of version 4.0 of the platform.

3.1.5 Platform Main menu Options

By clicking on the red cross in the top-left hand corner of the platform (Figure 3.5), the user can access the main menu (Microsoft Office 2007 – based) which contains the input-output functions.
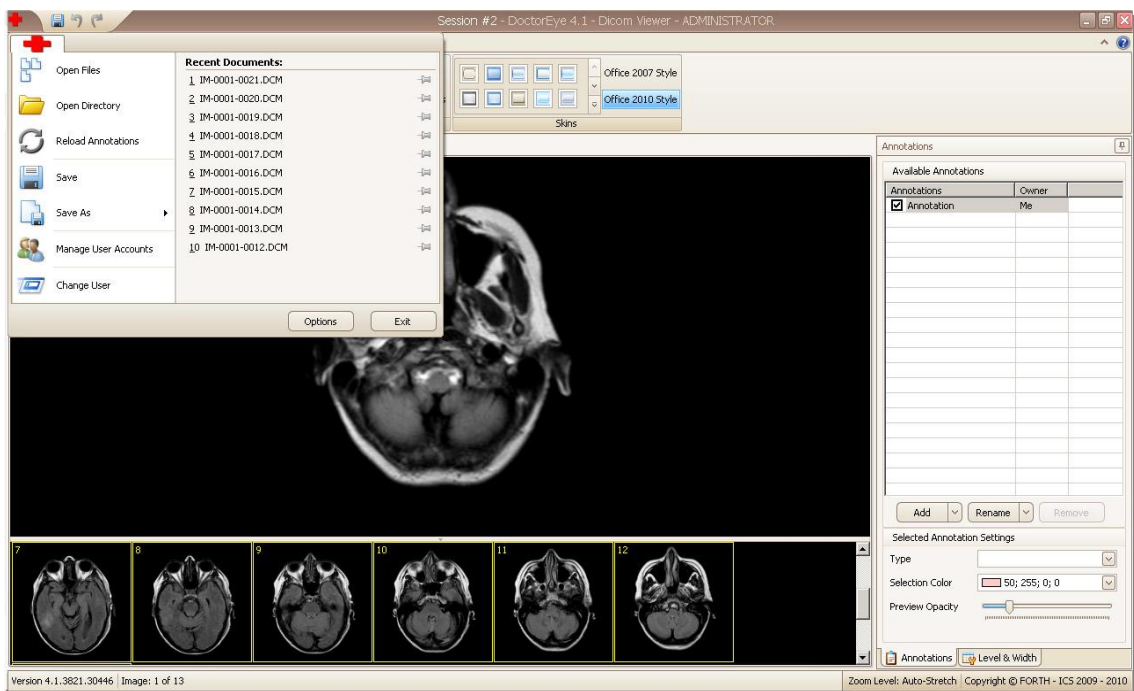
Figure 3.5: DoctorEye Main menu options

- ***Open files***

    From a list of dcm files the user can choose the files indented to be processed.

- **Open Directory**

  A directory is chosen by clicking on it. The dcm files stored there, as well as those in all the subdirectories, are imported into the platform and are presented in two windows. The main window depicts by default the first image of the dataset (or later any selected one), while the thumbnails of all the images of the dataset are depicted in the second resizable window, below the main one (Figure 3.5).

- **Reload Annotations** (technique used in image retrieval systems to organise and locate regions of interest in images)

  Having been working on an MRI dataset, the user judges that the results are not satisfactory and processing needs to be carried out from the beginning. On condition that this work has not been saved, the annotations already stored from previous work can be reloaded.

- **Save**

  In the same way as in *Microsoft Office* programs, the user must select the *save* option to save current work in the medical files.

- **Save As**

  Selections (annotations) can be alternatively saved in many types:
  - *Annotation* (store the selected areas of annotations in a *txt* file).
  - *Annotation Outline* (store the contour of annotations in a *txt* file).
  - *Xml file* (store the area of annotations in an *xml* file).
  - *3rd party application* which produces 3 files:
    - the *Size.dat* which includes the size of the MRI Images and the number of the slices in the specific MRI dataset (ex. 512,512,22 means that the dimension of the images are 512 rows x 512 columns x 22 slices).
    - The *TumourPoints.dat* which includes the position of the tumour points in all the slices.
    - The *Volume.dat* which includes all the points of the tumour in all slices, starting from the first point until the last one continuously (as a volume).

In addition, the *Manage User Accounts* window provides the *Administrator* with the following options:
  - To disable the access of a specific user.
  - To allow other users to become Administrators as well.
  - To reset the password of a user (create new one).

The *Change user* option gives the ability to log off (close current work without closing the program), allowing another user to log on.

3.1.6 Importing Medical Images

The user can select any number of medical images in DICOM format (dcm files) from a group of thumbnails to process. These thumbnails will appear in a resizable area at the bottom of the screen (Figure 3.5).

At this point, the user can adjust the *window level* and *window width* values by using a system of axes. These two parameters represent a more sophisticated approach to the brightness and contrast of an image.

The *window level* is the midpoint of the grey-scale while the *window width* is the number of grey-shades (Figure 3.6).
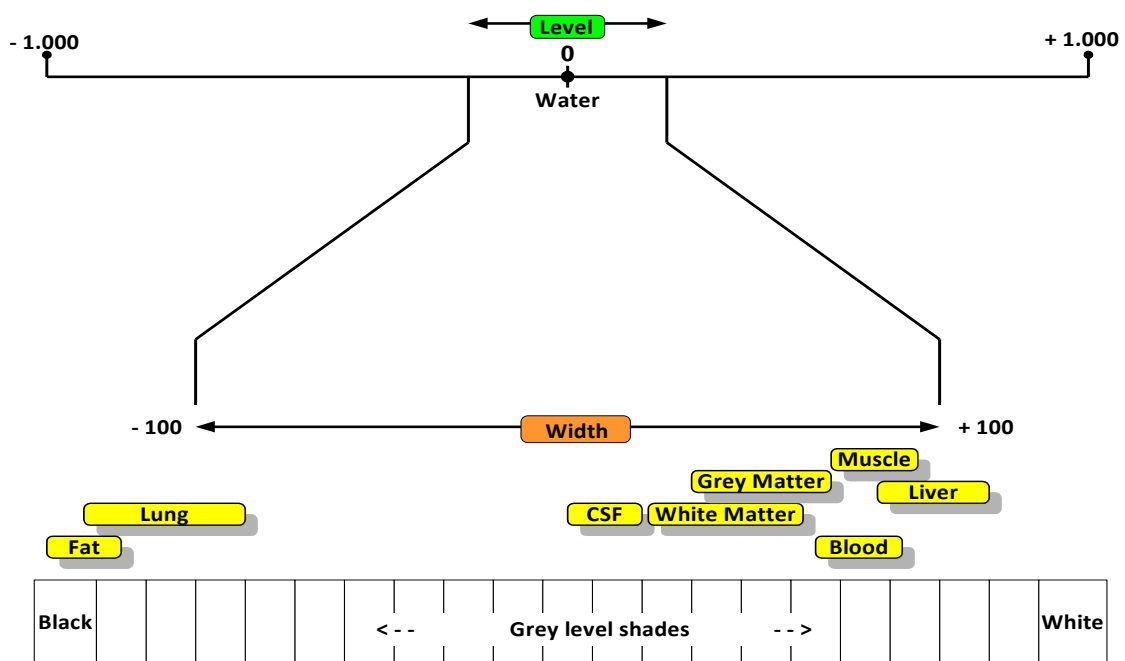
Figure 3.6: *Window level* and *Window width* adjustment

DICOM images are stored as 8-bit, 12-bit or 16-bit images containing a considerable amount of information. The main drawback of JPEG images relative to DICOM ones, is that JPEG images have only an 8-bit (256 shades) grey-level depth.

This means that a mapping system is needed to map the actual pixel values of the image (16 bits), within the range of 256 grey shades (8 bits) of the grey colour. With the adjustment of these values, the user can focus on and optimise visualisation of specific structures.

As an example, to evaluate an organ (e.g. the lung), the window level is set to the area that contains this organ and the window width is set relatively wide to allow detailed assessment of that area.

The user has also two options here: The first allows to *zoom in* or *out* and the second to shift the position of the selected image on the screen in order to have a better view of the regions of interest.

3.1.7 A Multi-functional Annotation system

The *Annotations* panel can be activated to delineate either areas or contours of potential tumours in the selected medical image. These areas can be annotated, categorised, deleted, added and redefined as depicted in figure 3.7.

Figure 3.7: A single slide is selected for further processing. A working area has been set (green rectangle) and the segmentation algorithm has been applied. The selected area is labelled in pink.

To start the processing, the user must first press the *Add* button in the *Annotations* panel to create a new label. This label can be added to a single slide or to a group of slides automatically by choosing those from a window using the thumbnailed medical images.

The segmentation process starts with the first image of the selected group of images and at this point the user has to choose a segmentation algorithm. A *working area* can be also defined, where the segmentation method is to be applied (Figure 3.7). At the end of this process the above mentioned label will correspond to the area which will be identified by the algorithm. The colour of the selected region (red being the default colour) can also be specified in order to define two or more areas in the same region of the image.

The label that was given at the beginning of the process is now available in the *Available Annotations* panel corresponding to this specified tumour. It can be selected and the specified tumour will be displayed. The platform also gives the ability to select and delineate multiple tumours (i.e. in the case of metastasis) with different labels and colours, either in the same or in any other slide as shown in figure 3.8.
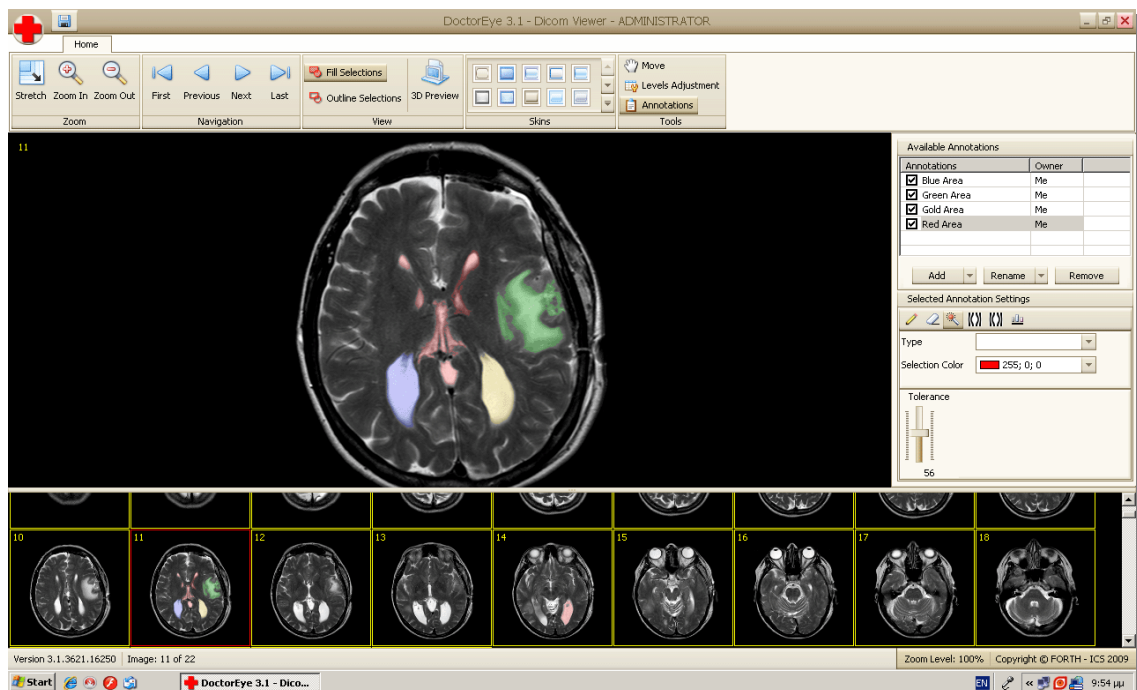
Figure 3.8: Different areas of interest may be annotated accordingly using respective labels in different colours. This can be done in the same slide in the case of metastasis. (Blue and Gold depict areas which are easy to segment while Red and Green depict more complex areas)

The user can also change the colour of the findings of his previous work as well as the opacity value, in order to have a better view of the areas of interest.

3.1.8 Integrated Segmentation Algorithms and Tools, Innovations

Two different, in terms of underlying theoretical concepts, segmentation algorithms are currently available in the platform: namely the *Region Growing* (or *Magic Wand)* and *Greedy Algorithm* (or *Spatially Adaptive Active Contours – Snake)*, while any other algorithm can be easily plugged-in as well.

The first is based on image intensity, whereas the *Greedy* algorithm (or *Spatially Adaptive Active Contours*) is a model-based segmentation method.

3.1.8.1 The *Region Growing* semi-automatic segmentation algorithm

The function of the *Region Growing* algorithm is based on finding and selecting all the pixels around a pre-specified user-selected initial point that are similar in grey intensity. A *tolerance* value must also be set by the user to determine how closely to match colours [Fujita H. & Fejri M., 2006]. Higher *tolerance* ends up in a larger selection as depicted in figure 3.9

(a) *Start Point* selection   (b) *Tolerance* = 0   (c) *Tolerance* = 0,25

d) *Tolerance* = 0,50   (e) *Tolerance* = 0,75   (f) *Tolerance* = 1
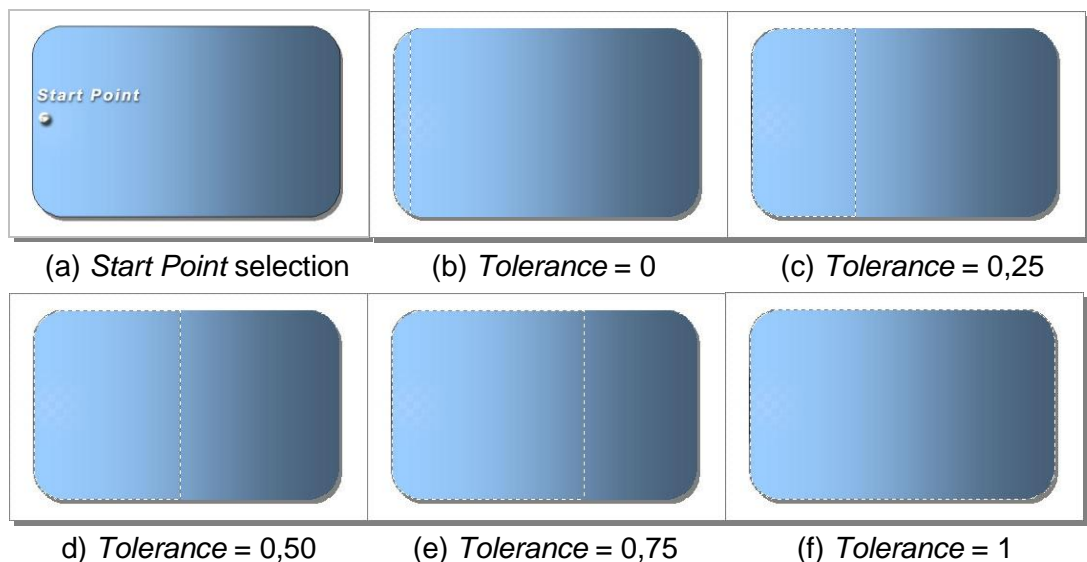
Figure 3.9: The *Region Growing* algorithm parameters (*Start Point*, *Tolerance, and Contiguous*)

There are three key points concerning the functionality of the *Region Growing* algorithm (Figure 3.9):

1. the *start point* where the user must select the point (colour value) of the image to start with.

2. the *tolerance* value which is used to define which pixels of the image have colour values similar to the *start point* colour value ± the *tolerance* value.

3. the *contiguous* property which allows spatially contiguous pixels under examination to be connected and grouped with the already selected pixels.

To enhance its effectiveness, we have implemented the algorithm in such way that just after the *Start Point* selection, a slider allows the user to adjust the *tolerance* value interactively and visually select the desired area in the image (Figure 3.10).

Figure 3.10: The *Region Growing* algorithm functionality – Interactive adjustment of the *tolerance* value

This means that the segmentation process is more user-friendly since it allows the definition of areas experimentally as there is no need to redefine the *Start Point* while adjusting the *Tolerance* value with the slider.

Moreover, the *Contiguous* property is integrated in the algorithm, so as to

always be active automatically.

At this point, segmentation errors are common, especially at the bounds of the tumour where the grey-level value profile may be similar to that of the tumour itself. This defect can be reduced by re-defining the *Start Point* for the algorithm and re-adjusting the slider for the *Tolerance* value to get a more precise delineation of the desired area.

All the points selected by the algorithm are automatically stored in an *Image Mask (array)* of the same size as the original image (Figure 3.11). Each pixel in the *Image Mask* represents the position of the selected pixels in the original image and is used to label the delineated areas.
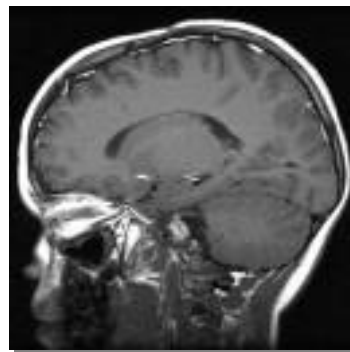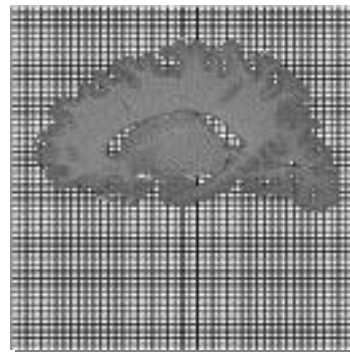
(a) Head MRI Image   (b) The corresponding *Image Mask*

Figure 3.11: The *Region Growing* algorithm functionality – Head MRI Image and the corresponding *Image Mask* (array)

In the example above (Figure 3.11), to get the selection illustrated at the corresponding *Image Mask,* a lighter area (*Start Point* definition) of the *cortex* is clicked on, to avoid selecting the relatively darker area of the c*erebellum* located at the right bottom area of the brain. The *Tolerance* value is set to 0,35 to include all the grey-level values appearing in the *cortex* of the head.

In order to facilitate the image processing task in the cases where the user must work with more complex images (e.g. tumours located in several distinct places), an integrated option allows the user to hold down the *shift* key to add a new area or the *ctrl* key to remove an area from the already selected ones.

All in all, the algorithm integrated into the platform is a fast version, which speeds up the segmentation process as it also ensures that pixels already examined will not be checked again.

3.1.8.2 The *Greedy Active Contours* algorithm

An alternative method to perform segmentation in two-dimensional possibly noisy images is based on iterative evolution methods such as *The Discrete Active Contours* algorithm, also called *Snakes.*

A number of methods are available to evolve *Active Contours.* The most commonly used ones are the *Variational approach* [Kass et al, 1987] and the *Greedy* algorithm [Williams and Shah, 1992], [Mille et al, 2006].

The platform implements the *Greedy* algorithm, which minimises the following discrete energy functional:

$$E(\ p'i\ ) = Econt(\ p'i\ ) + Ecurv(\ p'i\ ) + Egrad(\ p'i\ ) + Ebal(\ p'i\ ) \qquad \text{Eq. 3.1.8.2}$$

In contrast with the initial location *pi*, we denote *p'i* the search location, whose energy is a weighted sum of various internal and external energies [Williams and Shah, 1992]. Global minimisation is carried out by means of successive local optimisation. The external energy is supposed to be minimal when the snake is at the object boundary position. The user only needs to add points in order to define an initial approximation.
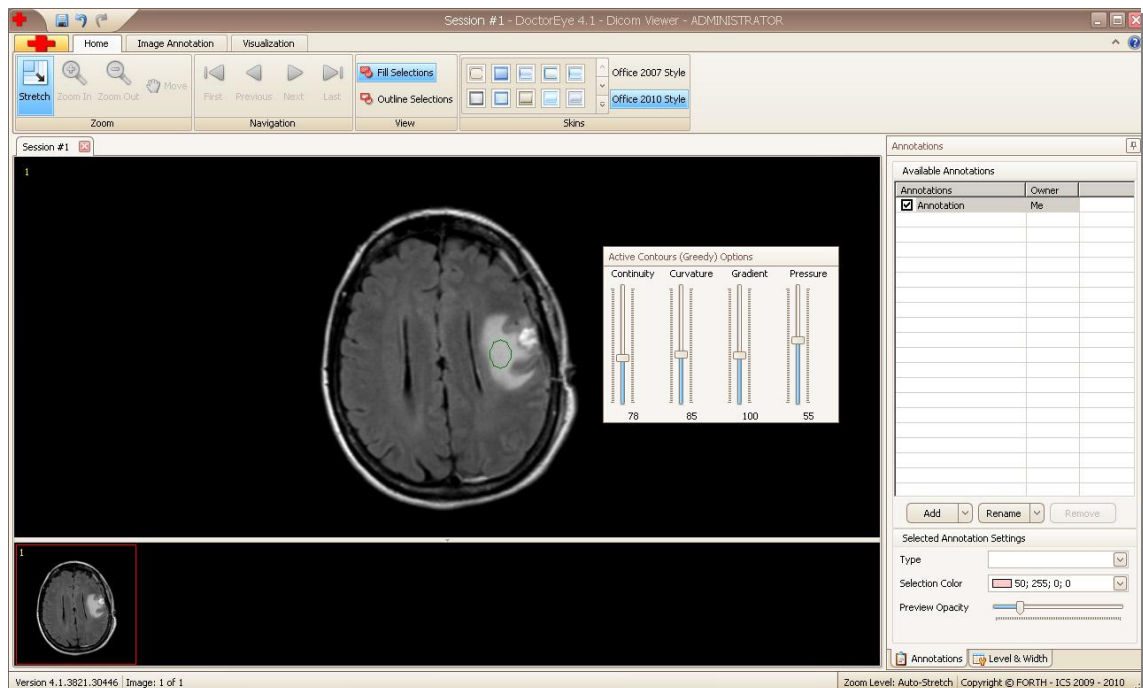
Figure 3.12: The *Greedy* algorithm functionality (Active Contours - Snake) – Interactive delineation of a tumour outline from a possibly noisy 2D image

The following parameters must be defined in order to achieve optimal segmentation results: *Continuity*, *Curvature*, *Gradient* and *Pressure* (or *Balloon*) (Figure 3.12).

Continuity

This internal constraint specifies how a snaxel (snake point) should locate itself, so that the distance between a snaxel (snake point) and its neighbours should be close to the average distance between snaxels.

Curvature

Another internal constraint that specifies the location of a snaxel so as to minimise the amount of curvature it introduces. In other words, it maximises the angle it defines between its neighbours.

Gradient

This is an external constraint. According to it, a snaxel should locate itself in areas where the gradient in the image is large. The Sobel gradient has been implemented in this example.

Pressure (or Balloon)

With this constraint, the snake behaves like a balloon, blowing up. As it expands, it stops if the contour of the edges is strong, or passes through if the contour is too weak. In any case, the initial snake needs not be too close to the final contour to converge. This approach modifies the definition external forces presented in traditional *Snake* [Kass et al, 1987] making the curve behave like a balloon.

Several other internal and external constraints may be defined for snakes, but only these four have been implemented in this version of the algorithm.

Finally, segmentation errors can also occur when using the *Active Contours* algorithm, mostly because it is not easy to adjust the algorithm parameters in an automated way.

3.1.8.3 Refinement Tools and Techniques

If the images are extremely complex, the segmentation results may require further refinement by the expert clinician, especially if the result is critical for

other applications (e.g. cancer growth simulation).

The integrated tools and techniques can assist the user to achieve refined delineations of the important areas. These tools are advanced versions of the *Pencil* and the *Eraser*.

Contour refinement is possible by using the *Eraser* and *Pencil* tools where any mistakenly selected or ignored pixel can be removed or added, respectively, in order to end up with the best possible delineation of the identified tumour.

The *Histogram* tool allows the user to interactively define the histogram in known tissue types and use this information for manually refining the tumour delineation result. This tool gives access to the values of the selected tumour.

By defining the upper and the lower limit of these values, the user can reject some values located in the areas around those limits, thus achieving a more precise selection of the tumour.

DoctorEye version 4.3 has integrated a multi-functional environment for histograms of any selected area providing 15 different views with optional markers and labels for each point. The user gets the information needed for further processing interactively.

The different views available are *Area, Area 3D, Bar, Bubble, Line, Line 3D, Point, Scatter Line, Spline, Spline 3D, Spline Area 3D, Stepline, Stepline 3D and Swift Plot.* Some examples are shown below:
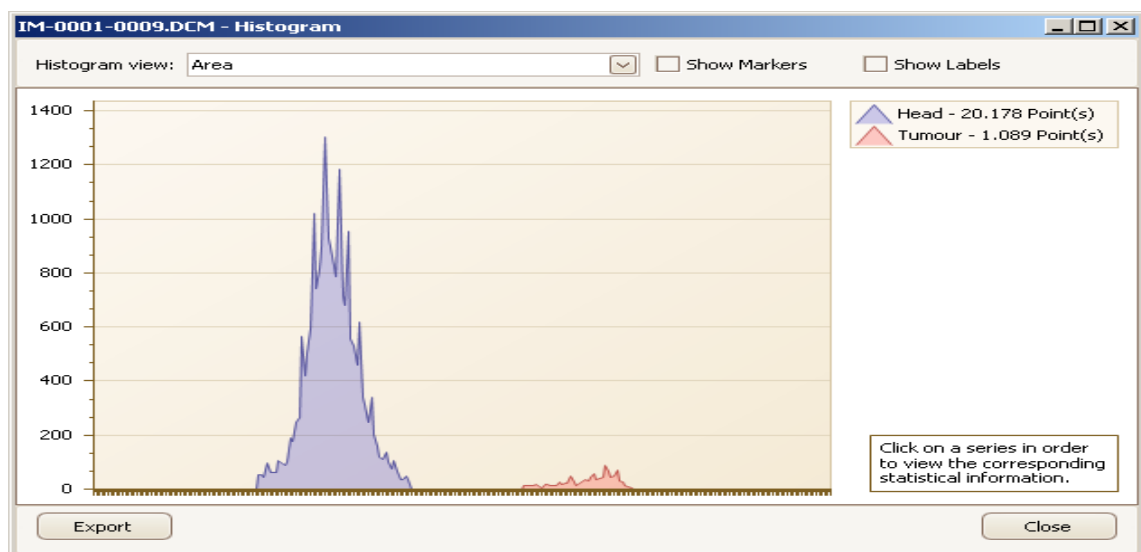
Figure 3.13: Histogram – Area view
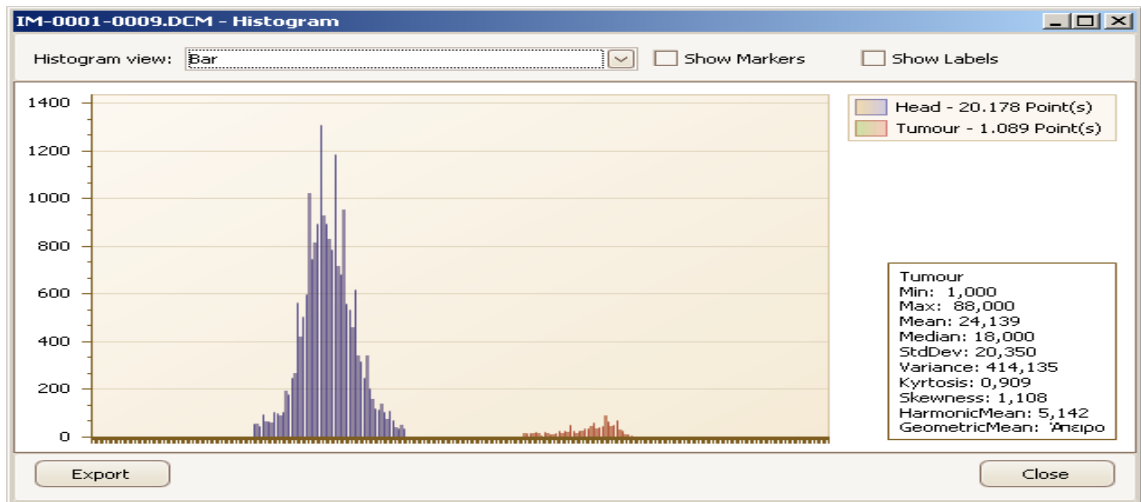
Figure 3.14: Histogram – Bar view
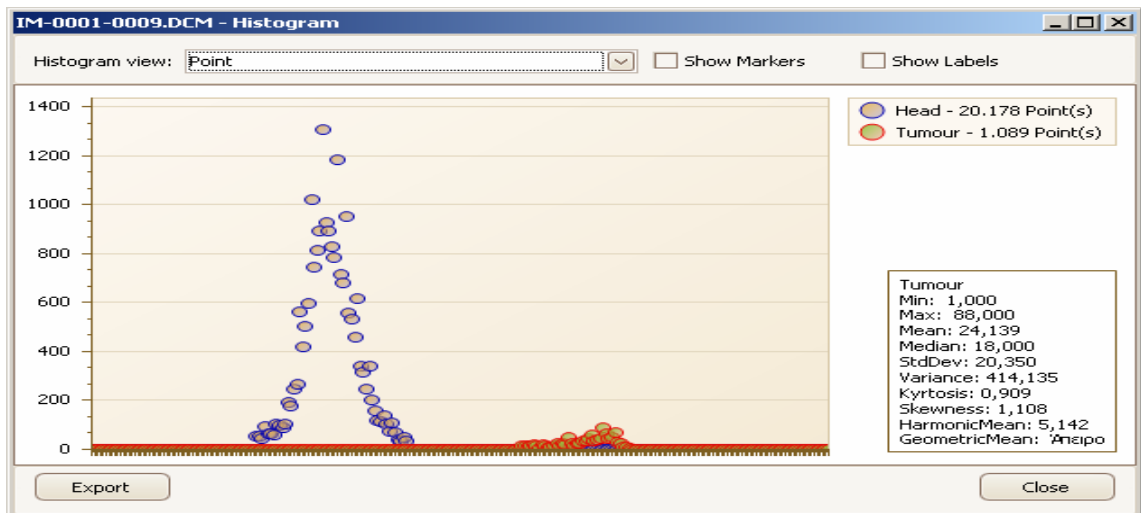
Figure 3.15: Histogram – Point view
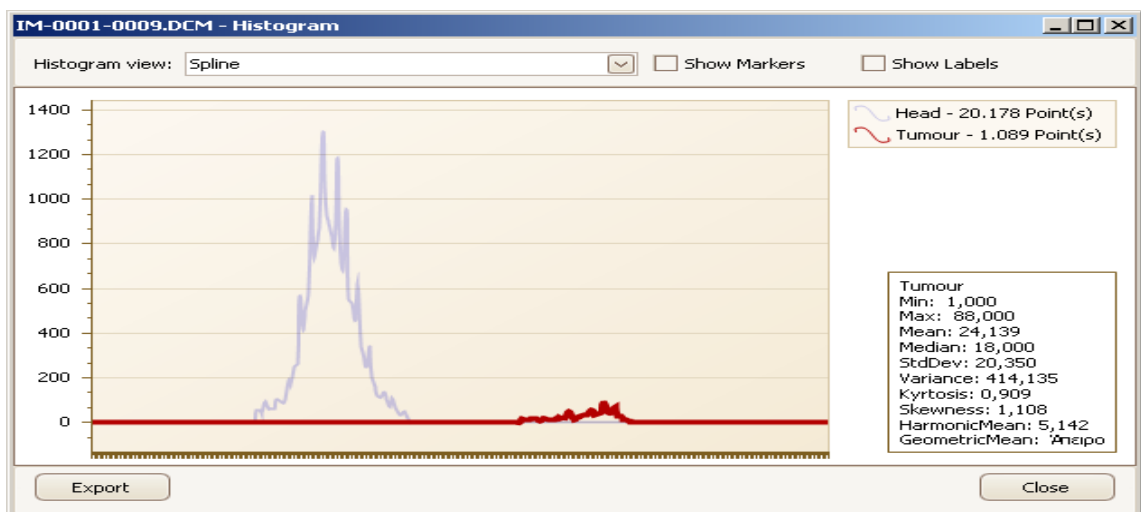
Figure 3.16: Histogram – Spline view

As shown in the above figures, the user, apart from the visual information of the delineated areas, has also the option to use metrics concerning these areas as well as the option to export this information and save it in an external file for further processing.

3.1.9 Export Data

The option *Save* in the main menu saves the selected areas in the corresponding medical images (DICOM Files) the user has been working on.

The stored information is displayed automatically and can be accessed when pressing *Open* a new image or a sequence of images.

The option *Save as* in the main menu provides the following options to save selections (annotations):

- *Annotation* (store the selected areas of the annotations in a txt file)
- *Annotation's Outline* (store the contour of the annotations in a .txt file)
- *Xml file* (store the area of the annotations in a .xml file)
- The *3rd party application* option produces 3 files:
    - The *Size.dat* which includes the size (number of rows x number of columns) of the MRI Images and the total number of the slices contained in the specific MRI dataset (ex. 512,512,22 means that the dimension of the images are 512 rows x 512 columns x 22 slices).
    - The *TumourPoints.dat* which contains data in the form of x,y,z,concentration. Here x and y are the coordinates for a specific point in the tumour in a slice while z indicates the number of the slice where this point is located. In order to get initial results in the experiments with tumour diffusion models, the concentration value is currently set to 200. Future research is expected to define an accurate concentration value to provide more realistic results.
    - The Volume.dat which includes all the points of the tumour, starting from the first point in the first slice and finishing in the last point in the last slice in a sequence (as a volume), showing the grey-level value of every point (takes values from 0 to 255).

Moreover, the user can save his work on the images in the same or separate

files, in several common image formats.

3.1.10 **The 3D Representation Procedure** (Initial Implementation by Angelos Armen)

The annotations saved into the images include information such as who made the annotations, the timestamp, the name of every annotation, the type as well as the points and colour of every tumour.

All the above mentioned information was added not only to support a better 3D visualisation of the tumour (depicts more than one tumour), but also to support potential future functions such as comparing the results given by two or more segmentation methods, etc.

For the 3D visualisation of the segmented areas, the Visualisation Toolkit (VTK) is used which is an open-access class library for 3D graphics and visualisation.

The 3D visualisation process is presented by an interactive and resizable window that provides the user with a choice of environment parameters for the best representation of the findings (Figure. 3.17).
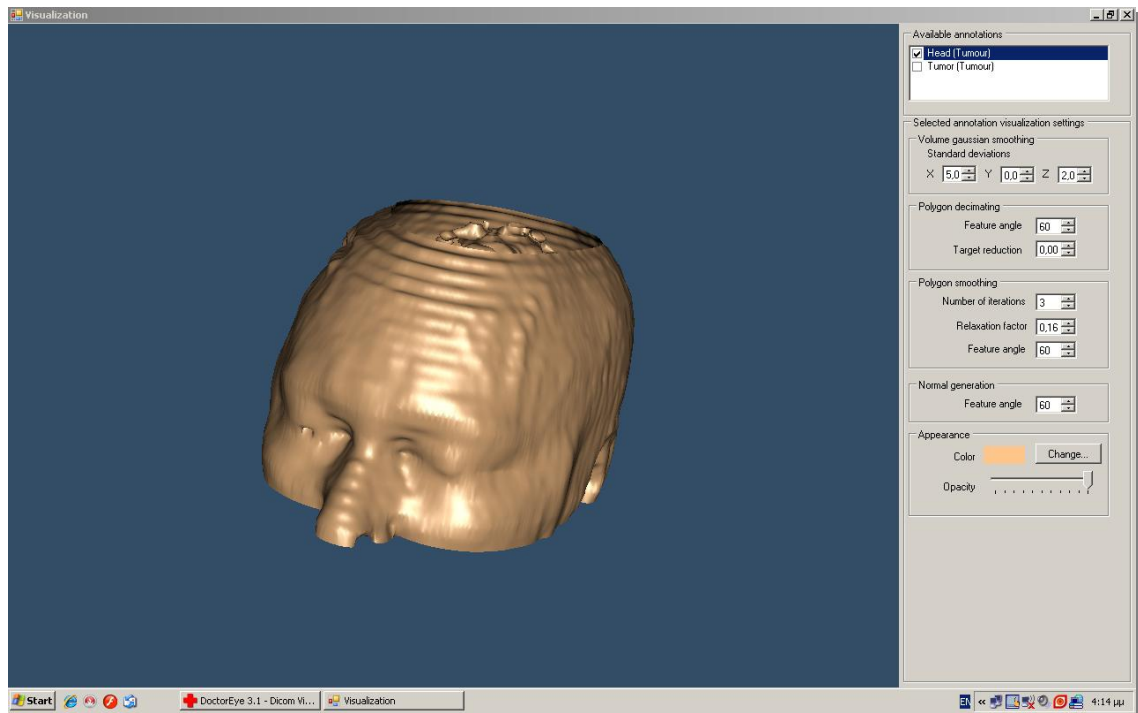
Figure 3.17: 3D representation of a head (derived from 22 slices)

The user can change parameters concerning the viewing angle of the findings, the colour of the annotated areas, the transparency level of each of them, etc (Figure 3.18).
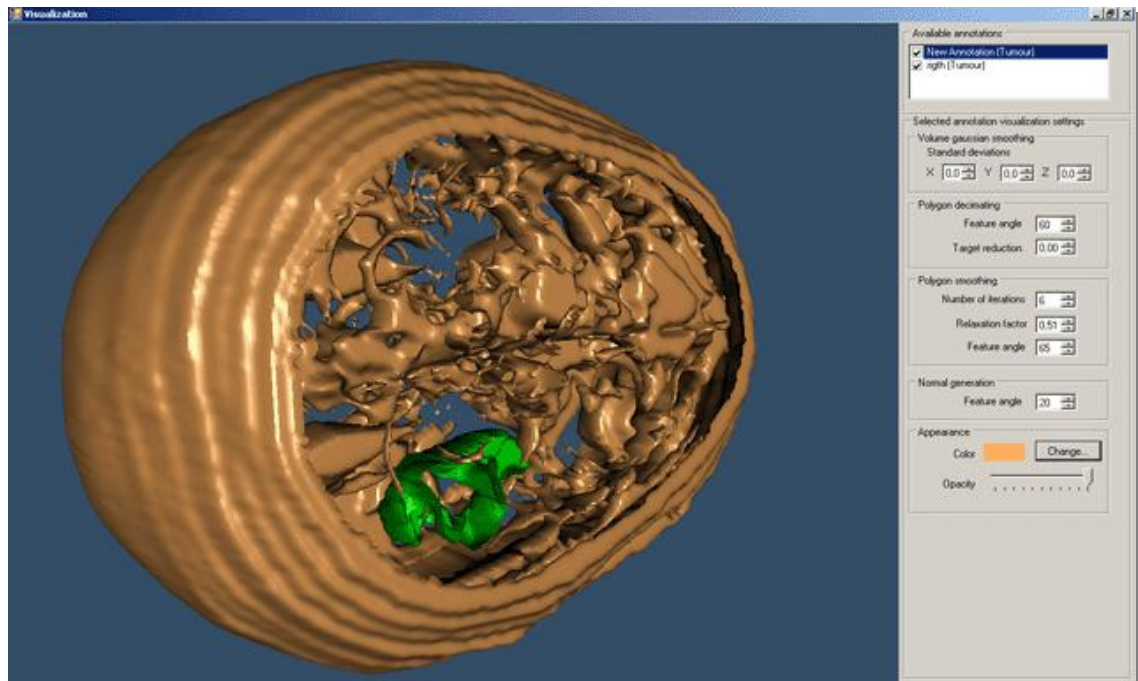
Figure 3.18: 3D representation of a head – different angle (derived from 22 slices)

The above illustrated example is the result of the segmentation of 22 brain images using the *BRAINIX - 401 MRI dataset* [DICOM sample image sets].

3.1.11 Processing Time (case study: MRI dataset with 22 slices)

Testing on 22 slices of a Brain MRI dataset, revealed that the average time that is required to reach the final 3D representation of the head and the pinpointed tumour (Figure 3.18) using the *Region Growing* algorithm on the *BRAINIX – 401 MRI* dataset [DICOM sample image sets] is:

- For the introduction of the 22 images in the platform: 6 seconds.
- For the implementation of the algorithm to the head and the tumour: 4 minutes and 20 seconds.
- For the application of the 3D representation algorithm: 2 seconds.

For the above mentioned procedure, a laptop was used with OS "Windows XP Professional SP2" having an Intel® Core™2 Duo processor at 1,73GHz and 1,73GHz, and 3 GB RAM memory.

3.1.12   A Multi-User Authorisation and Management System

Additionally, a *Multi-User authorisation and management system* has been implemented where the *Administrator* can manage not only his work but also the work (ex. Annotations) of all the other users (Figure 3.19).

However, the difference between a *simple user* and the *Administrator* is that the former can only see the work of the other users, while the *Administrator* can have real access to the data of all the users.

That is, he has the authorisation to manage (add, rename or delete) other users' annotations.
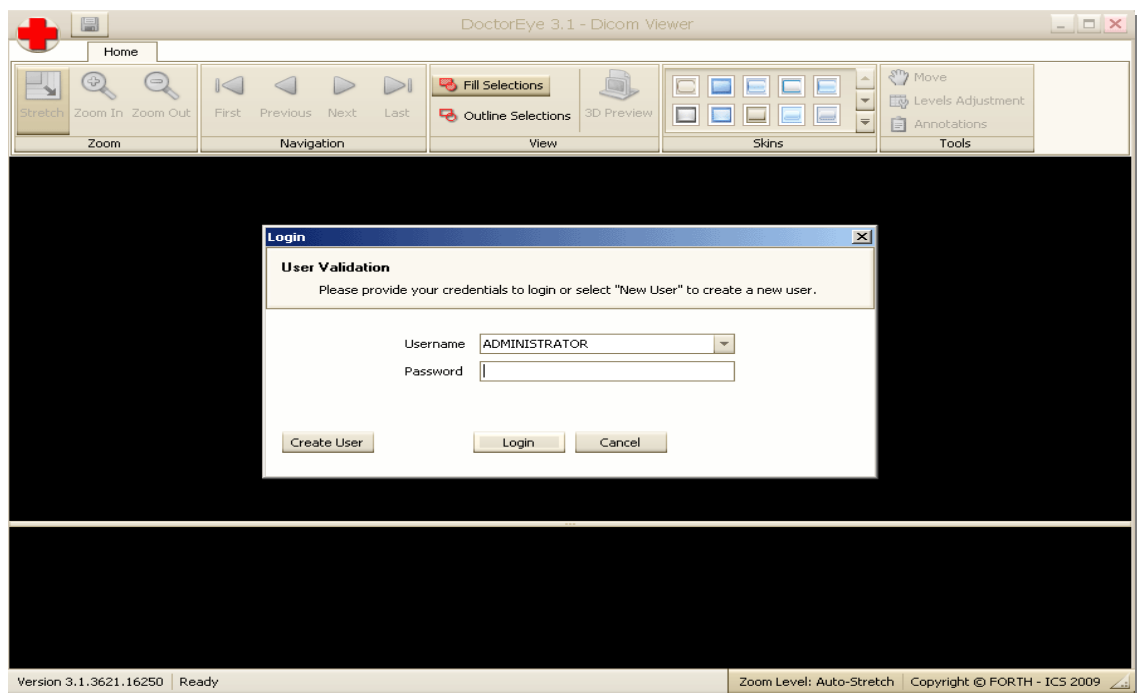
Figure 3.19: A multifunctional management system is implemented

This way, a number of different users can delineate the same tumour.

The *Administrator* (Expert Clinician) can choose the best delineated tumour in every single slice presented by different users, and has the option to rename it (ex. *Left Kidney Tumour final*) in order to integrate it into the final result so as to achieve the best 3D representation of the tumour.

3.1.13 Plug-ins Technology

The development of a clinically driven powerful plug-in structure based on the *.NET Reflection* mechanism allows the deployment of plug-in modules from third party developers (Section 4.1.3).

This is achieved with the *reflection* technique of the *.NET framework*. Each plug-in is an *assembly*, a dynamic-link library (dll) containing all necessary information internally as metadata. This feature defines the structure of plug-ins and allows other scientists to use the platform to implement and test their algorithms.

Through the *reflection* technique the developer can access information in the assemblies concerning the contained types, their members, their accessibility and attributes.

The main interface of the platform can be used as a primary step, in the creation of a new plug-in. In this way, the developer takes advantage of the capabilities of the platform while the platform gains a new additional feature.

The plug-in structure (*SDK* files) is developed in two languages: VB.net and C#.

A sample about how to use the plug-in technology of the system to make a new session with 10 new DICOM Images is presented in vb.net and in C# with detailed comments at *Appendix A* and *Appendix B* respectively.

After using the above sample, the user has to copy the resulting dll file to the *Tools* directory, and then has to start the platform. At the top of the platform the *Samples* tab will appear with two options available: The first one creates a new session with 10 new DICOM Images, while the second one inverts the selection of the selected image (e.g. the user selects the black area surrounding the head with the use of the region growing algorithm and then presses the invert selection tool to select the head).

Another more sophisticated sample (the *Compare Sessions*) where the user compares the corresponding images from two MRI datasets is presented in vb.net at *Appendix C*.

The source code with detailed comments, allows the user to change the code in a very simple way and by using logical operators achieve any result.

3.1.14 Experimental Process

To start the platform, a user account is required (Figure 3.20).
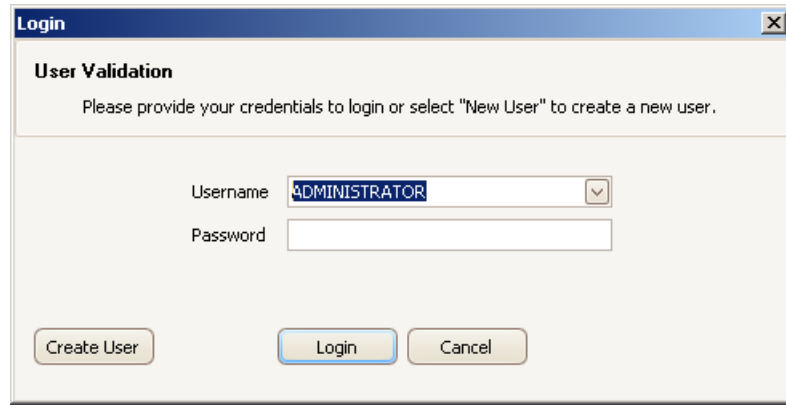
Figure 3.20: User validation/creation login window

By clicking on the *Menu* button (red cross) in the top-left-hand corner of the main window, the user may open a folder to get all the contained images, select images from a specific folder or access recent DICOM images.

A window depicts a number of thumbnails allowing the visual selection of the images to be processed (Figure 3.21).

Figure 3.21: DoctorEye layout – Selecting images

Once the selection has been completed, the selected thumbnails appear in a

session at the bottom of the screen in a resizable area with the first image appearing automatically enlarged in the main window, above them.

The *Level/Width* options allow adjustment of the contrast and the brightness of the image to be processed, so as to provide a better view of the areas of interest in the image (Figure 3.22).

Figure 3.22: DoctorEye layout – Home tab options and Level / Width adjustment

As depicted in figure 3.22, the main procedures are clearly defined with the *Home*, *Image Annotation* and *Visualisation* tabs.

- The *Home* tab contains four panels for the manipulation of the images, their delineations and the appearance of the layout of the platform.

- The *zoom* panel is equipped with *Stretch*, *Zoom in*, *Zoom out* and *Move* settings that enable the adjustment of the position and the appearance of the picture in the main window.

- The *navigation* panel allows easy access to every image in the dataset.

- The view panel gives the option for choosing either contour or area, defining in this way how the regions of interest will appear in the image

annotation process.

- The skins panel provides a number of colour themes in order for the user to change the layout of the platform (colours and appearance of the controls).

By selecting the *Image Annotation* tab, a number of options are available for the segmentation process (Figure 3.23).
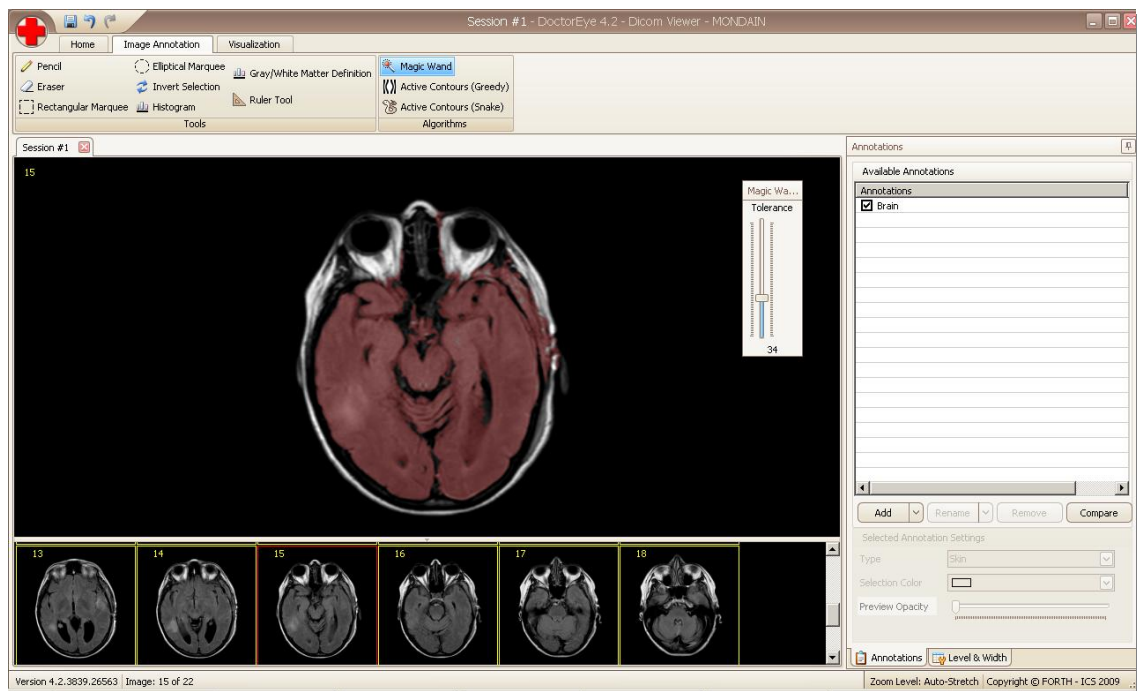
Figure 3.23: DoctorEye layout – Image Annotation tab options and the Region Growing algorithm

First of all, a segmentation algorithm must be selected in order to delineate regions of interest.

These algorithms include the *Region Growing*, the *Greedy Active Contours and* the *Snake Active Contours.*

With the *Region Growing* algorithm, delineation important areas can be achieved in a very simple way (Figure 3.23). Only one *start point* (colour value) in the image needs to be selected and the *tolerance* value (similar pixels to start point colour value) must be adjusted interactively.

With the *Greedy Active Contours* algorithm to delineate an area of interest, a

click and drag to form an ellipse inside the tumour's area is needed (Figure 3.24).
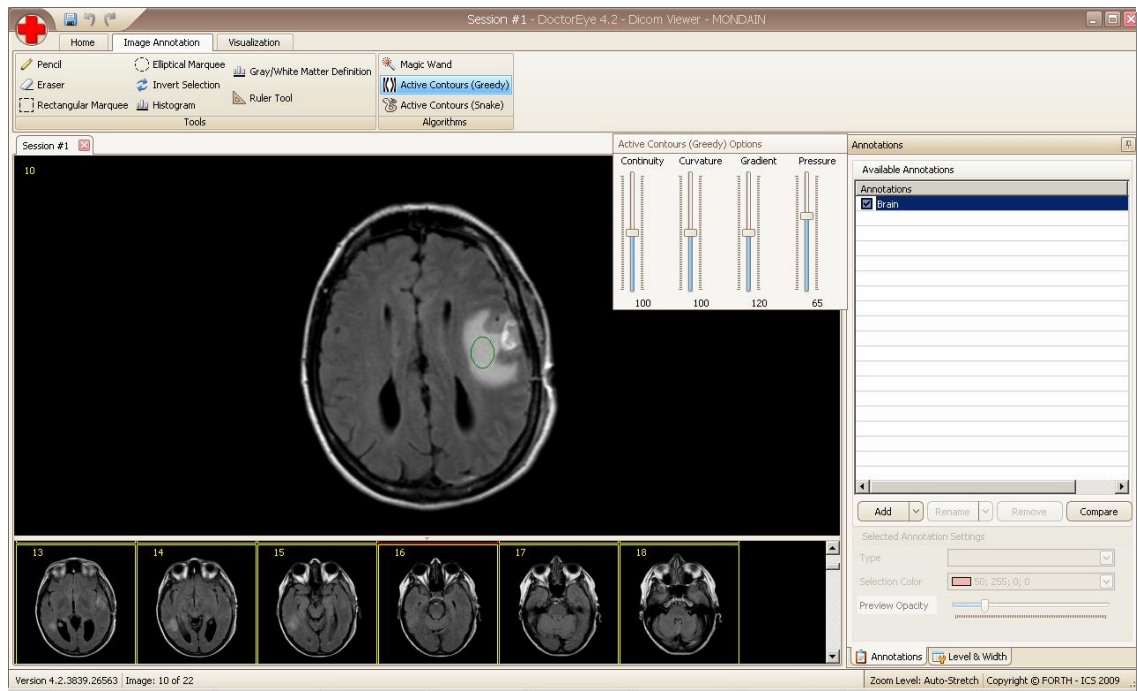
Figure 3.24: DoctorEye Segmentation Algorithms – The Greedy Algorithm

After defining the four parameters (*Continuity*, *Curvature*, *Gradient* and *Pressure* or *Balloon* (Figure 3.24) as described in section 3.1.8.2, the contour (or *snake*) moves one iteration outwards closer to the contour of the desired area with each press of the spacebar button until a steady state is reached and the snake no longer expands.

The last algorithm *Active Contours – Snake* [Farmaki et al., 2010] is an alternative form of snake (Section 4.1.3.2).

The *Tools* panel contains several options for the refinement of the delineated areas such as advanced versions of the pencil and the eraser, which keep the neighbour pixels connected.

At this point, a label and a specific colour must be assigned to the corresponding delineated area.

The integrated multi-functional annotation system allows the definition of more than one area with multiple colours and opacities.

At the end of the process, the *Visualisation* tab provides a multifunctional environment with 3D representations of the delineated areas.

3.1.15 Summary

In brief, the DoctorEye platform is a powerful clinical tool facilitating imaging biomarker extraction. Key features include:

- A user friendly environment (Microsoft Office 2007-based).
- Customizable Interface (similar to windows skins technology).
- Compatibility with any Windows-based computer with the .NET framework ver. 2.0 or later.
- Compatibility with any medical image modality which provides dcm images (CT, MRI, etc).
- Simultaneous processing of multiple datasets (in sessions) similar to the tabbed windows functionality.
- A multiple user management system supporting user accounts.
- Image Settings and View options (advanced zoom options – in stretch mode and image adjustments (width and level parameters).
- Intuitive segmentation tools (advanced versions of the Pencil and Eraser & Invert Selection).
- Advanced version of semi-automatic segmentation algorithms and techniques (Region Growing algorithm, Greedy algorithm, Histogram tool).
- Full automatic Extraction of *Grey/White Matter* areas.
- Advanced multifunctional annotation system which supports unlimited annotations per image. The user can view/hide annotations, rename, delete and define the colour and the opacity of the annotations.
- An advanced and easy to use plug-in mechanism based on the *.Net Reflection* functionality, allowing third party developers to develop their algorithms and introduce them into the platform to extract results.

3.2   The *Automatic Tumour Detector (ATD)* Project

3.2.1 Introduction

Much like the *DoctorEye*, *ATD* has been developed to support clinicians in the recognition of organs and their possible abnormalities. However, *ATD* is a more sophisticated platform and was designed to integrate more advanced

techniques and algorithms in order to enhance processes such as image handling, segmentation, visualisation and storage.

The main advantage here is the implementation of a fully automatic recognition process of regions of interest which does not require any previous complicated knowledge of medical image processing.

Compared to *DoctorEye*, *ATD* is based on a completely different philosophy concerning interface, functionality and the data management system offering fully automatic recognition of organs and their dysfunctions even in the case of more complicated images such as abdominal images.

3.2.2 Platform design

The platform development was based on the .NET framework architecture [Benefits of the Microsoft .NET Framework, 2013], so that it could be deployed in any Windows-based computer with the .NET Framework version 4.0 or later versions.

Moreover, given that the system uses the *Mono project functionality* and libraries [The Mono project, 2013], the user can run the application in many other Linux based environments through the No-Touch Deployment [Benefits of the Microsoft .NET Framework, 2013].

The user-interface design is clinically-led and its features follow the Windows 8 layout (i.e. the Metro Design, already applied to windows-based smart phones) (Figure 3.25).

Figure 3.25: Platform Design. The clinician has finished the segmentation task on slide no. 12. The Segments panel on the right side contains the delineated regions of interest (Left Kidney, Right Kidney and Right Kidney Tumour)

3.2.3 Importing Medical Images

The user can introduce any number of DICOM images into the platform. These images will appear as thumbnails at the bottom of the screen, below the enlarged selected image (Figure 3.25).

A system of axes allows the adjustment of the *Window level* and *Window width* values providing a better view of the areas of interest in the image. *Window Width* is the difference between the brightest and dullest pixel value and *Window Level* is the mid value between the brightest and dullest pixel value.

The *zoom-in / zoom-out* options and the *hand* tool allow the user to adjust the size and the position of the selected image on the screen so as to be able to focus on specific sections of the image for more detailed examination.

3.2.4 Manual Segmentation Panel

This panel integrates an advanced implementation of the *Region-Growing* segmentation algorithm (top-left corner of Figure 3.25). This semi-automatic segmentation method is to assist clinicians in rapidly defining the regions of

interest in the image interactively, in order to define the *Standard Golden Models.* These models are necessary for the evaluation of the results and the efficiency of the integrated full-automatic Region – Oriented Segmentation framework.

In order for clinicians to define the *Standard Golden Models* accurately, boundary refinement can be achieved by using sophisticated versions of the *Pencil* and *Eraser* tools allowing the expansion or shrinkage of the selected areas by automatically keeping similar neighbouring points connected so as to add or remove any mistakenly selected or ignored pixels.

At the end of this process, the *Segments* panel on the right side of the platform contains the user-defined labels corresponding to the selected areas.

This acts essentially as a clinical examination dashboard.

3.2.5 A Multi-functional Annotation system

The integrated multi-functional annotation system facilitates the delineation of areas of interest in the selected image. These areas can be labelled, coloured, renamed or deleted as depicted in figure 3.25.

When the user clicks on the *Add* button in the *Segments* panel, the *Annotation Selection* window appears. This allows the user to select thumbnail images in order to add annotations either by choosing from a list of already existing labels, or by typing in a new label.

The process can be applied to a single image or to a number of images simultaneously. The user can visually select any of the images to delineate and colour an area of interest by using either the manual or the automatic segmentation methods from the *Framework* panel.

Any such designated labels that may have been assigned as annotations for a single or group of images can be modified through the *Re-name* button.

The user can also select and delete any annotations by pressing the *Remove* button.

3.2.6 Automatic Segmentation Panel

The framework is based mainly on a region-oriented segmentation method [Bassmann H., Besslich P., 1995], for automatic identification of organs and their possible structural abnormalities/pathologies such as cysts, stones and tumours.

A panel enables the medical technician to interactively adjust the parameters used in this method and check the corresponding results in real time.

The medical technician can perform preliminary checks to help select the imaging parameters experimentally in a single slide. Once the result is acceptable, the parameters and the rules can be applied automatically to the entire image dataset and can be saved in a *Template* with a name that corresponds to the (sub) area identified (e.g. kidney, right or left).

For highly complex images, the medical technician also has the option of using a *Region of Interest (ROI)* focusing technique by defining a *working area* where the framework will be applied.

3.2.7 Validation Panel

To check accuracy and precision, the result from the *Automatic Segmentation process* (Section 3.2.6) can be compared to the semi-automatic result of the clinician's output (Section 3.2.4).

This can be achieved by means of comparison of the resulting 3D Volume models (clinician's *Golden Standard* volume model versus the medical technician's volume model) by using the metrics from the *3D Rendering* process (Section 3.2.8).

Alternatively, the *Validation* panel allows a more precise evaluation by comparing the results for every single slide between the two models (Figure 3.26).

Using this platform, both medical technician and a clinician can work on the same slide and annotate areas of interest. These areas can subsequently appear automatically in every single slide.
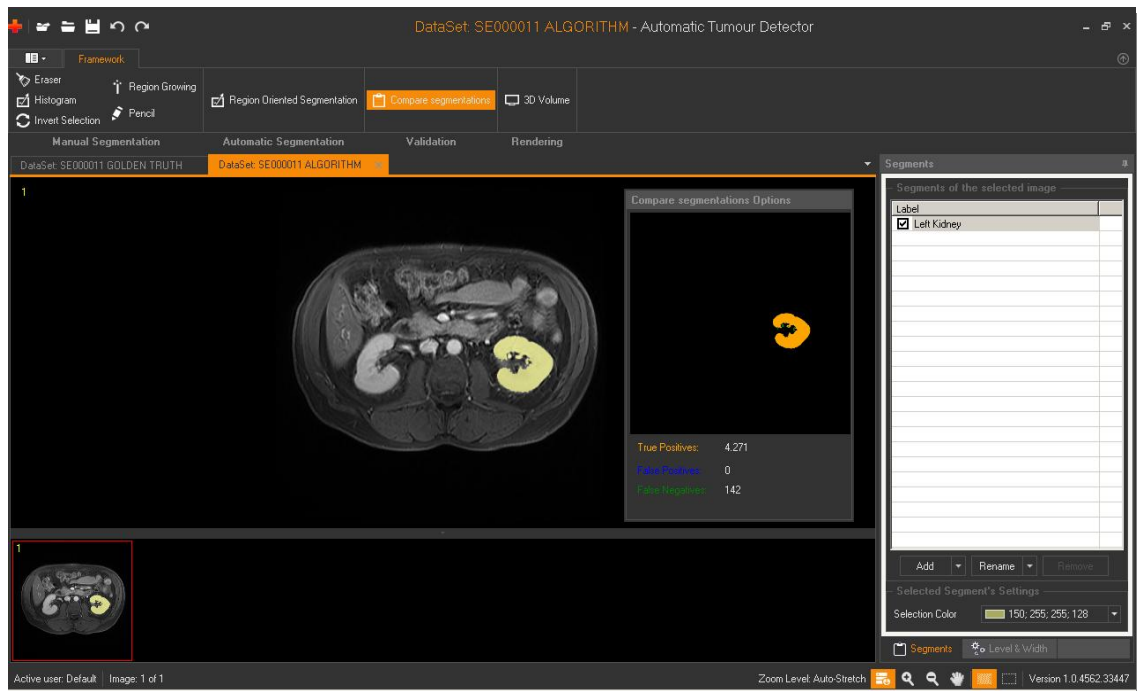
Figure 3.26: Validation Panel – Single Slide Validation Process
(Clinician's (Golden Truth) vs Medical Technician's (Algorithm) delineation)

By pressing the *Compare segmentations* button, a panel appears allowing visual comparison of the previously delineated areas.

This panel shows the *True Positives* (Correctly Selected) pixels which are the common pixels in the two methods (orange), the *False Negatives* pixels which are presented only in the clinician's work (blue) and the *False Positives* (Mistakenly Selected) pixels which are presented only in the second image produced with the automatic method (green) (Figure 3.26).

A video demonstration for both the semi-automatic and fully automatic segmentation techniques along with the user interface is available at: www.creteportal.gr/ATDSegmentation.zip

3.2.8 3D Rendering process - A Visualisation Toolkit (VTK) Implementation

Once the user has annotated all the regions of interest in the specific image dataset, the *3D Volume* rendering panel (top-middle of figure 3.27) provides a 3D view and thus enables the manipulation of the resulting volume model.

For this implementation the open source *Visualisation Toolkit* [The Visualisation Toolkit (VTK)], has been deployed; which supports a wide variety of visualisation algorithms in a 3D interactive process.

The *ATD* platform allows a full 3D representation of the organ along with any defined structural abnormalities within it (Figure 3.27) providing a realistic view of the area in 3D as well as a quantitative analysis of the medical imaging data.
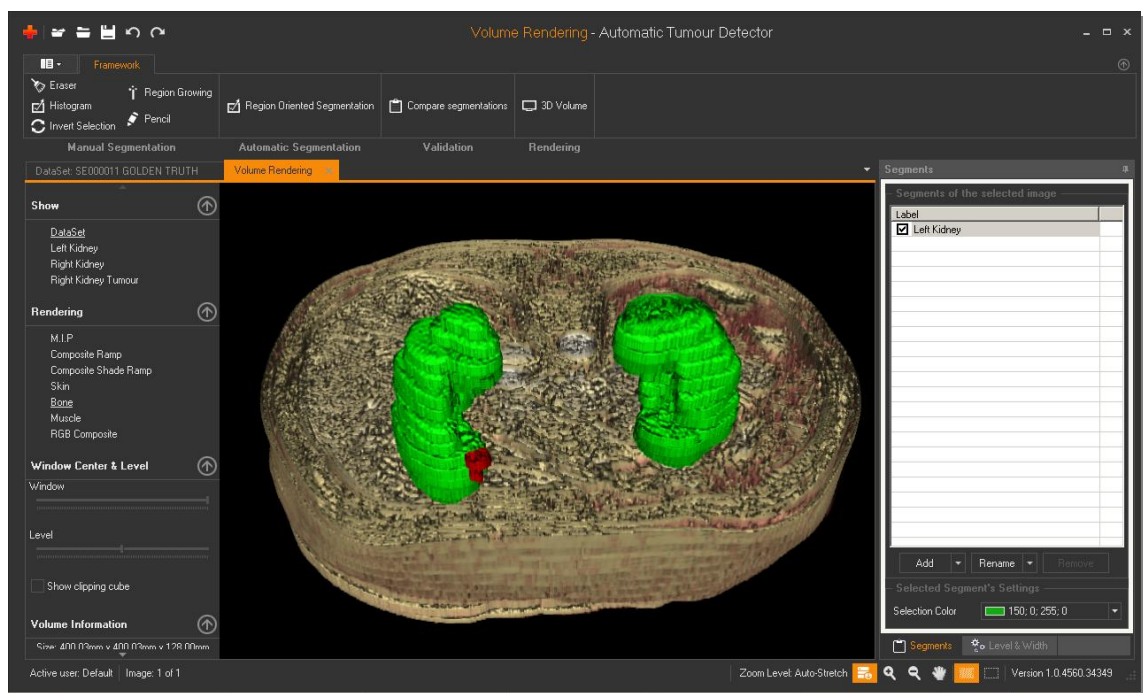
Figure 3.27: 3D model of the body integrating the previously delineated areas. Green represents the kidneys while red identifies the tumour

In this case the implemented rendering algorithms used were *Volume rendering* and *Surface rendering*.

Volume rendering is an algorithm that converts 3D objects into cube-like geometric elements called voxels. This has the advantage of preserving data integrity but at the expense of computation time and increased complexity.

Surface rendering is an alternative, well established algorithm that is often used in virtual reality scenarios capable of converting the 3D objects into geometric primitives for fast rendering. Future versions of this platform will utilise even newer volume rendering methods, as described at [Hadwiger et al., 2003] and [Dehui et al., 2011].

3.2.9 Storage Information and transmission

The selected areas in the corresponding medical images are finally saved in external (XML-structured) anonymised files. A typical file size of a complete image dataset is about 500 Kbytes (uncompressed) which enables efficient exchange of such data across remote sites for example for sending them to another expert for a second opinion.

The user has also the option to e-mail a *Template* to another radiologist, to automatically reveal important findings in seeking a second opinion. A typical size of a *Template* file is about only 2 Kbytes.

In the next revision of the system, the capability for transmission of selected compressed images to a mobile device or smartphone will be added. This will allow clinicians to either receive such clinical information or offer opinions while they are on the move.

3.2.10   Integrated Segmentation Algorithms and Tools, Innovations
3.2.10.1 The Region Growing semi-automatic Segmentation Algorithm

The function of the algorithm is based on finding and demarcating organ structures as a mass of neighbouring pixels in image areas; starting from a single (seed) pixel.

It achieves this by examining the intensity levels of the neighbouring pixels and spreads the selection outwards starting from a pre-defined (seed) pixel whose grey-level intensity value, plus/minus a so-called *tolerance* value, forms the reference value for such recruitment of similar pixels.

The goal in setting the *tolerance value* is to determine how similar in colour a neighbouring pixel must be in order to be selected as belonging to the region being grown.

If the *tolerance* value is relatively low this will result in the algorithm selecting those pixels with colour values equal or near to the reference pixel that is being currently designated as such by the cursor/pointer. Alternatively, high *tolerance* values would allow a broader range of neighbouring pixels to be included as part of the region that is being grown [Fujita H. & Fejri M., 2006].

In practice, when seeking to demarcate the outer boundaries of the organ

image being processed, the choice of the *tolerance* value can be iteratively adjusted for the best trade-off between selecting too many pixels that, at the next stage, will have to be rejected as irrelevant, or, missing some important pixels that belong to the organ image being demarcated.

To label the delineated organs areas and any abnormalities such as tumours, an image mask (array) is used; this is of the same size as the original image. The pixels in the image mask represent the corresponding positions of the selected pixels in the original image; for enhanced efficiency, the proposed algorithm checks only the pixels that have not already been examined.

Thus the key objective of the *Region Growing Methods* is the accurate definition of the boundaries of designated areas of interest (e.g. left kidney) (Figure 3.28).
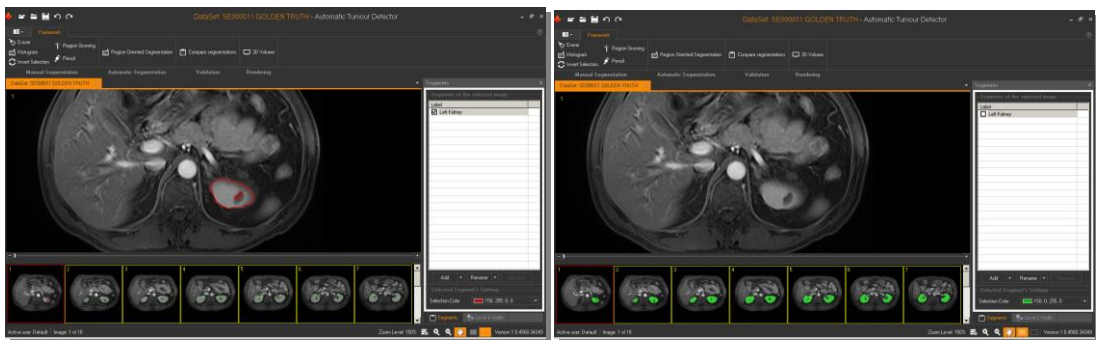
Figure 3.28: Addressing the fuzzy boundaries problem by applying specialised tools

The fuzzy transition zones which span the tissue boundaries lack colour homogeneity, making the delineation process difficult [Marcotegui B. & Zanoguera F., 2002].

To solve the problem with the fuzzy transition zones at the boundaries of the designated areas of interest (e.g. left kidney) and to support the clinicians when attempting to delineate complex images, an advanced digital pencil and the eraser tool are integrated with the *Region Growing* functionality within the platform to automatically keep the similar neighbouring points connected, providing the clinicians with the option to swiftly refine their delineations.

The *ATD* platform integrates an enhanced version of the *Region Growing semi-automatic segmentation algorithm* with the following features, which speed up the segmentation task:

- A slider allows the adjustment of the *tolerance* value interactively and visually for the selection of the desired are in the image, just after the *Start Point* selection.
- An image mask speeds up the segmentation process by ensuring that pixels already examined will not be checked again.

3.2.10.2 A Fully Automatic Region Oriented segmentation Framework

In order to best support the clinical diagnosis process, the proposed *Imaging-enabled Assistive Diagnosis system (IAD)* has to address the following challenges:

1. Locate the clinician's area of interest (e.g. kidney) in the image
2. Calculate the average intensity difference of pixel grey-level values within the clinician's area of interest as distinct from the intensity of the surrounding areas
3. Initially delineate the structures of interest in the image by simply defining *intensity* and *tolerance* values; resolve the delineation and annotation of the area and any abnormalities within it either through using a reference pixel value and iteratively optimised tolerance margins or by following the clinician's delineation and annotation of abnormalities in that area, and finally,
4. Accurately describe the delineated areas in detail

The system responds to the above challenges, through the following steps as applied to the recognition of the Kidneys as a demonstrator case.
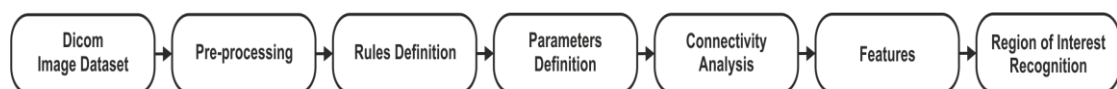
Figure 3.29: The proposed Region-Oriented Segmentation Framework

1st Step – Pre-processing

As depicted in figure 3.29, the segmentation process starts with a pre-processing procedure using an edge-preserving anisotropic (or Perona–Malik) diffusion filter [Perona P. & Malik J., 1990] (Figure 3.30 & Figure 3.31), so that small image artefacts are smoothed (intra-regional smoothing), whilst objects of interest such as edges are enhanced (inhibiting inter-regional smoothing).
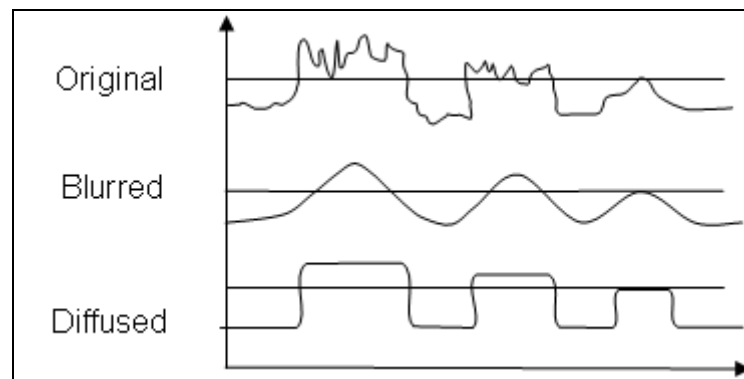
Figure 3.30: Anisotropic Diffusion Filtering (Perona-Malik)

This is an efficient method of noise removal, used to clarify the images compared to the application of blurring filters to the image which result in smooth, noiseless areas with fuzzy contrast (Figure 3.31).
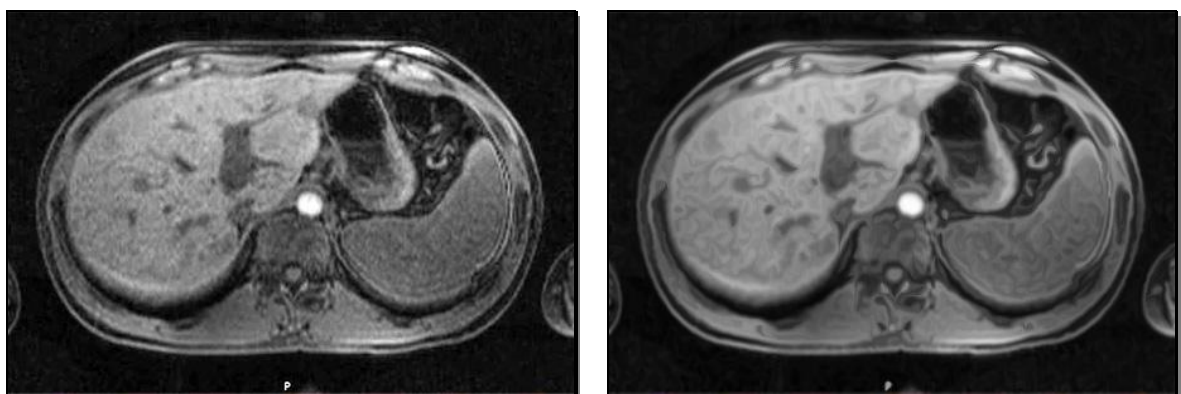
Before   After

Figure 3.31: Anisotropic Diffusion Filtering Example

The use of the *Anisotropic Diffusion Filter* prevents the loss of fine details and smoothing across boundaries. So, with the use of this filter, precise boundaries of areas in the image can be achieved.

2nd Step: *Rules Definition*

In clinical practice, the first step towards the recognition of regions of interest is to target their location. The platform gives the clinician the option to define a *working area* in the sequence of images to ensure that it includes the targeted objects (e.g. in our demonstrator case these are *Kidneys*).

Defined *working areas* are stored in *Templates* and can be used in the

identification of specific objects in a given medical image dataset. This avoids false positives and minimises the amount of information which needs to be processed.

3rd Step: Parameters Definition

Generally, a histogram displays the frequency of the grey-levels in an image. If there exists no user-specified region of interest as a *working area* where the organ is located, the automatic process would typically result in a larger area being designated as the region of interest.

To resolve this, in this step the system deploys a modified algorithm as introduced by H. Bassman and P. Besslich [1995].

In the equation below (Eq. 3.2.10.2(a)), *h(gv)* is the histogram value for a specific grey-scale value *gv*, *Max* is the maximum value of the histogram and *NormMax* is the normalised maximum value defined by the user.

$$h(gv) = \text{int}((float)h(gv) * NormMax/Max) \qquad \text{Eq. 3.2.10.2(a)}$$

A normalisation of the histogram process through the right definition of the associated *NormMax* parameter is required to avoid problems in the next step due to overflow events.

To identify the abnormalities located in a designated area, the dynamic range of the histogram entries has to be compressed in such a way that the lower entries of the histogram are emphasised. This is achieved by using Eq. 3.2.10.2(b).

$$h(gv) = 10\sqrt{h(gv)} \qquad\qquad \text{Eq. 3.2.10.2(b)}$$

In this way, small peaks in the histogram corresponding to small areas in the image are emphasised, allowing the algorithm to detect them more accurately.

As a *start point*, a process of smoothing the histogram must be applied to homogenise and successfully detect relatively large areas (organs) avoiding the insignificant local peaks (i.e. variations in colour inside the organ image area).

The histogram is smoothed by applying the computational method whereby all the intensity values of the pixels in the image are re-calculated by determining the average of a pre-defined number (the link *width*) of neighbouring pixels of

the histogram.

This interpolation *width* parameter is defined experimentally by the user, supported by real-time visualisations (Fig. 3.37). The higher *width* values are associated with large areas being designated as part of the organ structure of interest; while low *width* values help the user pick out the smaller structures thus attempting to avoid missing any important parts of the image. If the *width* parameter is set to 1 the smoothing process is disabled.

By detecting the falling and rising histogram edges the number of valleys in the histogram can be determined, thus inferring the threshold values (Figure 3.32).
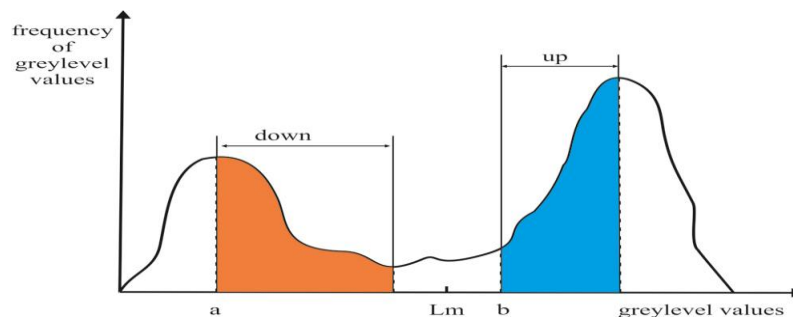
Figure 3.32: Automatic definition of Thresholds (Lm) process (Eq. 3.2.10.2(c))

A *Threshold* (Lm) is defined as:

$$Lm = a + down + [b - (a + down)]/2 \qquad \text{Eq. 3.2.10.2(c)}$$

In this equation, *a* represents a local maximum value and *b* is the point where the histogram starts to rise again (ignoring any small peaks under a predefined limit value). These local minimum values *Lm* are used to segment objects and to create a *Label Image* (Figure 3.33). In this figure, two thresholds are used (*Lm1* = 0, *Lm2* = 5) to identify two different zones.

For example, the left Kidney in figure 3.28 corresponds to the second curve in the histogram (Figure 3.32). The closer the peak of this curve is to *Lm*, the more the delineated boundary moves inwards towards the centre of the kidney.

The platform provides the clinician with the option to define the *up* and *down* parameters which are also stored in the *Templates* in order to achieve the desired *Lm* values in complex images.

Applying any filter to an image introduces a certain amount of noise. This noise can be removed by using erosion-dilation linear morphological filters. By applying a 3x3 erosion filter, the user defines a *Threshold* (the number of the neighbours, max 8 in a 3x3 mask), whereby a value of *0* removes the central pixel of the 3x3 mask.

Conversely, using a dilation filter the user defines a *Threshold* to place a pixel at the central position of the 3x3 mask with an intensity corresponding to the same colour value of the mask region.

4th Step: Connectivity Analysis

In order to create the final *Mark Image* which depicts the regions of interest, L-shaped masks are used (based on 6-connected neighbourhood technique) [Horn B.K.P., 1986] to compare the label value of every pixel to the values of the neighbouring pixels. The pixels with the same values in the *Label Image* but different values in the *Initial Image* are included in the list of pixels to be considered later when identifying the number of the different objects in the image.

Initial Image							Label Image							Mark Image					
1	1	1	0	7	7		1	1	1	0	2	2		a	a	a	-	c	c
1	1	1	0	7	7		1	1	1	0	2	2		a	a	a	-	c	c
1	1	1	0	7	7		1	1	1	0	2	2		a	a	a	-	c	c
4	4	7	7	7	7		1	1	2	2	2	2		b	b	c	c	c	c
4	4	7	7	7	7		1	1	2	2	2	2		b	b	c	c	c	c
4	4	4	4	7	7		1	1	1	1	2	2		b	b	b	b	c	c

Figure 3.33: Automatic identification of objects using L-shaped masks (3 Objects a, b and c are identified)

In this example (Figure 3.33), the *Mark Image* contains 4 identified regions. This is based on the work of Bassmann and Besslich [1995] which sets out this method in detail.

Thus the modifications applied to the *Fully Automatic Region Oriented Segmentation Framework* include the addition of a pre-processing procedure (Perona–Malik diffusion filter), (Eq. 3.2.10.2(b)) to remove the noise of medical

images (e.g. abdominal), an implementation of an L-shaped mask based on 6-connected neighbourhood pixels in the *Connectivity Analysis (CA)* process, and a top-down connectivity analysis of the detected regions.

The *CA* method requires at least one common point between one image slide and the next so as to verify the region boundary. Moreover, the average intensity of the grey-level values of the selected region is calculated and a tolerance value is defined.

This criterion must also apply to every following slide in order to successfully detect the desired region.

5th Step: Features

The above-mentioned *Region-Oriented Segmentation Framework* applied to a CT/MRI image dataset can delineate regions of interest which can be categorised based on features such as the *compactness*, the *centre of gravity* (the central point of a defined area), *total area* (number of the pixels) and the *perimeter* of a specific region.

The *compactness and* the *average density* are features that are independent of the exact position, rotation and scaling of the object, so they are very useful in the identification process.

The current version of the *IAD* system additionally stores another two parameters from the above-mentioned features in the *Template* file. Firstly the *total area* which is a criterion to be considered for objects of interest so as to avoid erroneously detecting very small objects during the organ identification and delineation process, and secondly, the *centre of gravity* of an object which must be located in the *working area* and must encompass all the pixels of the object.

Finally, the medical technician in creating the *Templates* needs to click only once on a designated object image (e.g. kidney) from the initially produced list, to obtain the average grey-level value of that object.

To avoid selection of other objects with similar intensities, this value is also stored in the *Template* with an additional tolerance value which can also be defined by the medical technician.

In the next version of the platform a procedure will be incorporated that will allow for the automatic selection of the organ without the need for an initial click. This process will be applied in the *working area* by using the *concentration value* of the desired object along with all the other parameters of the framework for fully automatic identification.

For the recognition of kidney abnormalities (tumours, stones and cysts), some statistical data can be additionally considered to arrive at the *threshold* values for the average grey-level intensity typical of some structures representing abnormal or pathological changes e.g. cysts. Cysts are relatively dark; tumours are grey, while stones have relatively higher grey-level values.

The *Analysis* panel (Figure 3.34) enables the medical technician to experiment with defining the three parameters for the identification of any of the above-mentioned abnormalities/pathologies consistent with the clinician's judgment.
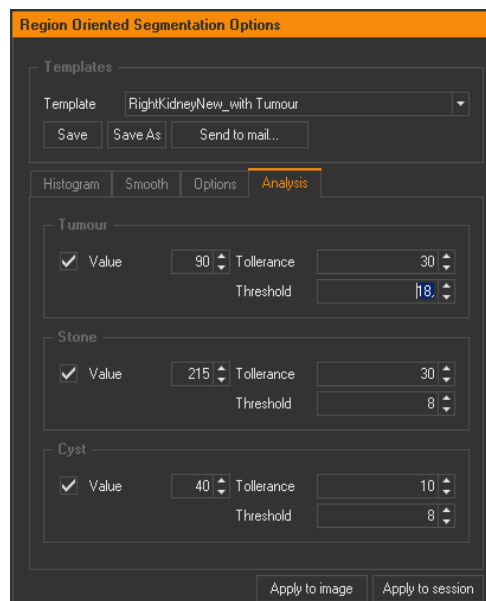
Figure 3.34: Creating Templates for the automatic identification of kidney abnormalities (tumours, stones and cysts)

The first parameter refers to the *grey-level* value that the pixels of an object (e.g. a pixel in an image of an abnormal kidney structure) are typically expected to be designated as such i.e. recognised e.g. as a stone, a tumour or a cyst.

Due to the non-homogenous distribution of grey-level values of the pixels in the MRI images of such organs, a *Tolerance* value must also be defined so that *grey-level* Value ± *Tolerance* corresponds to the range of intensities of pixel

values typically expected to depict such abnormal structures. In this way, pixels which meet the above criteria (potential seeds) are selected.

However, this methodology can also erroneously designate a number of irrelevant pixels with similar intensities scattered in the organ image (classification noise).

In order to identify only the best candidate seeds corresponding to the abnormalities and thus minimise the classification noise, a 9 x 9 erosion filter is used.

Here, the medical technician must declare the number of neighbourhood pixels (*threshold*) to be taken into account (Maximum 9 x 9 = 81-1 = 80 neighbourhood pixels).

Finally, the best candidate seeds with intensity levels closest to the respective *thresholds* are used in a filling process (region growing) to fill up and this helps to demarcate the sub-structural areas which represent the kidney abnormalities.

3.2.10.3 Tools

In the case of extremely complex images, integrated tools and techniques allow for refined delineations of areas of importance.

These tools include advanced versions of the *Pencil* and the *Eraser,* which enable contour refinement by allowing neighbouring pixels to remain connected.

Moreover, the *Invert Selection* tool gives the option of changing the current selection, so that contents which were previously outside of the selection are now inside it, and vice versa.

With the *Histogram* tool, the values of the selected area are depicted in a histogram. Additionally, these values can be stored in an external file for further processing.

3.2.11 Experimental Process

3.2.12 The method for creating and validating the outputs of the *ATD* platform is presented in figure 3.35.
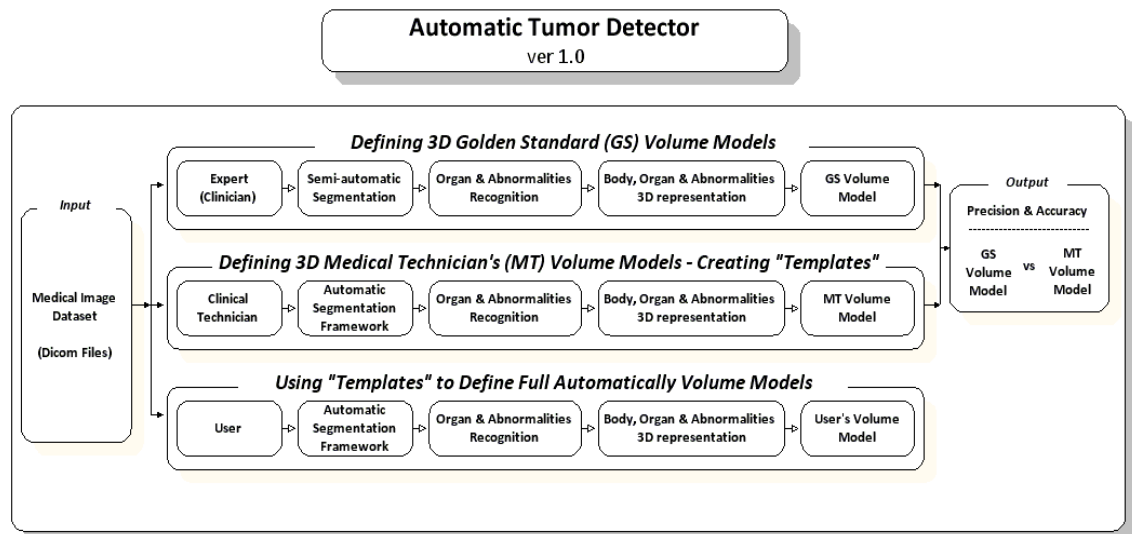
Figure 3.35: Methodology used for the evaluation of the automatic segmentation Framework. Clinician's (or Golden Standard (GS)) Volume Model vs the Medical Technician's (MT) Volume Model

In summary, it involves a clinician using semi-automatic segmentation techniques (e.g. the *Region growing*) and advanced correction tools (working with areas and not with pixels) for a fast and easy identification and annotation of the important areas thus creating and storing 3D models.

Following this, a medical technician is using the *Automatic Segmentation Framework* panel to achieve results similar to the clinician's work and consequently store the results in a *Template*. The platform allows the evaluation of the results by comparing the annotations coming from these two works.

More analytically, the above process is described by the following three steps:

1st Step - Defining *3D Golden Standard Models*

In medical image analysis, the main problem is that the outcome must be compared with a baseline (*Golden Standard model*) in order to validate the performance of the image processing algorithms applied to the dataset.

As shown in figure 3.35, the process calls for clinicians to identify important areas to be delineated and annotated (e.g. kidneys, tumours, stones and cysts) in the medical image dataset in order to define a *Golden Standard Model* for the evaluation of the outcome in a specific medical image dataset.

Accordingly, the clinician imports a medical dataset into the platform. By using

a fast implementation of the *Region Growing* semi-automatic segmentation algorithm and the advanced refinement tools in the *Manual Segmentation* panel, the clinician can accurately define the delineated areas of interest in the images (Figure 3.25).

Once the delineation process has been completed on the image slide where the regions of interest are depicted, the *3D Volume Rendering* option creates a 3D model of the organ structure by integrating the previously delineated areas. By providing a realistic 3D view of the resulting data, this process supports the clinician's attempts to perform an efficient and effective differential diagnosis of possible pathologies in the organ under investigation.

Seven different views of the 3D model are available along with corresponding metrics. They include: M.I.P. (pH-sensitive Molecularly Imprinted Polymer), Composite Ramp, Composite Shade Ramp, Skin, Bone, Muscle and RGB Composite as shown in figure 3.36 below:
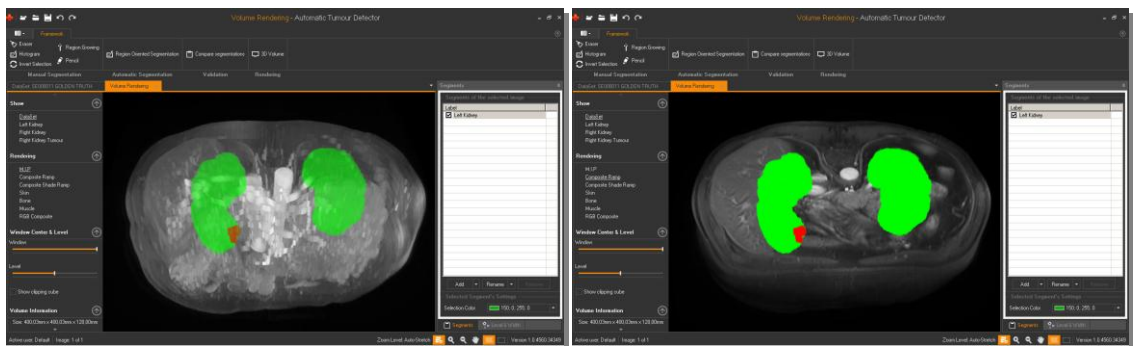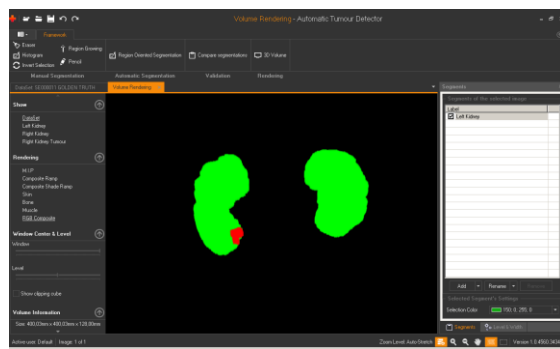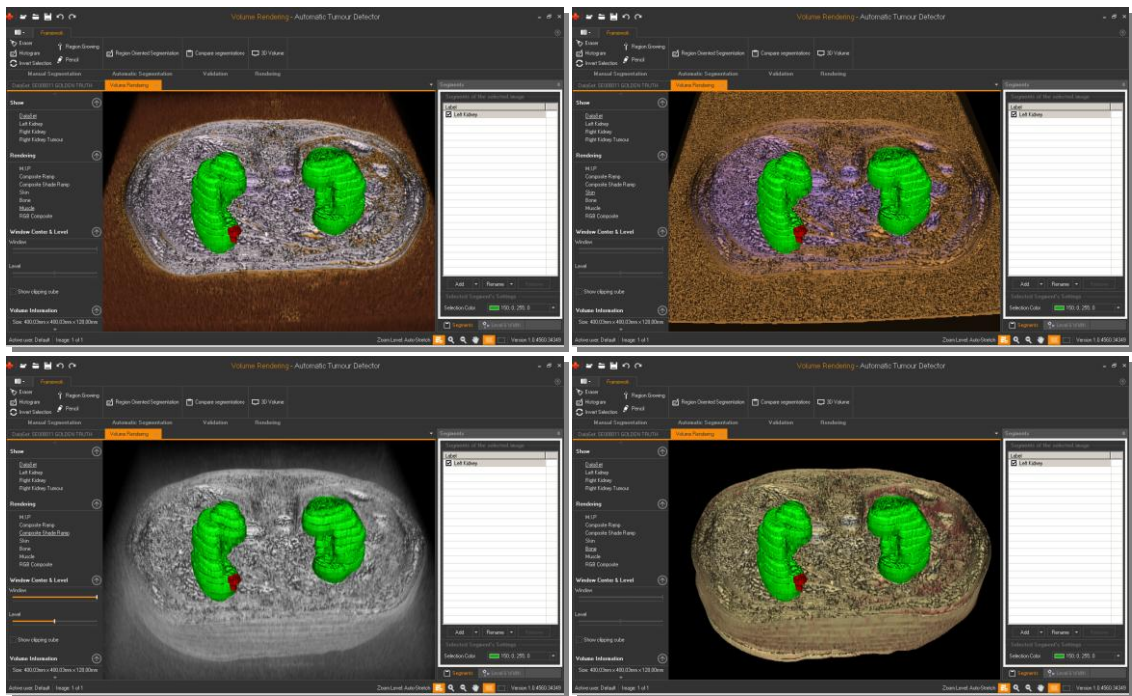
Figure 3.36: The platform supports seven different views of the 3D models presenting the organs and their abnormalities (M.I.P., Composite Ramp, Composite Shade Ramp, Skin, Bone, Muscle and RGB Composite)

The initial information presented to the clinician based on the resulting 3D model is exemplified in the table below:

Table 3.2: Metrics resulting from the produced 3D model; measurements show actual physical sizes of organ structures.

	Body	**Left Kidney**	**Right Kidney**	**Right Kidney Tumour**
X axis (mm)	400,03	84,38	75,00	16,41
Y axis (mm)	400,03	146,88	154,69	18,75
Z axis (mm)	128,00	104,00	112,00	16,00
pixels	4.194.304	46.157	44.415	423
percentage	100,00%	1,10%	1,06%	0,01%

2nd Step - Creating Templates with Rules and Parameters to Identify Specific Areas of Interest

The medical technician uses image slides from the medical image dataset, some of which have been previously delineated and annotated by the clinician, to form rules and parameters to create *Templates*.

Specifically, by experimenting with the parameters of the *Automatic Region*

Oriented Segmentation Framework, the medical technician attempts to achieve a segmentation result closest to that of the clinician's (Figure 3.37). The *Validation* panel allows the evaluation of segmentation results (section 3.2.7).

Figure 3.37: Defining parameters and rules (Templates) for the Automatic Segmentation process

Once the medical technician achieves a result that is very close to the clinician's opinion, it can be stored in a *Template* and can be applied automatically later to a single image or to a series of images (datasets) at once.

3rd Step -Using existing *Templates* for fully automatic Identification of Specific Areas of Interest
A clinician (or trainee) can import a medical image dataset of the same type as the previous ones (e.g. abdominal images).

Using the existing *Templates*, the clinician can automatically select a *Template* to apply (e.g. Left Kidney) in order to find a specific organ and view the potential abnormalities in that organ.

Since the location of the organs can vary from one dataset to another, in order to identify the initial position of the organ, the clinician simply loads the *Template* in any of the images including that organ and then clicks on the organ

to select it from the list of objects. Future version of the platform will integrate an automatic procedure for the identification of the initial position of the organ, based on the concentration value of that organ.

3.2.13 Summary

ATD is a new, easy-to-use platform supporting multi-colour object annotations resulting in a fully automated identification method of kidneys and their potential pathologies (tumours, stones and cysts) as well as a 3D multi-modal interactive visualisation environment.

The development of this system has been clinically driven, providing the clinicians with useful visual information and real metrics of the detected areas.

The advantages of this platform include rapid processing of CT/MRI datasets on a large scale, easy and accurate delineation of highly complex medical images, an easy-to-handle multifunctional annotation system and a fully automatic framework for the recognition of kidneys and their structural anomalies/pathologies.

Moreover, it allows the storage of the information in small anonymous external files to ensure their fast transmission via networks to other computers or mobile devices.

The user also has the option to send a *Template* file to a second radiologist to get one more opinion about the findings.

This is a first step towards the implementation of a complete telemedical application for mobile clinicians.

Chapter 4 – Results and Discussions

This chapter presents the results of the development of both platforms.

DoctorEye experimental results are presented in terms of *Training*, *Clinical* and *Research* modes.

In the case of the *ATD* platform, experimental results are related to the use of the *Fully Automatic Region Oriented Segmentation Framework.*

4.1 The *DoctorEye* Project

The *DoctorEye* platform facilitates the 3D annotation, image analysis and visualisation of important medical image entities, such as cancer, from either MRI datasets or any other medical image modality.

There are four basic features that characterise the platform. It is flexible, easy to use, fast to operate and since no registration or activation is needed it is freely distributed for testing.

4.1.1 Experimental results (Training mode)

In training mode, clinical trainees can work on the same medical image dataset delineating organs and their potential abnormalities.

Figure 4.1: Generally, one of the basic ideas for an advanced medical platform is to support processing of the same dataset by different clinicians for training purposes. Photo comes from [The Views of MRI Scans, 2013]

After this process is completed, the *Clinical Expert* can log in on the platform as an *Administrator* having full access to the data of the clinical trainees.

According to the scenario, he opens the same dataset loading the trainees' annotations. By changing the opacity of the annotated areas he can present all the delineations simultaneously on one screen.

At this stage, the *Administrator* can select and rename (e.g. Final Tumour) the best annotated areas in each image of the current dataset. He also explains to the clinical trainees the reasons why those annotations were selected as more accurate.

This way, the *Administrator* can select the most accurate delineations in the whole dataset achieving the most realistic 3D representation of the selected organs and their possible dysfunctions.

4.1.2 Experimental results (Clinical mode)

DoctorEye ver 4.3 supports 3D delineation, annotation and representation of regions of interest (ROIs) such as organs and their abnormalities in a very easy way.

Thus, clinicians may have a better view and manipulate *in silico* human internal structures in a multifunctional environment.

The figure 3.36 contains five different views of a 3D model of a head and tumour.

The main steps of the process the clinician needs to follow to achieve a 3D delineation of a head and tumour to create a 3D model are:

- Load an MRI dataset (e.g. the 301- BrainIx Dataset) [DICOM sample image sets, 2013].
- Select a point in the dark area around the head in the first image with the *Region Growing* tool and with the *Invert selection* tool create a delineation of the head.
- Rename the label in the annotation panel to *head.*
- Execute the same process on all the slices of the dataset.
- Select the first slice where the tumour appears.

- Add the new label *Tumour* in the annotation panel.
- Use the *Region Growing* tool or one of the other semi-automatic segmentation algorithms and the *Tools* available in the *Annotations panel* to achieve the best delineation of the tumour.
- Execute the same process on all the slices containing the tumour in the dataset.
- Press the *3D Visualisation* button in the *Visualisation panel* to enable the multifunctional environment where a 3D model of the selected areas can be manipulated.

Figure 4.2: Delineation of head and tumour (derived from 22 slices)

The 3D multifunctional environment shown in the figures below, allows different views of regions of interest (ROIs) such as tumours, presenting the volume under investigation in 3D interactively.
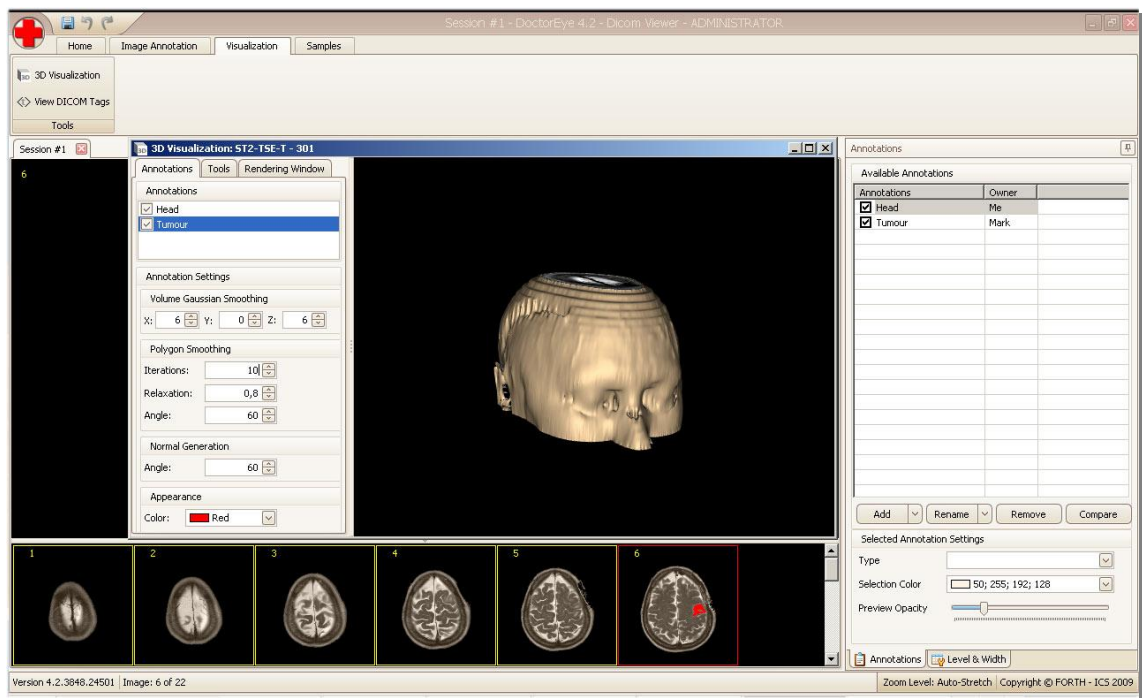
Figure 4.3: 3D representation of head and tumour (derived from 22 slices)
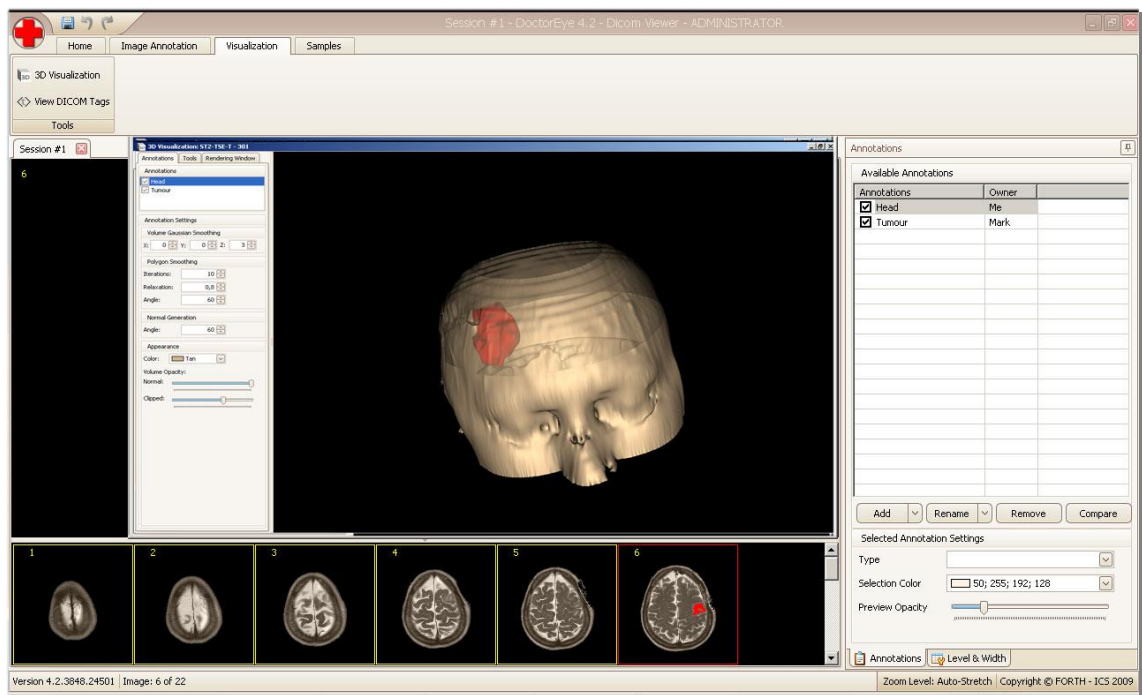
Figure 4.4: 3D representation of head and tumour (derived from 22 slices) by changing the head volume opacity value
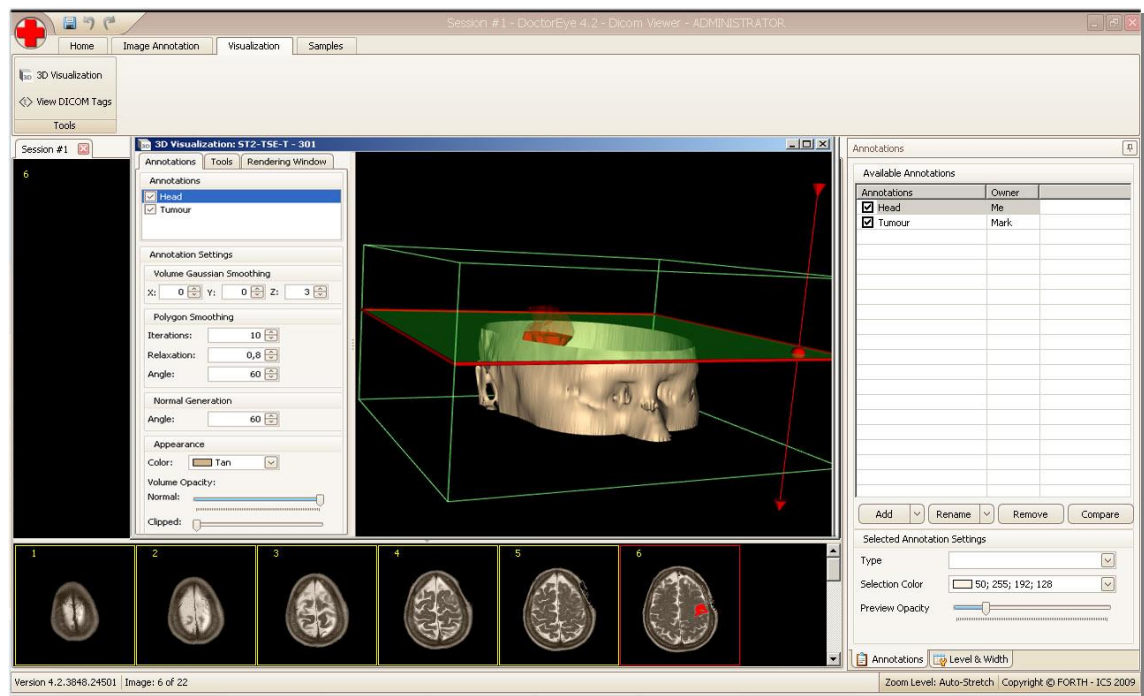
Figure 4.5: 3D representation of head and tumour (derived from 22 slices) - clipped using the Plane tool
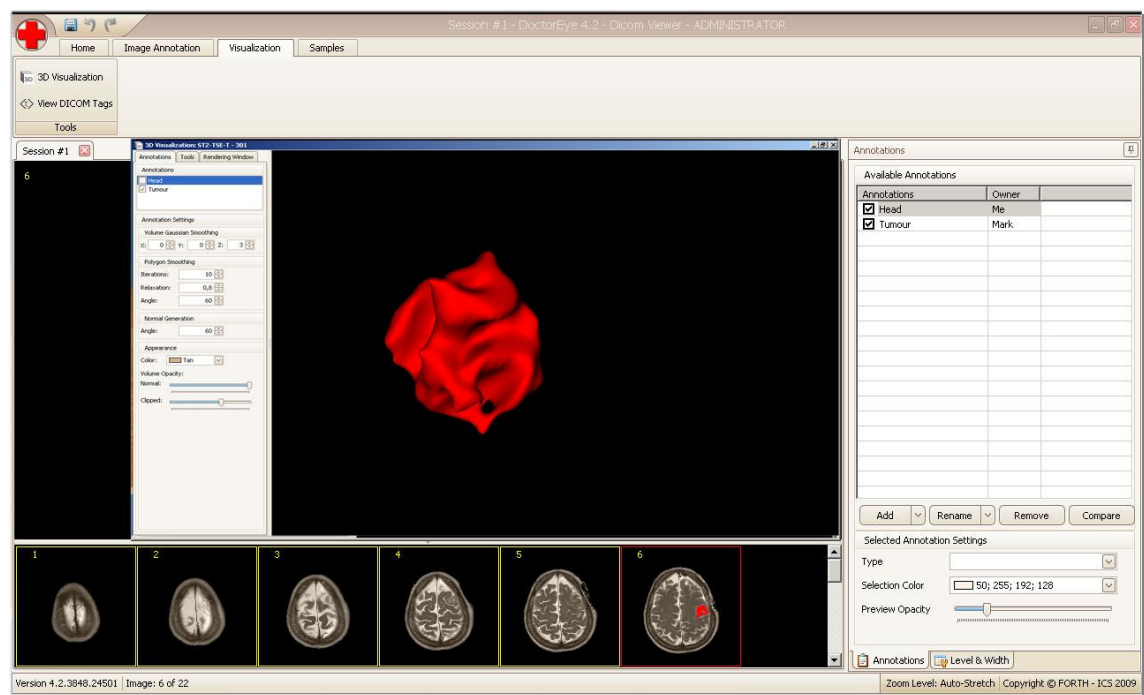
Figure 4.6: 3D representation of the tumour (derived from 22 slices) – zoom-in mode

The above illustrated example is the result of the segmentation of 22 brain images using the *BRAINIX - 301 MRI dataset* [DICOM sample image sets, 2013].

4.1.3 Experimental results (Research mode)

Apart from the fact that the platform can assist a senior Doctor to train other Doctors in the visual identification of abnormalities appearing in a specific medical image dataset (Section 4.1.1) and to produce 3D views for clinical use (Section 4.1.2), DoctorEye can also assist researchers in the development of new techniques and methods for medical image processing.

4.1.3.1 Experimental results (Research mode) – Histograms (CSF, Necrosis and Tumour)

Accurate identification of diseased tissues in clinical practice is not an easy task. In an ideal case, the diseased and non-diseased areas would show as separate areas with different colours in the histogram as depicted in figure 4.7.
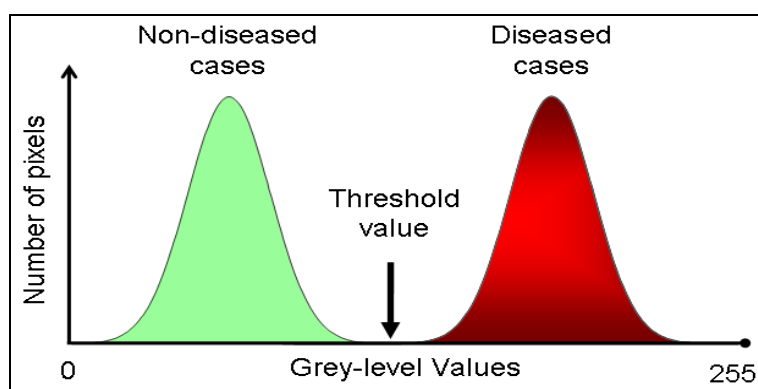
Figure 4.7: Subjective judgement of likelihood that a case is diseased

However, in reality, in most images there is a certain degree of overlapping of the diseased and non-diseased areas (Figure 4.8) requiring more sophisticated approaches for their accurate identification.
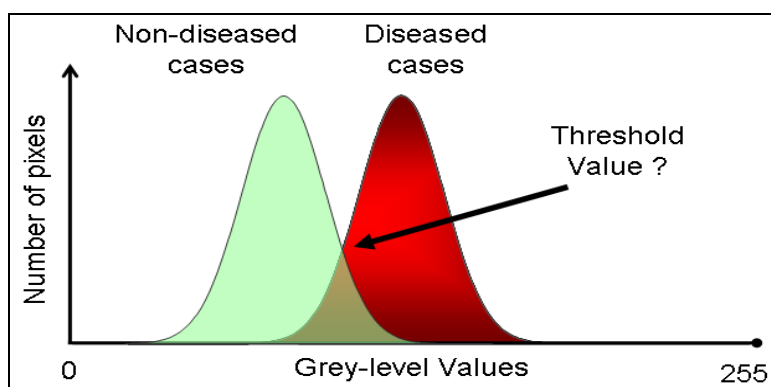
Figure 4.8: Non-diseased vs diseased cases, a more realistic approach

Definition of the *Threshold* value needed for the accurate description of these cases is crucial.

As an example, in order to run precise oncology models *in silico*, accurate data from individual patients are needed [Zepp et al, 2010].

Using *DoctorEye*, vital, necrotic and cystic areas within a tumour can be defined accurately by clinical experts, through the visual interpretation of high resolution magnetic resonance images (MRI).

The histograms of the segmented areas (gliomas) presented in figure 4.9 show that they can add value for a better description of tumours for use *in silico* oncology models.

Figure 4.9: In this figure 5 different glioblastoma cases where CSF, necrotic and tumour areas are presented. Histogram figures come from [Zepp et al, 2010]

To identify a clear demarcation between tumour and healthy tissue in gliomas, a correlation between signal intensities and histological features must be defined.

DoctorEye provides histograms of signal intensities and their corresponding mean and median values between cerebrospinal fluid (CSF), vital tumour,

necrotic and cystic areas within the tumour.

A correlation between tumour texture and signal intensities in MRI expressed by histograms of signal intensities is a step forward in the right direction.

4.1.3.2 Experimental results (Research mode) – A new Active Contours (Snake) semi-automatic segmentation algorithm

The *DoctorEye* multifunctional platform supports the integration, testing and comparison of new segmentation algorithms with the already integrated ones.

A new *Active Contours* (Snake) semi-automatic segmentation algorithm [Farmaki et al, 2010] is also integrated into the platform.

Compared to the *Greedy Active Contours* algorithm which requires the adjustment of four parameters to execute (*Continuity*, *Curvature*, *Gradient* and *Pressure* (or *Balloon*)) (Section 3.1.8.2), the new algorithm requires the adjustment of only one of them (*Force (or Balloon)*). The other three parameters of the snake evolution are automatically predefined by the new algorithm. The user needs to draw an ellipse within the area of interest (e.g. tumour) and then press once only the spacebar button to describe the boundaries of this area (Figure 4.10).
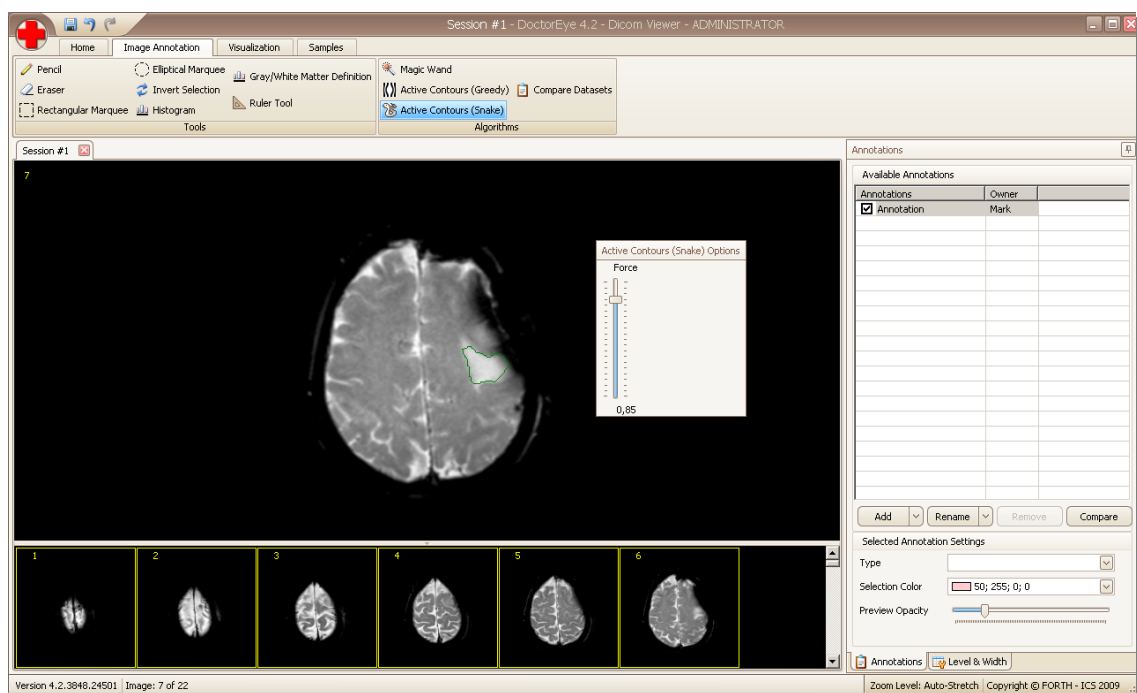
Figure 4.10: A new Active Contours (Snake) semi-automatic segmentation algorithm

Farmaki et al. [2010] claim that this semi-automatic segmentation method presents better tumour segmentation results in comparison with the two previous segmentation methods and that its use ensures more accurately defined boundary details, and overcoming of small inhomogeneities within the tumour area.

4.1.3.3 Experimental results (Research mode) – Diffusion models

The *DoctorEye* platform also supports the development of methods and techniques by other researchers for medical image processing, with the use of plug-in technology.

For example, the plug-in of the platform allows the development of diffusion models in order to simulate the glioma growth procedure in space and in time [Roniotis A. et al, 2009].

The clinician here has to delineate the boundaries of the brain such as bone or outer skull area, where tumour cells cannot migrate.

The *Diffusion Panel* (plug-in technology) (Figure 4.11) allows the adjustment of the modelling parameters, in order to get the diffusion result.
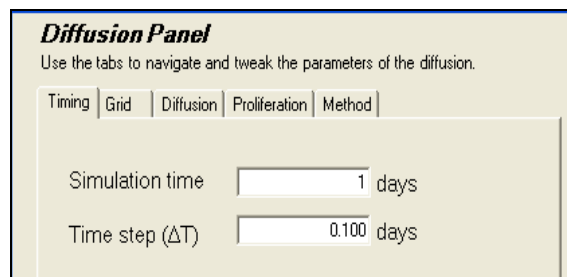
Figure 4.11: Diffusion Panel (plug-in technology) - Figure comes from [Skounakis E. et al, 2010]

The result of this process can either present the volume reconstructed in 3D, or visualised in slices

After 100 days of diffusion, the simulated tumour cell concentration is represented with a heat-colour area (Figure 4.12).
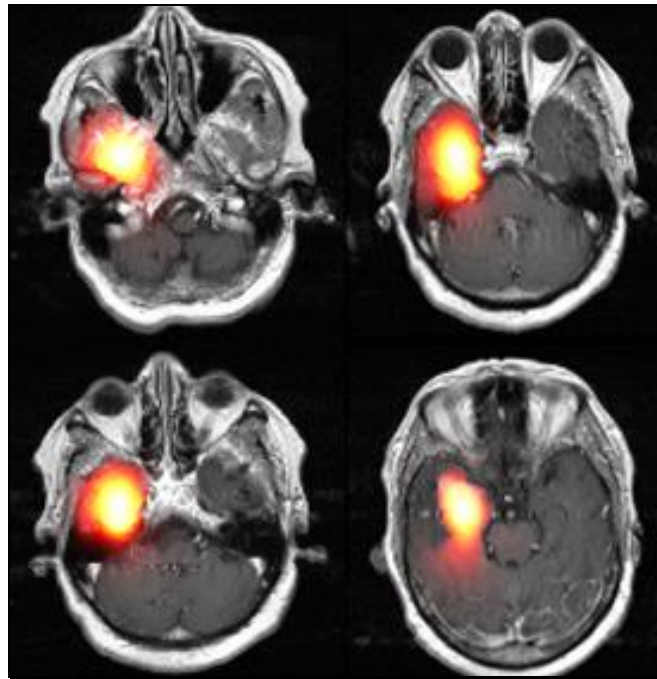
Figure 4.12: Representation of the diffusion modelling results showing the tumour cells in space after 100 days of diffusion - Figure comes from [Skounakis E. et al, 2010]

This functionality can assist clinicians to improve optimal treatment design.

4.1.3.4 Experimental results (Research mode) – DoctorNo plug-ins

The *Medical Image Analysis Group* from the *Institute for Surgical Technology and Biomechanics* at University of Bern, Switzerland has developed *DoctorNo*, a suite of plug-ins for the *DoctorEye* platform [DoctorNo plug-ins, 2013].

This suite of plug-ins can be used in the *DoctorEye* platform offering additional tools for the analysis of 3D brain tumour magnetic resonance images (MRI).

The *Doctor-Strip* tool extracts the brain region from images of the head.

The *Doctor-Regi* tool can register multi-modal and multi-temporal images of the patient in a common reference space.

The *Doctor-Resa* tool resamples images to have a resolution of 1mm, which is necessary for tumour simulation studies.

Finally, the *Doctor-Classi* tool classifies the brain tissues into healthy (CSF, GM, WM) and pathologic ones (necrotic, active and edema region).

The development of these tools was supported by the European Union within the framework of the *ContraCancrum* project (grant number: EU FP7 - IST-223979) [ContraCancrum, 2013].

4.1.3.5 Developing Frameworks and Algorithms

DoctorEye, as a multifunctional platform, provides visual and quantitative useful information for the researchers to design and develop frameworks and algorithmic approaches in medical image processing.

This way the process of creating algorithms or frameworks (algorithmic approaches and groups of processes) is simplified.

For example, a user opens with the *DoctorEye* platform the *IM-0001-0009.dcm* DICOM medical image from the *sT2-TSE-T - 301 BRAINIX* MRI dataset [DICOM Sample image sets, 2013] (Figure 4.13).
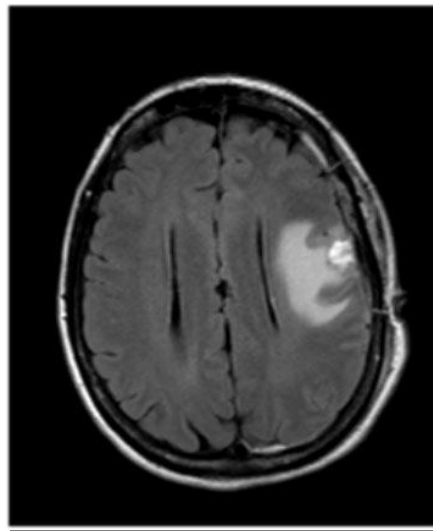
Figure 4.13: Image sample (Im-0001-0009.dcm) from the sT2-TSE-T – 301 BRAINIX MRI dataset [DICOM Sample image sets, 2013]

As explained in the previous sections, delineation of the head and tumour areas with corresponding labels can be achieved accurately (Figure 4.14).

Figure 4.14: Delineation of the head (blue colour) and the tumour (red colour) with corresponding labels

According to the analysis mentioned in Section 4.1.3.1, there is overlapping between tumour texture and signal intensities of the normal brain tissue. This is also confirmed by the signal intensities shown in the histogram below where in this case, the *Head* label corresponds to the Skull and the Cerebrum: (Figure 4.15).
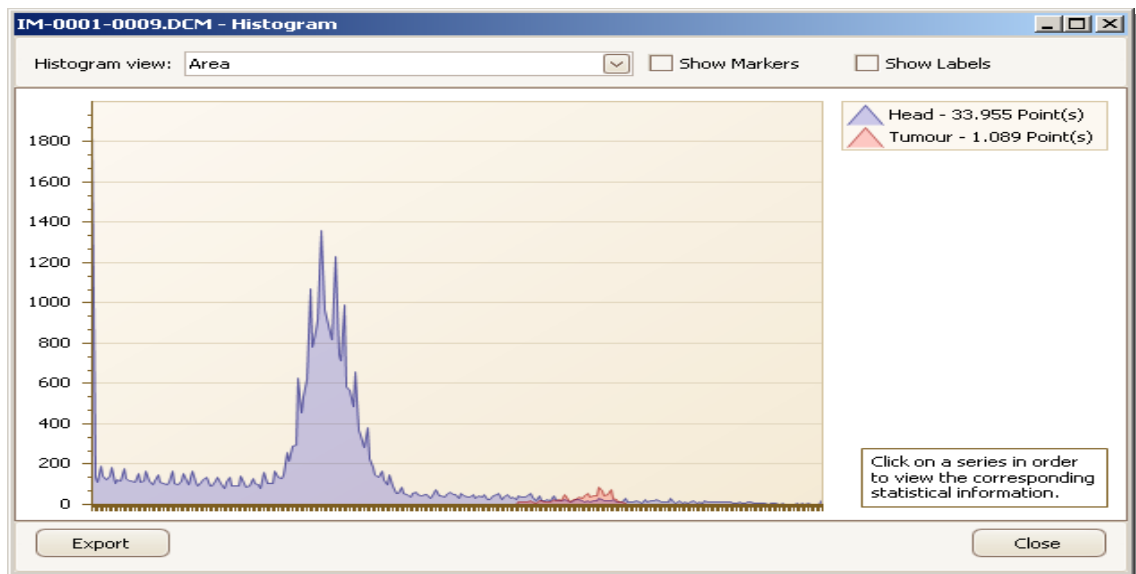
Figure 4.15: Histogram showing the information from the delineated areas (Head and Tumour) of the Im-0001-0009.dcm MRI image. The Head label in this case, corresponds to the Skull and the Cerebrum.

From figure 4.15, it is obvious that some normal cells in the head have grey-level values which are the same as or similar to those of the tumour's cells, thus rendering their distinction very difficult.

In case the user selects only the Cerebrum area for the *Head* label, avoiding the Skull cells, the result is shown in figure 4.16:
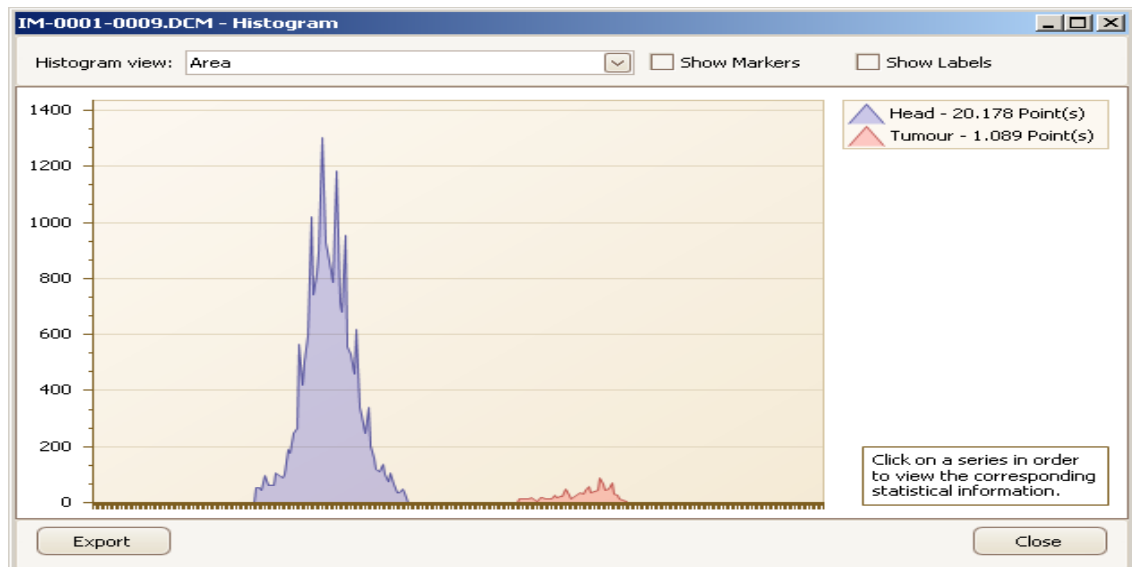
Figure 4.16: Histogram showing the information from the delineated areas (Head and Tumour) of the Im-0001-0009.dcm MRI image. The Head label corresponds only to the Cerebrum.

Here, there is no overlapping between tumour texture and signal intensities of the normal brain tissues.

The two areas are not close to each other and thus, accurate delineation can be achieved by simple algorithmic techniques such as *Adaptive Thresholding*.

So, in order for the user to develop a *Framework* so as to automatically delineate the *Cerebrum* and the *Tumour* areas accurately, the process to follow is:

- Open the image
- Define and exclude the pixels of the *Skull* (to avoid overlapping with the pixels of the *tumour* area)
- Make use of a method to find a compact area of the *Cerebrum*
- Run a *Region Growing* algorithm in this area with a predefined *tolerance* value to select all the pixels contained there (Figure 4.16 – Blue area)

- The rest of the information should be the *tumour* area (Figure 4.16 – Red area)

The above mentioned example is a simplified approach to the creation of a simple *Framework* for medical image segmentation.

Since the subject is medical images, the *Framework* must be enriched with texture-based algorithmic approaches to ensure that the information produced at the end of this process will be the desired one.

4.1.4 Discussion

Although the original idea was the development of a platform to meet the needs of clinicians (Clinical use), in its current version it has come to support three modes: *Training*, *Clinical* and *Research* mode.

In *Training mode* an expert clinician can help other clinicians to expand their knowledge and evaluate their work in special issues.

In *Clinical mode*, *DoctorEye* platform as a multifunctional powerful clinical tool facilitates multilevel imaging biomarker extraction with no need of prior knowledge in segmentation/annotation systems.

The *Research mode* is supported with the integrated plug-ins sophisticated technology and the fact that it is distributed free to test and requires no registration or activation.

These properties make this platform a friendly environment for the evaluation of results coming from the use of new techniques in biomedical information extraction, annotating organs and their potential pathologies.

The platform has already been adopted for annotating a large number of tumours in the EC *ContraCancrum* Project ICT-2007-223979 [ContraCancrum, 2013].

4.2 The *Automatic Tumour Detector* Project

4.2.1 Evaluation Metrics

Evaluation of the *Automatic Segmentation Framework* is based on the following five criteria [Mahalakshmi T. et al, 2009]: *Accuracy*, *Precision*, *Sensitivity*, *Specificity* and *Dice Similarity Coefficient*. These metrics provide a means of benchmarking of performance of *IADS (Imaging-enabled Assistive Diagnosis Systems)*.

Generally, pixels are classified into four categories: *True Positives* (Correctly Selected), *True Negatives* (Correctly Rejected), *False Positives* (Mistakenly Selected), and *False Negatives* (Mistakenly Rejected). The number of pixels in these categories can be used in the following formulae to calculate the values of the above metrics.

Accuracy is the proportion of true results (*True Positives* and *True Negatives*) in the population of the results, as shown in Eq. 4.2.1(a) below:

$$Accuracy = \frac{TruePositives + TrueNegatives}{TruePositives + TrueNegatives + FalsePositives + FalseNegatives} \quad \text{Eq. 4.2.1(a)}$$

Precision is defined as the proportion of *True Positives* against all the positive results (*True Positives* and *False Positives*); as shown in Eq. 4.2.1(b) below:

$$Presision = \frac{TruePositives}{TruePositives + FalsePositives} \quad \text{Eq. 4.2.1(b)}$$

Sensitivity refers to the ability of the system to identify positive results. In other words, it measures the proportion of positives which are correctly identified as such; this is shown in Eq. 4.2.1(c) below:

$$Sensitivity = \frac{TruePositives}{TruePositives + FalseNegatives} \quad \text{Eq. 4.2.1(c)}$$

Specificity refers to the ability of the system to identify negative results, which means that it measures the proportion of negatives correctly identified as such; this is shown in Eq. 4.2.1(d) below:

$$Specificity = \frac{TrueNegatives}{TrueNegatives + FalsePositives}$$ Eq. 4.2.1(d)

Dice Similarity Coefficient (DSC), defines the similarity measure over two 3D volume models; as shown in Eq. 4.2.2(e) below:

$$DSC(GS, MT) = \frac{2|GS \cap MT|}{|GS| + |MT|}$$ Eq. 4.2.2(e)

Where *GS* is the clinician's volume model (Golden Standard) and *MT* is the medical technician's volume model (Automatic Segmentation Framework).

At this point, it is worth mentioning that although the medical technician is involved in this process, his/her subjective opinion has very little effect on the overall process: the medical technician creates a 3D model that is based on that of the Doctor for a specific dataset concerning the organs and their potential dysfunctions.

Once this process is finished, the accuracy / sensitivity / specificity of the results coming from the *Automatic Segmentation Framework* can be verified by introducing several medical image datasets of the same type (e.g. abdominal) and comparing the automatic results with the output of the doctor's work.

Therefore, any misguided selection performed by the medical technician will be cancelled out since the main 3D model of the findings has been initially defined by the Doctor.

4.2.2 Experimental results
As an example, after applying the *Fully Automatic Region Oriented Segmentation Framework* to the SE00011 MRI dataset, the following results are obtained for the automatic identification of objects (Left Kidney, Right Kidney and Right Kidney Tumour):
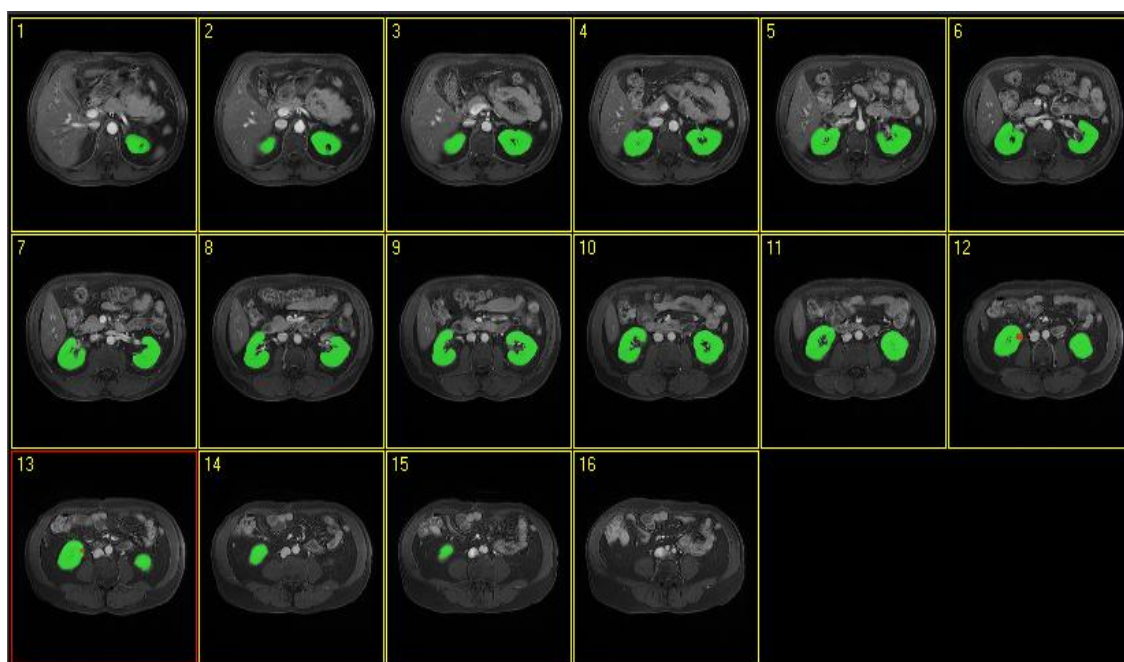
Figure 4.17: Automatic identification of objects (e.g. Left Kidney, Right Kidney and Right Kidney Tumour on No. 12 & No 13 slides) – SE00011 MRI dataset)

After applying formulas 4.2.1(a) & 4.2.1(b), we get the following results for the accuracy and precision of the delineations:

Table 4.1: Delineation of the Left Kidney (SE00011 MRI dataset) – Accuracy and Precision

a/a	SE000011 MRI Dataset	True Positives	True Negatives	False Positives	False Negatives	Accuracy	Precision
1	MR000000	1.692	260.452	0	202	89,33%	100,00%
2	MR000001	3.280	258.864	71	89	95,35%	97,88%
3	MR000002	4.274	257.870	133	13	96,70%	96,98%
4	MR000003	3.940	258.204	0	104	97,43%	100,00%
5	MR000004	4.134	258.010	161	9	96,05%	96,25%
6	MR000005	3.539	258.605	110	111	94,12%	96,99%
7	MR000006	3.563	258.581	143	10	95,88%	96,14%
8	MR000007	3.638	258.506	273	13	92,71%	93,02%
9	MR000008	4.271	257.873	142	0	96,78%	96,78%
10	MR000009	4.494	257.650	10	38	98,94%	99,78%
11	MR000010	3.876	258.268	42	116	96,08%	98,93%
12	MR000011	2.724	259.420	0	97	96,56%	100,00%
13	MR000012	1.235	260.909	6	0	99,52%	99,52%
14	MR000013	0	262.144	0	0		
15	MR000014	0	262.144	0	0		
16	MR000015	0	262.144	0	0		
					Average	95,80%	97,87%

In the following example, after applying the automatic identification method to the SE00004 MRI dataset in a similar manner, the following results were obtained:
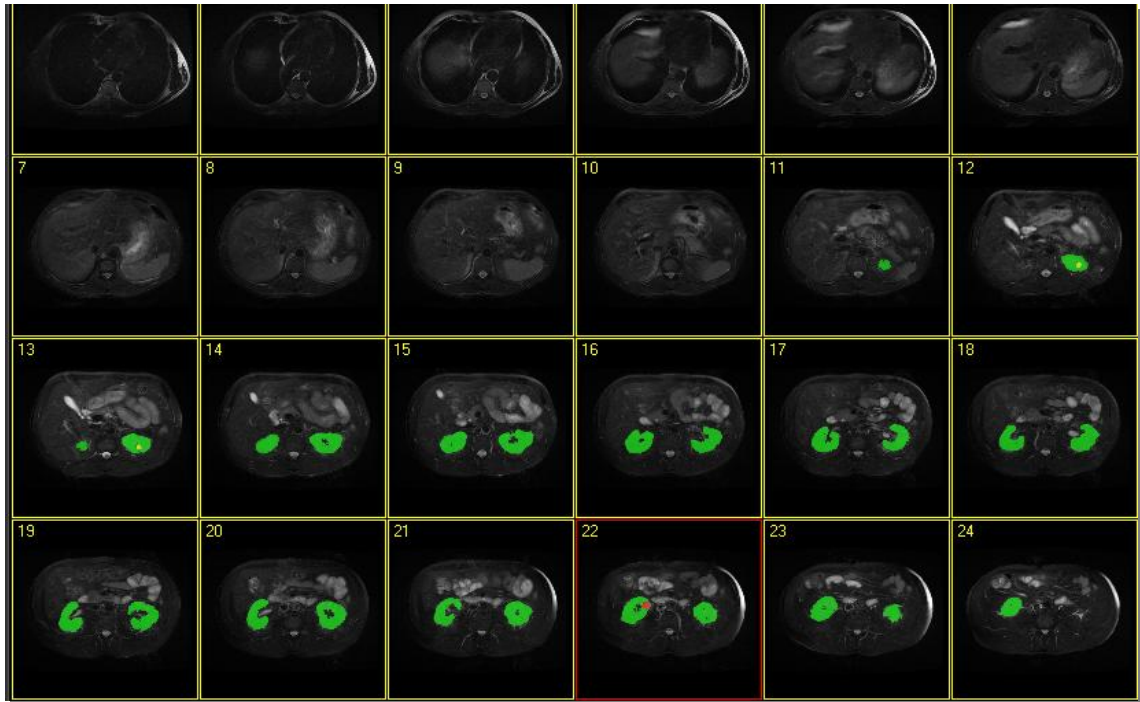
Figure 4.18: Automatic identification of objects (e.g. Left Kidney, Right Kidney, Right Kidney Tumour (No 22 slide) & Left Kidney Stone (No 12 & No 13 slides) – SE00004 MRI dataset)

By applying equations 4.2.1(a), 4.2.1(b), 4.2.1(c), 4.2.1(d) & 4.2.1(e) to the above mentioned dataset (SE0004), we obtained the following results:

Table 4.2: Delineation of the Left Kidney (SE000004 MRI dataset) – Evaluation metrics

a/a	SE000004 MRI Dataset	True Positives (Correctly Selected)	True Negatives (Correctly Rejected)	False Positives (Mistakenly Selected)	False Negatives (Mistakenly Rejected)	Accuracy	Precision	Sensitivity	Specificity	Dice similarity
1	MR000000	0	262.144	0	0					
2	MR000001	0	262.144	0	0					
3	MR000002	0	262.144	0	0					
4	MR000003	0	262.144	0	0					
5	MR000004	0	262.144	0	0					
6	MR000005	0	262.144	0	0					
7	MR000006	0	262.144	0	0					
8	MR000007	0	262.144	0	0					
9	MR000008	0	262.144	0	0					
10	MR000009	0	262.144	0	0					
11	MR000010	651	261.493	47	43	99,97%	93,27%	93,80%	99,98%	93,53%
12	MR000011	2.238	259.906	26	118	99,95%	98,85%	94,99%	99,99%	96,88%
13	MR000012	3.254	258.890	12	258	99,90%	99,63%	92,65%	100,00%	96,02%
14	MR000013	4.225	257.919	72	120	99,93%	98,32%	97,24%	99,97%	97,78%
15	MR000014	3.954	258.190	8	208	99,92%	99,80%	95,00%	100,00%	97,34%
16	MR000015	3.727	258.417	21	201	99,92%	99,44%	94,88%	99,99%	97,11%
17	MR000016	3.472	258.672	13	108	99,95%	99,63%	96,98%	99,99%	98,29%
18	MR000017	3.603	258.541	32	239	99,90%	99,12%	93,78%	99,99%	96,38%
19	MR000018	4.250	257.894	112	160	99,90%	97,43%	96,37%	99,96%	96,90%
20	MR000019	4.408	257.736	148	107	99,90%	96,75%	97,63%	99,94%	97,19%
21	MR000020	4.018	258.126	120	91	99,92%	97,10%	97,79%	99,95%	97,44%
22	MR000021	3.021	259.123	109	53	99,94%	96,52%	98,28%	99,96%	97,39%
23	MR000022	1.850	260.294	115	74	99,93%	94,15%	96,15%	99,96%	95,14%
24	MR000023	0	262.144	0	0					
					Average	99,92%	97,69%	95,81%	99,98%	96,72%

Table 4.3: Delineation of the Left Kidney Tumour (SE000004 MRI dataset) – Evaluation metrics

a/a	SE000004 MRI Dataset	True Positives (Correctly Selected)	True Negatives (Correctly Rejected)	False Positives (Mistakenly Selected)	False Negatives (Mistakenly Rejected)	Accuracy	Precision	Sensitivity	Specificity	Dice similarity
22	MR000021	349	262.144	26	0	99,99%	93,07%	100,00%	99,99%	96,41%
					Average	99,99%	93,07%	100,00%	99,99%	96,41%

Table 4.4: Delineation of the Left Kidney Stone (SE000004 MRI dataset) - Evaluation metrics

a/a	SE000004 MRI Dataset	True Positives (Correctly Selected)	True Negatives (Correctly Rejected)	False Positives (Mistakenly Selected)	False Negatives (Mistakenly Rejected)	Accuracy	Precision	Sensitivity	Specificity	Dice similarity
12	MR000011	184	262.144	13	0	100,00%	93,40%	100,00%	100,00%	96,59%
13	MR000012	171	262.144	9	0	100,00%	95,00%	100,00%	100,00%	97,44%
					Average	100,00%	93,40%	100,00%	100,00%	96,59%

Table 4.5: Average times taken for Semi-automatic and Fully Automatic Segmentation of kidneys and their potential dysfunctions (Tumours, Stones and Cysts)

(20 MRI Datasets - 552 Dicom Images, Average Times)		
	Segmentation Methodology	
Stages	Semi-automatic	Fully Automatic
Input of a Single Medical Image MRI Dataset (Average number 28 Images)	9,47 secs	9,47 secs
Load annotations	1,87 secs	1,87 secs
Kidney Segmentation	4 mins 54 secs	55 secs
Segmentation of Dysfunctions (Tumours, Stones and Cysts)	5 mins 55 secs	
Save Annotations	1,4 secs	1,4 secs
Save Template's parameters	0	0,5 secs
Total Time	11 mins 2 secs	1 min 8 secs

4.2.3 Discussion

Overall, this *IAD* system has performed as a multi-functional system with the following features as evaluated against CT/MRI-image datasets showing its capability to support clinical diagnosis; specifically with a demonstrator case focusing on assisting in diagnosis of kidney pathologies.

- A multi-functional easy-to-use annotation system.
- The ability for real-time detection of kidneys and their abnormalities (i.e. tumours, stones and cysts – if any present).
- A multi-functional 3D visualisation system providing actual geometry (real physical sizes) measurements.
- Evaluation of the results based on a 3D volumetric evaluation, as well as on five other measurement methods

After initial development, the system was tested by clinicians and their feedback was used to improve the usability of the system.

Generally, the clinicians commented favourably on the speed and accuracy of the system, as well as on its large variety of functions with an emphasis on

the 3D view.

A notable shared view expressed by the clinicians was that given that the system was able to recognise kidneys and any abnormal tissue located within them, it should be possible for it to also detect any abnormal tissue that may also be present in the surrounding areas as this is what the clinician would want to examine particularly if there is already clinical evidence of abnormal tissue within the organ.

This function is being currently integrated whilst the system is undergoing a large clinical trial to include at least 100 MRI datasets of an average of 25 slides each.

Since the input of the system is CT/MRI datasets, it follows that these must be produced by well calibrated CT/MRI scanners in order to ensure maximum effectiveness.

Results have shown that currently the system is able to accurately detect *relatively compact* regions such as stones, cysts and tumours.

In more complex cases where, for example, a tumour has spread into different areas with varying intensities, the system can recognise the tumours but with decreased accuracy; this is being addressed through a set of more advanced algorithmic approaches.

Concerning the applicability of the work on different patients and in the case of using another MRI scanner for the same type of images (e.g. abdominal), the medical technician must create another *Template* to achieve accurate results, as not all medical image modalities are calibrated in the same way. They depict important areas of the body with similar but not identical range of grayscale values and the way each MRI scanner represents fuzzy areas (e.g. contours of the organs and tumours) is different. This calls for calibration of the sensitivity parameters on the platform (*Width, Ascending* & *Descending*, *Threshold* and *Area* as already explained), for more accurate delineations.

In summary, the platform's accuracy depends on the modalities and not on the different patient datasets: a *Template* is created from a medical image dataset for a specific scanner. This *Template* is highly accurate in the detection of the organs and the potential dysfunctions for any image dataset produced by that

scanner. For images coming from another MRI scanner, the *Template* must be readjusted but this is a one-off process as after saving the new *Template* corresponding to the new MRI, this *Template* can be used on any datasets coming from this MRI.

In order to deal with the possible inhomogeneity of images used, the platform performs the following steps:

- The Region of Interest (ROI) is defined.

- The parameters used to accurately find the organ and its boundaries are defined: *Width* (for smoothing the histogram and get the correct boundaries of the organ), *Ascending & Descending* (for identifying local minimums), *Threshold* (for removing the noise from the use of filters) and *Area* (for initial identification of the organ ignoring very small areas).

- The parameters to find the correct seeds for the pathology detection to feed to the region growing algorithm are also defined: *Greyscale* and a *Tolerance* value for the range of values to represent the dysfunction, and a *Threshold* value to change the sensitivity of the method to ignore seeds that are not strong enough.

In this way, the *Framework* remains highly immune to datasets coming from different patients and even from different pathologies.

Finally, care was taken to ensure that the output files were anonymised and were also of a small size and thus easier to download by clinicians over a clinic network.

This would also enable the system to securely and efficiently transmit files, including images, to client applications running on smartphones (Windows or Android) so that, clinicians and consultants could view the results, on the move, as and when required to save time and increase diagnostic accuracy through second opinions.

Chapter 5 - Conclusions

In this chapter, important conclusions for both medical platforms are drawn from this research. Their contribution to knowledge and recommendations for future research are presented separately for both platforms.

5.1 The *DoctorEye* project

5.1.1 Research Summary

DoctorEye is a novel, free-to-use platform designed to assist doctors to visualise *in silico* so as to better interpret organs and their dysfunctions (e.g. tumours) in medical images.

The platform is already being used in a related tumour modelling EC project (*ContraCancrum*) and offers several robust tools for fast segmentation, annotation and 3D visualisation, assisting clinicians in better understanding the pathology and defining the treatment.

The user-friendly GUI environment has been developed to meet the needs of clinicians as result of an effective collaboration with expert clinicians, clinical staff and engineers.

Moreover, the application interface is flexible and can be easily adjusted to suit different viewing setups ensuring optimal representations of the findings. The algorithms are fully integrated into the platform and run on the fly and not as calls to external programs.

The integrated multi-user annotation system supports training of clinicians in the accurate identification of areas of interest.

The sophisticated plug-in technology supports other researchers' experiments.

Finally, it is free to test upon request and requires no registration or activation, thus not limiting its use in any way. A link for freely downloading and using the software can be found at: http://biomodeling.ics.forth.gr/?page_id=8 [DoctorEye, 2013].

5.1.2 Contributions of the Research

The *DoctorEye* platform can assist doctors to identify any number of 3D distinct regions of interest - such as tumours - in complex medical images, and annotate them individually.

The platform currently focuses on aiding the clinician to rapidly and accurately annotate/segment organs and any potential dysfunctions in them (e.g. tumours). It is designed to offer robust tools and services for aiding the clinician to delineate the tumour with a 3D visualisation, providing metrics, in order to assess the stage of the disease.

The platform in its current stage facilitates the segmentation/annotation/storage processes incorporating even more tumour-specific semi-automatic segmentation methods and tools in order to improve its robustness and make annotation even faster for the clinician.

The multi-user and multi-functional annotation system supports training of clinicians in the accurate identification of organs and their potential pathology. Thus, it can be a useful tool assisting in the training of the clinicians' process to recognise and treat pathologies.

The platform already facilitates clinicians to share and combine their medical expertise e.g. in tumour delineation. Therefore, medical images with the original annotations can be shared with another clinician for re-evaluation, in order to improve accuracy.

The sophisticated plug-in technology supports researchers in experimentation with new segmentation/classification/visualisation algorithms, simplifying this process.

Due to the scalable architecture of the platform it can serve as the basis of an integrated system for visualising cancer in three dimensions, as well as hosting models of cancer growth or response to therapy.

All these functions justify that *DoctorEye* is a multifunctional, easy to use innovative platform that contributes to the research as an advanced 3D medical analysis tool that can work in training, clinical and research mode*.*

5.1.3 Suggestions for Further Research

A problem currently under consideration is the size of the files used to store the different labels and segmented regions. It is planned to develop a more sophisticated data management system in order to avoid creating data files that are large and difficult to handle.

Future work focuses on incorporating even more tumour specialised segmentation algorithms and measuring their performance. This requires the knowledge of the true borders of the tumour under investigation and a precise definition of the validation metrics.

Although the platform has been designed by clinicians for clinicians it is crucial to design several validation experiments that will deal with the effectiveness of the tools in annotating organs and their dysfunctions (e.g. tumours). The latter requires the comparison of the annotations of experts (used as gold standard) to the generated segmentations and report the sensitivity / specificity score.

Future work also includes a further development of the platform to be used as a wider medical e-health management system, able to store complete electronic patients' records together with disease specific clinical data and findings.

As such, it could be used for remote consulting, especially in cases where the diagnosis is difficult and requires a second opinion.

5.2 The *Automatic Tumour Detector* project

5.2.1 Research Summary

This research has resulted in the development and evaluation of a CT/MRI Imaging Diagnosis Assistive (*IAD*) platform for organ detection and delineation as well as their potential pathology simultaneously.

Although the *IAD* demonstrator has focused on abdominal images and supports the clinical diagnosis of kidneys using CT/MRI imaging, it can be adapted to work on image delineation, annotation and 3D real-size volumetric modelling of other organ structures, such as the brain, spine, etc.

The *IAD* provides advanced real-time 3D visualisation and measurements with fully automated functionalities as developed in two stages.

In the first stage, via the clinically driven user interface, expert clinicians use CT/MRI imaging datasets to accurately delineate and annotate the kidneys and their possible abnormalities, thus creating *3D Golden Standard Models.*

Based on these models, in the second stage, medical technicians interactively define model-based rules and parameters for the integrated *Automatic Recognition Framework* to achieve results which are closest to that of the clinicians.

These specific rules and parameters are stored in *Templates* and can later be used by any clinician to automatically identify organ structures i.e. kidneys and their possible abnormalities simultaneously.

The system also enables clinicians to send the outcome of the analysis to another clinician for a second opinion.

A 3D model of the body, the organs and their possible pathology with real metrics is also integrated.

Clinicians who participated in the trials expressed satisfaction with the integrated semi-automatic method in that it offered better visualisation of regions of interest, as it simplified and sped up the image annotation process even in very complex medical image datasets enabling higher accuracy organ and abnormality identification. As using the system requires no previous knowledge of auto-labelling, it is easy to use to support the clinical diagnosis process throughout; from the input stage of the CT/MRI image datasets to the generation of 3D models; its fully *Automatic Segmentation Framework* has been tested on 20 MRI datasets corresponding to an equal number of patients (552 Images).

The system provides metrics for the evaluation of the results, in terms of *Accuracy*, *Precision*, *Sensitivity*, *Specificity* and *Dice Similarity Coefficient (DSC)* so as to enable benchmarking of its performance.

The first IAD prototype has produced promising results as its performance accuracy based on the most widely deployed evaluation metric DSC, yields

97,2% for the recognition of kidneys and 96,1% for their abnormalities, compared to other systems with a mean DSC 95% and 91% respectively at best.

5.2.2 Contributions of the Research

In summary, the algorithms and methods presented in this research to identify the organs and their potential pathology have significant advantages over the ones in existing literature.

The semi-automatic segmentation region growing algorithm used among others in this platform with additional controls and fuzzy rules, opens pathways for other types of detection of areas of interest in other sciences (e.g. in Seismology, in the creation of Seismic Group Maps [Skounakis et al, 2011])

Concerning the implementation of the *Fully Automatic Segmentation Framework*, apart from being more accurate, it is notably faster compared to any existing method to date for the automatic recognition of the kidneys.

ATD is also the first platform that identifies simultaneously abnormalities in the organ's area such as tumours, stones and cysts in practice with notable accuracy.

To achieve this, extra control mechanisms are added to every step in the abnormalities detection procedure in order to avoid selecting isolated and irrelevant pixels.

5.2.3 Suggestions for Further Research

Future developments of the system will include an additional collection of *Templates* to be used in the recognition of other organs and their associated abnormalities simultaneously (e.g. brain, spine, knees, etc).

In future versions, a transmission process of selected compressed images to a mobile device or smartphone will also be added. This will allow clinicians to either receive information or offer opinions while they are on the move.

References

Akbari H. and Fei B.W., "Automatic 3D segmentation of the kidney in MR images using wavelet feature extraction and probability shape model", *Proceedings of SPIE 2012*, Vol. 8314, Medical Imaging 2012: Image Processing, pp. 83143D1-83143D7, 2012. [Doi: 10.1117/12.912028]

Amira: multifaceted software platform [Online]. Available at: http://www.amira.com/ [2013]

Annotor: annotation software [Online]. Available at: http://www.montefiore.ulg.ac.be/services/stochastic/biomod/doku.php?id=software [2013]

Bassmann H. and Besslich P.W., *Ad Oculos – Digital Image Processing - Student Version 2.0*, I.S.B.N 1-850-32132-9, pp. 117-152, 1995.

Benefits of the Microsoft .NET Framework [Online]. Available at: http://msdn.microsoft.com/en-us/kb/kbarticle.aspx?id=829019 [2013]

Bomans M., Hohne KH., Tiede U., and Riemer M., "3-D segmentation of MR images of the head for 3-D display", *IEEE Trans Med Imaging*; Issue 9(2), pp. 177-183, 1990.

Brummer M., "Optimised intensity thresholds for volumetric analysis of magnetic resonance imaging data.", Proceeding SPIE 1808; Visualization in Biomedical Computing, pp. 299–310, 1992. [DOI:10.1117/12.131086]

Campadelli P., Casiraghi E., and Pratissoli S., "Fully automatic segmentation of abdominal organs from ct images using fast marching methods", *21st IEEE International Symposium on Computer-Based Medical Systems* (CBMS 2008), pp. 554-559, June 2008.

Chen X., Summers R. and Yao J., "FEM-Based 3-D Tumour Growth Prediction for Kidney Tumour", *IEEE Transactions on Biomedical Engineering (2011)*, Vol. 58, No 3, pp. 463-467, March 2011. [DOI: 10.1109/TBME.2010.2089522]

Chest X-ray [Online]. Available: http://www.cancerresearchuk.org/cancer-help/about-cancer/tests/xrays [2013]

Clarke P., Velthuizen P., Camacho M., Heine J., Vaidyanathan M., Hall L., Thatcher R. and Silbiger M., "MRI segmentation: Methods and applications", *Magnetic Resonance Imaging*, Volume 13, Issue 3, pp. 343-368, 1995.

ContraCancrum Project [Online]. Available http://www.contracancrum.eu [2013]

Dellepiane S., "Image segmentation: errors, sensitivity, and uncertainty", *Proc IEEE-Eng Med Biol Soc*, Issue 13, pp. 253–254, 1991.

DoctorNo plug-ins [Online]. Available: http://www.istb.unibe.ch/unibe/medizin/istb/content/e8060/e8092/e9657/e9986/files10635/DoctorNo-manual.pdf [2013]

ClearCanvas [Online]. Available: http://www.clearcanvas.ca [2013]

Computed Tomography (CT) of the brain [Online]. Available: http://www.minclinic.ru/KT/KT_eng/KT-brain_eng.html [2013]

Dehui X. et al., "Skeleton Cuts—An Efficient Segmentation Method for Volume Rendering," Visualization and Computer Graphics, IEEE Transactions on, vol.17, no.9, pp.1295,1306, Sept. 2011. [DOI: 10.1109/TVCG.2010.239]

DicomLookup [Online]. Available: http://dicomlookup.com/ [2013]

DicomObjects [Online]. Available: http://www.medicalconnections.co.uk/DicomObjects.NET [2013]

DICOM Sample image sets [Online]. Available: http://www.osirix-viewer.com/datasets/ [2013]

Dicom.dll software [Online]. Available: http://www.sermis.polito.it/tc-25/software/dicom.pdf [2013]

DoctorEye software [Online]. Available: http://biomodeling.ics.forth.gr/?page_id=8 [2013]

El-Baz, A. et al., "New motion correction models for automatic identification of

renal transplant rejection", International Conference on Medical Image Computing and Computer-Assisted Intervention, (MICCAI 2007), pages 235-243, Brisbane, Australia, October 29 - November 2, 2007.

El-Baz A. et al., "Image analysis approach for identification of renal transplant rejection", 19th International Conference on Pattern Recognition (ICPR 2008), pp.1-4, December 8-11, 2008. [DOI: 10.1109/ICPR.2008.4761694]

Farag et al., "A framework for the detection of acute renal rejection with dynamic contrast enhanced magnetic resonance imaging," 3rd IEEE International Symposium on Biomedical Imaging: Nano to Macro (ISBI 2006), pp.418-421, Arlington, Virginia, USA, April 6-9, 2006 [DOI: 10.1109/ISBI.2006.1624942]

Farmaki C., Marias K., Sakkalis V. and Graf N., "Spacially adaptive active contours: a semi-automatic tumour segmentation framework", International Journal CARS issue 5, pp. 369:384, 2010. [DOI: 10.1007/s11548-010-0477-9]

Fujita H. and Fejri M., "New trends in software methodologies, tools and techniques: How to create the magic wand?", *Proceedings of the Fifth SoMeT-06,* IOS press, ISBN 1-58603-673-4, pp. 127-132, 2006.

Gloger O., Tonnies K.D., Liebscher V., Kugelmann B., Laqua R. and Volzke H., "Prior Shape Level Set Segmentation on Multistep Generated Probability Maps of MR Datasets for Fully Automatic Kidney Parenchyma Volumetry", *IEEE Transactions on Medical Imaging*, Vol. 31, No. 2, pp. 312-325, February 2012. [DOI: 10.1109/TMI.2011.2168609]

Hadwiger M. et al., "High-quality two-level volume rendering of segmented data sets on consumer graphics hardware," Visualization, 2003. VIS 2003. IEEE, vol., no., pp.301,308, Oct. 24, 2003. [DOI: 10.1109/VISUAL.2003.1250386]

Horn B.K.P., Robot vision. Cambridge, London: *MIT Press*, ISBN 0-262-08159-8, 1986.
How MRI works [Online]. Available: http://www.howstuffworks.com/mri.htm [2013]

Jose J. et al., "An Efficient Diagnosis of Kidney Images Using Association Rules", International Journal of Computer Technology and Electronics

Engineering (IJCTEE) Volume 2, Issue 2,, ISSN 2249-6343, 2012.

Kass M., Witkin A., and Terzopoulos D., "Snakes:active contour models", *International Journal of Computer Vision*, vol.1, no.4, pp. 321-331, 1987.

Khalifa F., et al., "Non-invasive image-based approach for early detection of acute renal rejection", Proceedings International Conference Medical Image Computing and Computer-Assisted Intervention (MICCAI 2010), pages 10-18, Beijing, China, September 20-24, 2010.

Kim D.Y. and Park J.W., "Computer-aided detection of kidney tumor on abdominal computed tomography scans", *Acta Radiologica (2004)*, Volume: 45, No 7, pp. 791-795, 2004. [DOI: 10.1080/02841850410001312]

Kumar K. et al., "Artificial Neural Networks for Diagnosis of Kidney Stones Disease", I.J. Information Technology and Computer Science, Vol. 7, pp. 20-25, 2012.

Kumar S. et al., "Automatic Segmentation of Liver and Tumor for CAD of Liver", Journal of Advances in information technology, vol.2, no 1, February 2011.

Li K. and Fei B., "A New 3D Model-based Minimal Path Segmentation method for Kidney MR Images", *The 2nd International Conference on Bioinformatics and Biomedical Engineering*, ICBBE 2008, pp. 2342 – 2344, 2008. [DOI: 10.1109/ICBBE.2008.918]

Lin D.T. Member IEEE, C.C. Lei, and S.W. Hung, "Computer-Aided Kidney Segmentation on Abdominal CT Images", *IEEE Transactions on Information Technology in Biomedicine*, Vol. 10, No. 1, pp. 59 – 65, January 2006. [Doi: 10.1109/TITB.2005.855561]

Lin I. and Chao H., "CMAS: a rich media annotation system for medical imaging", in Proc. Medical Imaging 2006: PACS and Imaging Informatics, Conf., San Diego, CA, USA, Proceedings of the SPIE, Volume 6145, pp. 34-41, 2006.

Mahalakshmi T., Aswathi B.L. and Achuthsankar S.N., "Connectivity Characteristic of Transcription Factor.", *World Academy of Science Engineering and Technology (WASET)*, International Journal of Information and

Communication Engineering, Vol. 5, No 7, pp. 471-474, 2009.

Manjori R. et al, "Comparison of Human and automatic segmentations of kidneys from CT images", *Int. J. Radiation Oncology Biol. Phys.*, Vol. 61, No. 3, pp. 954–960, 2005.

Marcotegui B. and Zanoguera F., "Image editing tools based on multi-scale segmentation.", In H. Talbot and R. Beare (eds.)", *Mathematical Morphology VI*, (Proc. ISMM02, Sydney, Australia). CSIRO, pp. 127-135, April 2002.

Mechouche A., Morandi X., Golbreich C. and Gibaud B., "A Hybrid System for the Semantic Annotation of Sulco-Gyral Anatomy in MRI Images", in Proc. of the 11th International Conference in Medical Image Computing and Computer-Assisted Intervention – MICCAI 2008, New York, NY, USA, pp. 807-814, 2008.

Medical Image Analysis, by Atam P. Dhawan, IEEE Press, 2003

Mille J., Bone R. , Makris P., and Cardot H., "Greedy Algorithm and Physics-Based Method for Active Contours and Surfaces: A Comparative Study", in 2006 Proc. of IEEE International Conference on Image Processing (ICIP), Atlanta, USA, pp. 1645-1648, 2006

Peng H., Long F. and Myers E., "VANO: a volume-object image annotation system", Bioinformatics 25(5): pp. 695-697, 2009.

Perona P. and Malik J., "Scale-space and edge detection using anisotropic diffusion.", *IEEE Transactions on Pattern Analysis and Machine Intelligence,* Vol. 12, No 7, pp. 629-639, 1990. [DOI: 10.1109/34.56205]

Prevost R., Mory B., Correas J.M., Cohen L.D., and Ardon R., "Kidney detection and real-time segmentation in 3D contrast-enhanced ultrasound images", *9th IEEE International Symposium on Biomedical Imaging* (ISBI 2012), Barcelone, Spain, pp. 1559-1562, 2012. [DOI: 10.1109/ISBI.2012.6235871]

Rao M. et al, "Comparison of human and automatic segmentations of kidneys from CT images.", *International Journal of Radiation Oncology, Biology, Physics,* Vol. 61, No 3, pp. 954–960, March 2005. [DOI: 10.1016/j.ijrobp.2004.11.014]

Roniotis A., Marias K., Sakkalis V., Tsibidis G., and Zervakis M., "A Complete

Mathematical Study of a 3D Model of Heterogeneous and Anisotropic Glioma Evolution.", *IEEE EMBS* Conference, Minneapolis, pp. 2807-2810, 2009. [DOI: 10.1109/IEMBS.2009.5333776]

Rusinek H. et al., "Performance of an Automated Segmentation Algorithm for 3D MR Renography", Magnetic Resonance in Medicine 57, pp. 1159-1167, 2007.

Skounakis E., Konstantaras A., Katsifarakis E., Maravelakis E., Banitsas K. and Varley M., "Seismic Data Clustering Management System", *European Geosciences Union General Assembly (EGU 2011)***,** Vienna, Austria, April 2011.

Skounakis E., Farmaki C., Sakkalis V., Roniotis A., Banitsas K., Graf N., and Marias K, "DoctorEye: A Clinically Driven Multifunctional Platform, for Accurate Processing of Tumors in Medical Images", *Bentham Open, The Open Medical Informatics Journal, Volume 4, pg 105-115,* March 2010. [ISSN: 1874-4311], [DOI: 10.2174/1874431101004010105]

Tamilselvi P. et al., "Computer Aided Diagnosis System for Stone Detection and Early Detection of Kidney Stones, Journal of Computer Science 7 (2): ISSN 1549-3636, Science Publications 2011.

The Mono project [Online]. Available: http://www.mono-project.com [2013]

The Visualisation Toolkit (VTK) [Online]. Available: http://www.vtk.org/ [2013]

Two Views of MRI Scans [Online]. Available: http://www.two-views.com/MRI/During.html [2013]

Wang G. et al., "A new segmentation framework based on sparse shape composition in liver surgery planning system", Med. Phys. 40 (5), May 2013.

Williams D.J. and Shah M., "A fast algorithm for active contours and curvature estimation.", *Computer Vision Graphics and Image Processing: Image Understanding*, vol. 55, no. 1, pp.14-26, 1992.

Zepp J., Graf N., Skounakis E., Bohle R., Meese E., Stenzhorn H., Kim Y., Farmaki C., Sakkalis V., Reith W., Stamatakos G. and Marias K., "Tumor segmentation: The impact of standardised signal intensity histograms in

glioblastoma", *4th International Advanced Research Workshop on In Silico Oncology and Cancer Investigation, (4th IARWISO 2010),* IEEE, Athens, Greece, Sept 2010.

Appendix A: SDK vb.net sample 1 – Create Sessions

```vb.net
Private Sub CreateSessions()
' Create the first session
MyFirstSession = Global.DoctorEye.Application.AddSession

'Add a new dataset to this session to store the images
MyFirstDataSet = MyFirstSession.AddDataset

' Add a new image to the dataset and load it
MyFirstImage = MyFirstDataSet.AddImage(Me.Label1.Tag)
MyFirstImage.Load(True)

Dim FirstSize = MyFirstImage.Size
' After the loading is done, show the session
MyFirstSession.Visible = True

' Create the second session
MySecondSession = Global.DoctorEye.Application.AddSession

'Add a new dataset to the session to store images.
MySecondDataSet = MySecondSession.AddDataset

' Add a new image to the dataset and load it
MySecondImage = MySecondDataSet.AddImage(Me.Label2.Tag)
MySecondImage.Load(True)

Dim SecondSize = MyFirstImage.Size
' We keep the maximum size of the two images for the result image
Dim OutputSize = New Size(Math.Max(FirstSize.Width, SecondSize.Width),
Math.Max(FirstSize.Height, SecondSize.Height))

' After the loading is done, show the session
MySecondSession.Visible = True

' Create the output session
MyOutputSession = Global.DoctorEye.Application.AddSession
```

```vb
'Add a new dataset to the session to store images.
MyOutputDataSet = MyOutputSession.AddDataset

' Create ten 512x512 DICOM Images and add them to the list
MyOutputImage = MyOutputDataSet.AddImage(Me.Label3.Tag, OutputSize)
MyOutputImage.Load(True)

' After the loading is done, show the session
MyOutputSession.Visible = True
End Sub
```

```vb
Private Sub ExecuteCalculations()
' Now we can perform any calculation with the images
Dim Ann = MyOutputImage.AddAnnotation("Execution Result")
Ann.SuspendLayout()

For x = 0 To Me.MyOutputImage.Size.Width - 1
   For y = 0 To Me.MyOutputImage.Size.Height - 1
      Ann.Selection(x, y) = (((x + y) Mod 2) = 0)
   Next
Next

Ann.ResumeLayout()
End Sub
```

Appendix B: SDK C# sample 1 – Create Sessions

```csharp
using System;
using System.Collections.Generic;
using System.Linq;
using System.Text;
using DoctorEye;
using DoctorEye.Plugins;

namespace Forth.Ics.DoctorEye.SDK.Tools.CS
{
    public class CreateSessionSamplePlugin : Plugin
    {
        Guid CreatedSessionId;

        public CreateSessionSamplePlugin()
        {
            this.Name = "Create Session sample";
            this.Description = "Creates a new session with 10 images and shows it.";
            this.Category = "Samples";
            this.CategoryGroup = "C#";
            this.Glyph =
global::Forth.Ics.DoctorEye.SDK.Tools.CS.Properties.Resources.ToolImage;
            this.Style = ToolButtonStyle.SimpleButton;
        }

        protected override void Activate()
        {
         // Since the plug-in deactivates and reactivates when the active session
         // changes, we need to keep track of the id of the session that we created.
         // If the active session's id is different from our saved session then we
         // have to create the session.
        if (this.CreatedSessionId != global::DoctorEye.Application.ActiveSession.Id)
           {
              // Save the new images to "My Documents" folder.
              var PathToSave =
System.Environment.GetFolderPath(Environment.SpecialFolder.MyDocuments);
```

```csharp
        // Create a new session
        var MySession = global::DoctorEye.Application.AddSession();


        // Store the session's id.
        this.CreatedSessionId = MySession.Id;


        // Add a new dataset to the session we created to store our images.
        var MyDataSet = MySession.AddDataset();


        // Create ten 512x512 DICOM Images and add them to the list
        for (int i = 1; i < 10; i++)
        {
            var MyImage =
MyDataSet.AddImage(System.IO.Path.Combine(PathToSave,
String.Format("TestImage_{0}.dcm", i)), new System.Drawing.Size(512, 512));
            // Initialize the image.
            MyImage.Load(true);
            // Now that the image is loaded we can use it.
        }


        // After the loading is done, show the session
        MySession.Visible = true;
      }
    }


    protected override void Deactivate()
    {
    }
  }
}
```

Appendix C: SDK vb.net sample 2 – Compare Sessions

```vbnet
Private Sub CreateSessions()
    ' Create the first session
    MyFirstSession = Global.DoctorEye.Application.AddSession

    'Add a new dataset to the session to store images
    MyFirstDataSet = MyFirstSession.AddDataset

    ' Add an image and load it
    MyFirstImage = MyFirstDataSet.AddImage(Me.Label1.Tag)
    MyFirstImage.Load(True)

    Dim FirstSize = MyFirstImage.Size

    ' After all the loading is done, show the session
    MyFirstSession.Visible = True

    ' Create the second session
    MySecondSession = Global.DoctorEye.Application.AddSession

    'Add a new dataset to the session to store images
    MySecondDataSet = MySecondSession.AddDataset

    ' Add the image and load it
    MySecondImage = MySecondDataSet.AddImage(Me.Label2.Tag)
    MySecondImage.Load(True)

    Dim SecondSize = MyFirstImage.Size

    ' We keep the maximum size of the two images for the result image
    Dim OutputSize = New Size(Math.Max(FirstSize.Width, SecondSize.Width),
Math.Max(FirstSize.Height, SecondSize.Height))

    ' After all the loading is done, show the session
    MySecondSession.Visible = True
```

```vb.net
    ' Create the output session
    MyOutputSession = Global.DoctorEye.Application.AddSession

    'Add a new dataset to the session to store images
    MyOutputDataSet = MyOutputSession.AddDataset

    ' Create ten 512x512 DICOM Images and add them to the list
    MyOutputImage = MyOutputDataSet.AddImage(Me.Label3.Tag, OutputSize)
    MyOutputImage.Load(True)

    ' After all the loading is done, show the session
    MyOutputSession.Visible = True
  End Sub
```

```vb.net
  Private Sub ExecuteCalculations()
    ' We get a list of unique annotation labels.
    Dim AnnotationLabels = (From ann1 In Me.MyFirstImage.Annotations _
                 Select ann1.Label _
                 From ann2 In Me.MySecondImage.Annotations _
                 Select ann2.Label).Distinct

    For Each label In AnnotationLabels
      Dim LabelToSearch = label

      Dim Ann1 = (From item In Me.MyFirstImage.Annotations _
            Where item.Label = LabelToSearch).FirstOrDefault

      Dim Ann2 = (From item In Me.MySecondImage.Annotations _
            Where item.Label = LabelToSearch).FirstOrDefault

      ' We need annotations that exist on both images
      If Ann1 IsNot Nothing AndAlso Ann2 IsNot Nothing Then
        ' We copy the first annotation to the output image
        Dim OutputAnn1 = MyOutputImage.AddAnnotation(String.Format("{0} (First
Image)", LabelToSearch))
        OutputAnn1.SuspendLayout()
        OutputAnn1.Color = Color.FromArgb(50, Color.Red.R, Color.Red.G,
Color.Red.B)
        OutputAnn1.Selection = Ann1.Selection
        OutputAnn1.ResumeLayout()
```

```vb.net
        ' We copy the second annotation to the output image
        Dim OutputAnn2 = MyOutputImage.AddAnnotation(String.Format("{0}
(Second Image)", LabelToSearch))
        OutputAnn2.SuspendLayout()
        OutputAnn2.Color = Color.FromArgb(50, Color.Green.R, Color.Green.G,
Color.Green.B)
        OutputAnn2.Selection = Ann2.Selection
        OutputAnn2.ResumeLayout()

   ' We create a third annotation with the common selection to the output image
        Dim OutputAnn3 = MyOutputImage.AddAnnotation(String.Format("{0}
(Common)", LabelToSearch))
        OutputAnn3.SuspendLayout()
        OutputAnn3.Color = Color.FromArgb(50, Color.Blue.R, Color.Blue.G,
Color.Blue.B)

' The common selection points must be at the common areas of the two images
        Dim MinX = Math.Min(Me.MyFirstImage.Size.Width,
Me.MySecondImage.Size.Width)
        Dim MinY = Math.Min(Me.MyFirstImage.Size.Height,
Me.MySecondImage.Size.Height)

        ' We select the common points of the two images
        For x = 0 To MinX - 1
          For y = 0 To MinY - 1
            OutputAnn3.Selection(x, y) = (OutputAnn1.Selection(x, y) And
OutputAnn2.Selection(x, y))
          Next
        Next
        OutputAnn3.ResumeLayout()
      End If
    Next
  End Sub
```

Appendix D: List of Thesis Publications

Skounakis E., Farmaki C., Sakkalis V., Roniotis A., Banitsas K., Graf N., and Marias K.. "DoctorEye: A Clinically Driven Multifunctional Platform, for Accurate Processing of Tumors in Medical Images", *The Open Medical Informatics Journal,* Volume 4, pg 105-115, Mar. 2010, Bentham Open. [ISSN: 1874-4311], [DOI: 10.2174/1874431101004010105]

Zepp J., Graf N., **Skounakis E.,** Bohle R., Meese E., Stenzhorn H., Kim Y., Farmaki C., Sakkalis V., Reith W., Stamatakos G. and Marias K., "Tumor segmentation: The impact of standardised signal intensity histograms in glioblastoma"**,** *IEEE 4th International Advanced Research Workshop on In Silico Oncology and Cancer Investigation (4th IARWISO 2010),* Athens, Greece, Sept. 2010. http://www.4th-iarwisoci.iccs.ntua.gr/proceedings.pdf

Sakkalis V., Marias K., Roniotis A. and **Skounakis E.**, "Translating Cancer Research into Clinical Practice: A Framework for Analysing and Modeling Cancer from Imaging Data", *International Conference on Intelligent Systems Design and Applications (ISDA 2009)*, IEEE Proceedings pages 347-350, Pisa, Italy, Nov 2009. [DOI: 10.1109/ISDA.2009.235]

Skounakis E., Sakkalis V., Marias K., Banitsas K., and Graf N., "DoctorEye: A multifunctional open platform for fast annotation and visualization of tumors in medical images", *31st Annual International Conference of the IEEE Engineering in Medicine and Biology Society (EMBS 09)*, Proceedings pages 3759 - 3762, Minneapolis, Minnesota, USA, Sept. 2009. [DOI: 10.1109/IEMBS.2009.5334479] http://www.ncbi.nlm.nih.gov/pubmed/19964810

Skounakis E., Banitsas K., and Marias K., *Member IEEE,* **"**A Proposed Platform for Intelligent Identification of Organs from Medical Images.". *3rd International Advanced Research Workshop on In Silico Oncology (3rd IARWISO 2008),* IEEE Proceedings pages 20-22, 23-24 September 2008, Istanbul, Turkey. [Presentation sponsored by EC Contra Cancrum Project ICT-2007-223979]. http://www.3rd-iarwiso.iccs.ntua.gr/procs.pdf

Appendix E: List of other Publications

Konstantaras A., Katsifarakis E., Maravelakis E., **Skounakis E.**, Kokkinos E. and Karapidakis E., "Intelligent Spatial-Clustering of Seismicity in the Vicinity of the Hellenic Seismic Arc", *Earth Science Research Journal*, Vol. 1, No. 2, 2012. [ISSN 1927-0542], [E-ISSN 1927-0550], [DOI:10.5539/esr.v1n2p1]

Skounakis E., Konstantaras A., Katsifarakis E., Maravelakis E., Banitsas K. and Varley M., "Seismic Data Clustering Management System", *European Geosciences Union General Assembly, (EGU 2011)*, April 2011, Vienna, Austria. http://meetingorganizer.copernicus.org/EGU2011/EGU2011-12120.pdf

Katsifarakis E., Konstantaras A., Maravelakis E., **Skounakis E.** and Varley M. "Seismic clustering algorithms", *European Geosciences Union General Assembly, (EGU 2011)*, April 2011, Vienna, Austria. http://meetingorganizer.copernicus.org/EGU2011/EGU2011-4259.pdf

Skounakis E. and Christodoulou M. "Selective Medical Image Compression via Intelligent Identification of Objects.", *The Eight International Conference on Signal and Image Processing (SIP 2006)* by **I.A.S.TE.D** (The International Association of Science and Technology for Development, USA), 14-16 August 2006, Honolulu, Hawaii, USA).

Skounakis E., Karagiannis V. and Vlissidis A., "A Versatile System for Real-time Analysing and Testing Objects Quality", Proceedings-CD of the *4th International Conference on "New Horizons in Industry, Business and Education" (NHIBE 2005)*, (pages 701-708), 25-26 August 2005, Dassia, Corfu Island, Greece. [Presentation sponsored by E.C.D.L. Hellas].